Contribution to the study of deformation twinning in titanium

Lei Bao

THESE

Présentée *à*

UNIVERSITÉ PAUL VERLAINE-METZ

Par

BAO Lei

Pour l'obtention du grade de:

Docteur de l'Université Paul Verlaine-Metz

Spécialité: Mécanique des matériaux

Option: Sciences des Matériaux

Contribution to the Study of Deformation Twinning in Titanium

Soutenue le 21Juin 2011 à Pékin devant le jury composé de:

Claude ESLING	Professeur à l'Université Paul Verlaine de Metz, France	Directeur de thèse
Xiang ZHAO	Professeur à Northeastern University, Chine	Directeur de thèse
Christophe SCHUMAN	Maître de conférences à l'Université Paul Verlaine de Metz, France	Co-directeur de thèse
Yandong WANG	Professeur à Beijing Institute of Technology, Chine	Rapporteur
Alain VASSEL	Docteur à Association TITANE, France	Rapporteur
Lei WANG	Professeur à Northeastern University, Chine	Rapporteur
Elisabeth GAUTIER	Directeur de recherche CNRS, France	Examinateur
Liang ZUO	Professeur à Northeastern University, Chine	Examinateur
Yongqing ZHAO	Professeur à Northwest Institute for Nonferrous Metal Research, Chine	Membre du Jury
Yafeng LU	Professeur à Northwest Institute for Nonferrous Metal Research, Chine	Membre du Jury
Isabelle MORELON	Docteur, International Program Manager ANR, Non-thematic Department, France	Invité
Jean-Sébastien LECOMTE	Ingénieur de recherches CNRS, Arts Metiers Paris-TECH, France	Invité
Philippe MARTINEAU	Conseiller adjoint, Service pour la Science et la Technologie, Ambassade de France en Chine, France	Invité

LEM3 - UMR CNRS 7239 Université Paul Verlaine-Metz - Île du Saulcy - 57045 METZ Cedex 1

Contents

Summary

Titanium and its alloys are widely used in aviation, space, military, construction and biomedical industry because of the high fracture strength, high ductility and good biocompatibility. The mechanisms of plastic deformation in titanium have been studied in detail, especially deformation twinning since it has a great influence on the ductility and fracture strength.

In this study, an interrupted "in situ" SEM/EBSD investigation based on a split sample of commercial titanium T40 was proposed and performed in rolling and channel die compression. This approach allows to obtain the time resolved information of the appearance of the twin variants, their growth, the interaction between them and the interaction with the grain boundaries or twin boundaries. With the orientation data acquired by the EBSD technique, we calculated the Schmid factor, crystallographic geometry, and plastic energy associated with each variant of primary twins, secondary twins and double twins to investigate the lattice rotation, the activation of twins, the growth of twins, and the variant selection criterion.

In this observation, two types of twin systems were activated: {10-12} tension and {11-22} compression twins. Secondary twins were also activated, especially the twin variants with the highest Schmid factors (e.g. higher than 0.4). The growth of the two types of twin is quite different. The {11-22} twin shows Multiple Variants System (MVS) whereas the {10-12} twin shows Predominant Variant System (PVS).

The twinning occurs in grains that have particular orientations. Generally, the reorientation induced by the twinning aligns the c-axis of the twinned part to the stable rolling texture orientations, so that no further secondary twinning can be induced. The secondary twinning occurs only when the primary twinning orientates the c-axis of the primary twins far away from the stable orientations. For twinned

grains, the lattice rotation of the matrix is similar to that of the grains having a similar crystallographic orientation but without any twin.

Two sets of double twins were observed in this study, classified as C-T1 and T1-C double twins respectively. All the variants of C-T1 and T1-C double twins were classified into three groups: A, B and C according to the crystallographic symmetry. The misorientations of theses three groups with respect to the matrix are 41.34°, 48.44° and 87.85°. Strong variant selection took place in double twinning. In C-T1 double twins, 78.9% variants belong to group B whereas in T1-C double twins, 66.7% variants belong to group C. The plastic energy and Schmid factor both play important roles in the variant selection of double twinning. Geometrical characteristics, like the common volume or strain accommodation do not contribute significantly to the variant selection.

Résumé

Le titane et ses alliages sont largement utilisés dans les domaines aéronautique, spatial, de l'armement, du génie civil, dans des applications commerciales et biomédicales en raison de sa résistance à la rupture élevée, d'une bonne ductilité et d'une grande biocompatibilité. Les mécanismes de la déformation plastique du titane ont été étudiés en détail par le passé, particulièrement sur l'étude de la déformation par maclage car il a une grande influence sur les propriétés mécaniques.

Une méthode d'essais "in situ" en EBSD basée sur des tôles polies et colées ensemble a été développée dans cette étude et utilisée en laminage et en compression plane. Avec cette méthode, des mesures EBSD sont effectuées à chaque étape de la déformation dans la même zone comprenant un grand nombre de grains. Par conséquent, l'information sur l'orientation de ces grains à chaque l'étape de la déformation est mesurées.

Le maclage apparait dans les grains qui ont des orientations particulières. En règle générale, la réorientation induite par le maclage aligne l'axe c de la partie maclées vers les orientations stables de la texture de laminage, de sorte qu'aucun autre maclage secondaire peut être induit. Le maclage secondaire se produit uniquement lorsque le macle primaire envoie l'axe c loin des orientations stables. Pour les grains maclés, la rotation du réseau de la matrice est semblable à celle des grains ayant une orientation cristallographique identique mais sans macles.

Deux types de systèmes de macles ont été activés au cours de la déformation à la température ambiante: des macles de tension (10-12) et des macles de compression (11-22). Dan le maclage primaire, les résultats montrent que les variantes de macle ayant des facteurs Schmid supérieurs à 0.4 ont une bonne chance d'être actifs. Les comportements des deux types de maclage sont complètement différents. Dans la déformation en compression, les macles (11-22) montrent le comportement de type

multiplication des variants (Multiply Variants System: MVS) alors que les macles (10-12) montrent le type de maclage prédominant (Predominant Twin System: PTS). Cette étude présente deux types de macles doubles dénommées C-T1 (= macle primaire de Compression et macle secondaire de Tension) et T1-C (= macle primaire de Tension et macle secondaire de Compression). Tous les variants sont classés seulement en trois groupes: A, B et C par symétrie cristallographique. Les désorientations de ces 3 groupes par rapport à l'orientation de la matrice sont respectivement de 41.34°, 48.44° et 87.85°.Une forte de sélection de variant se déroule dans le maclage double. Pour les macles doubles CT, 78.9% des variantes appartiennent à la B et pour T1-C, 66.7% des variantes appartiennent à C. Le facteur de Schmid joue un rôle prépondérant dans la sélection des variants des macles doubles. Les caractéristiques géométriques, associant " volumes communs " et l'accommodation de la déformation ne contribuent pas de manière significative à la sélection des variants.

Acknowledgements

This work was carried on at Laboratoire d'Etude des Textures et Application aux Materiaux (LETAM CNRS FRE 3143), University of Metz in France. First of all, I would like to give my hearted thanks to all the members at this laboratory for their kind help.

I would like to sincerely thank my supervisors, Prof. Claude Esling, Dr. Christophe Shuman at University of Metz, and Prof. Xiang Zhao at Northeastern University for guiding me into this research field and for their constant help and support on my research work. Every progress in this work coagulated their care and enlightenment. Special thanks should be given to Prof. Marie-Jeanne Philippe for her enriching ideas and the fruitful discussions. I am also deeply indebted to Dr. Jean-Sébastien Lecomte, who is a friendly co-worker of outstanding practical ability and active thinking. At last, I would like to give my hearted thanks to Dr. Yudong Zhang for her constant help not only on my research work but also on my daily life in France. As an illuminating guider, she exhibits the characters of being reliable, modest, serious and sympathetic. I did extremely enjoy working with them all.

During my study, I always received direct help from the French Ph. D students at LETAM, especially Pierre Blaineau and Jean-Christophe Hell. Their kind care, selfless help and the deep friendship between us have made up of large part of the support and enjoyment of my study. I will cherish our friendship deeply in my mind.

Last but not least, I would like to give my hearted thanks to my mother and my wife. Their deep love, understanding, constant support and encouragement over the years are the great impetus to my study.

Chapter 1: Basic understanding and review of the literature on the plastic deformation of hexagonal materials

This chapter is devoted to introducing the basic concepts and definitions essential to the understand of the present work topic. It also proposed a review of the literature on plastic deformation mechanism in materials with hexagonal crystal structure, especially in titanium. At first, an introduction of the concepts about the hexagonal close-packed structure and a detailed description about deformation modes, twinning and slipping are proposed. Then we provide a review on some hexagonal metals often studied in the field of research in materials science.

1. Metals with hexagonal close-packed structure

The hexagonal structure materials such as titanium and magnesium are especially interesting because of their properties. The properties of titanium are particularly appreciated by the aerospace and biomedical industry. Magnesium is applied in automotive, computers or sports equipment. Zirconium is studied for its use in nuclear reactors. However, since their slip systems are not as sufficient as cubic's, so the twinning becomes more common in these materials. It becomes important to know the characteristics of deformation, including the activity of twinning, shear critical resolved on different slip systems... These relevant issues on hexagonal structure materials are the subject of many research works from 1950s until recent years (Schmid and Boas 1950).

1.1 Hexagonal close-packed crystal structure

The atom positions in the hexagonal close-packed structure are shown in Figure 1-1. If atoms are assumed to be hard spheres, the closest arrangement in an atom plane produces a series of hexagonal placed closely. The stacking sequence of close-packed atom planes one upon another produces is ABAB… (Figure1-1). In an ideal closed-packed structure, the axial ratio $\gamma = c/a = \sqrt{8/3} \approx 1.633$.

The coordination number of an ideal hexagonal close-packed structure is 12, as same as the FCC structure. However, no pure metal has the ideal 1.633 axial ratio. The pure metals with axial ratio higher than 1.633, have 6 nearest atoms in the basal plane; in the other case, the metals with axial ratio lower

than 1.633, have 6 nearest atoms, three above the basal plane and three under basal plane (Hume-Rothery and Raynor 1962; Christian 1965).

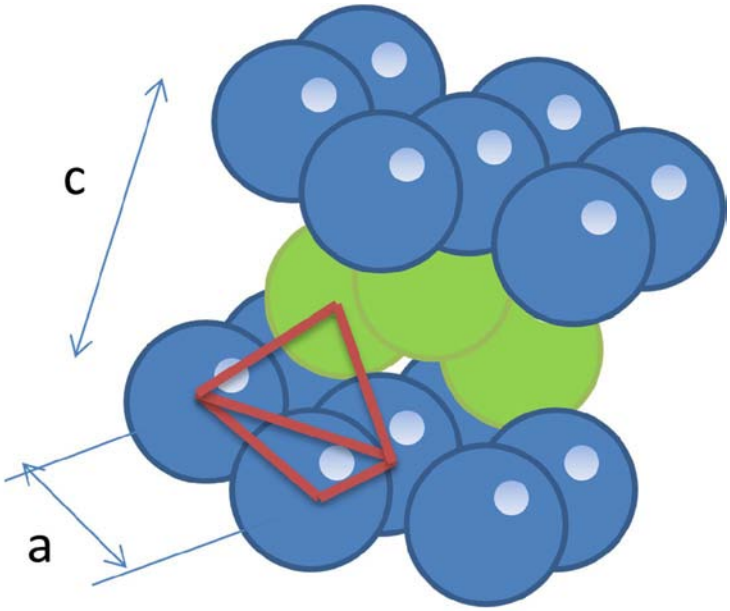

Figure 1-1: Atoms in the hexagonal close-packed structure.

Because the Miller indices of the crystallographic planes and directions from a same family appear quite dissimilar, and in order to avoid the possibility of confusion and the inconvenience, A Miller-Bravais indices were developed to describe the crystallographic planes and directions in hexagonal system (Taylor 1961; Reed-Hill and Abbaschian 1964; Barrett and Massalski 1966). This Miller-Bravais indices base on a 4-axis system, where the coplanar vectors a_1, a_2 and a_3 are at 120° to each other and vector c is perpendicular to the plane consists of vectors a_1, a_2 and a_3. (Figur 1-2) The vector a_3 is redundant since $a_3=-(a_1+ a_2)$. In the Miller-Bravais indices, a crystallographic direction *d* will have 4 indices [uvtw], such as $d=ua_1+va_2+ta_3+wc$, and then the crystallographically equivalent directions have similar indices.

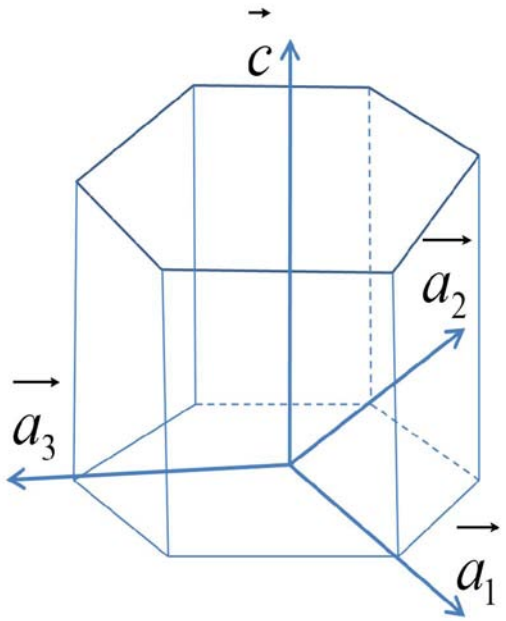

Figure 1-2: Four-axis system in Miller-Bravais indices.

1.2 Deformation mode in hexagonal materials

1.2.1 Twinning modes

Twinning in hexagonal metals is of great important because the limited slip modes in these metals make twinning a necessary way to accommodate the deformation. Unlike the slip mode, twinning products a specific new orientation in crystal by shear.

The geometry description of twinning shear is illustrated in Figure1-3. All points of the lattice on the upper side of plane K_1 are displaced in the direction η_1 by an amount of u_1 proportional to their distance above K_1. The plane containing η_1 and the normal to K_1 is called the plane of shear S. And it is evidently that all vectors in that plane through which is normal to plane S are unchanged in length, although rotation. The plane K2 in Figure 1-3 conventionally called the second undistorted plane. K1 is neither rotated nor

distorted, and it is called the first undistorted plane and also twin plane. When a crystal is completely converted to a twin, all directions lying in the initially acute sector between K_1 and K_2 are shortened, while all directions lying in the obtuse sector are lengthened. Since that twin can been seen as a specific type of crystalline structure relationship between the twin part and the matrix, we can describe twin in the same way as describe two crystalline structure relationship, with a rotation angle and a rotation axis. {10-12}, {11-21} and {11-22} twins in titanium are illustrated in Figure1-4.

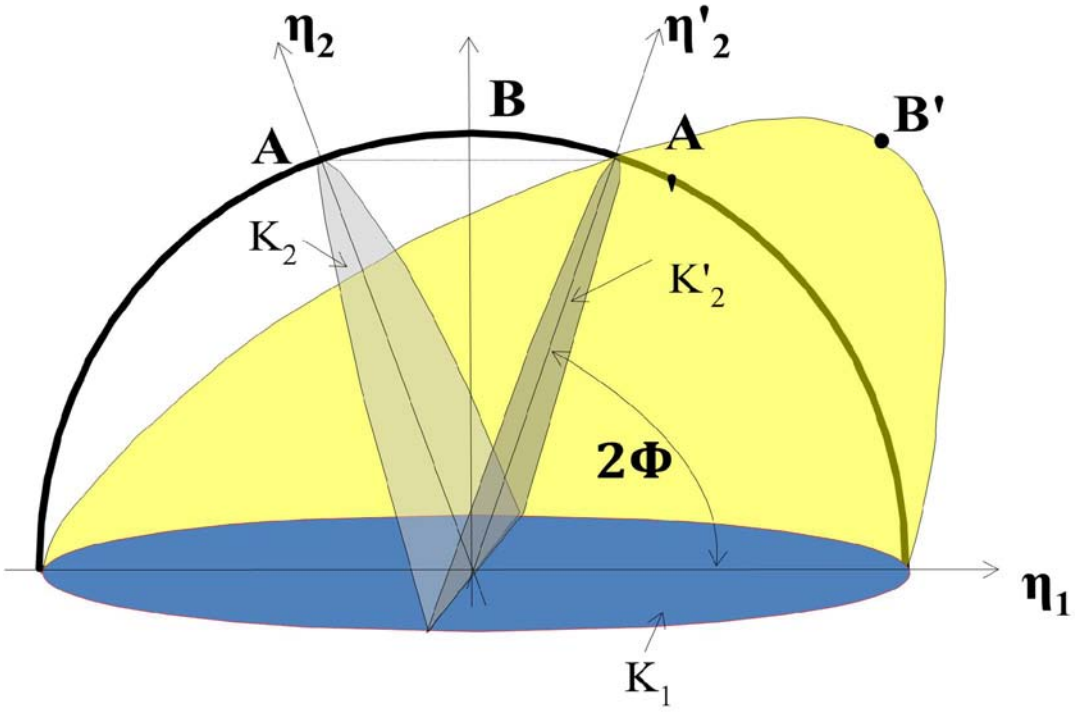

Figure 1-3: The geometry description of twinning shear.

In hexagonal metals, many types of twinning are exhibited, and the type can be related to the c/a ratio of the metal. Generally speaking, the lower c/a ratio, the greater the variety of twinning exhibited.

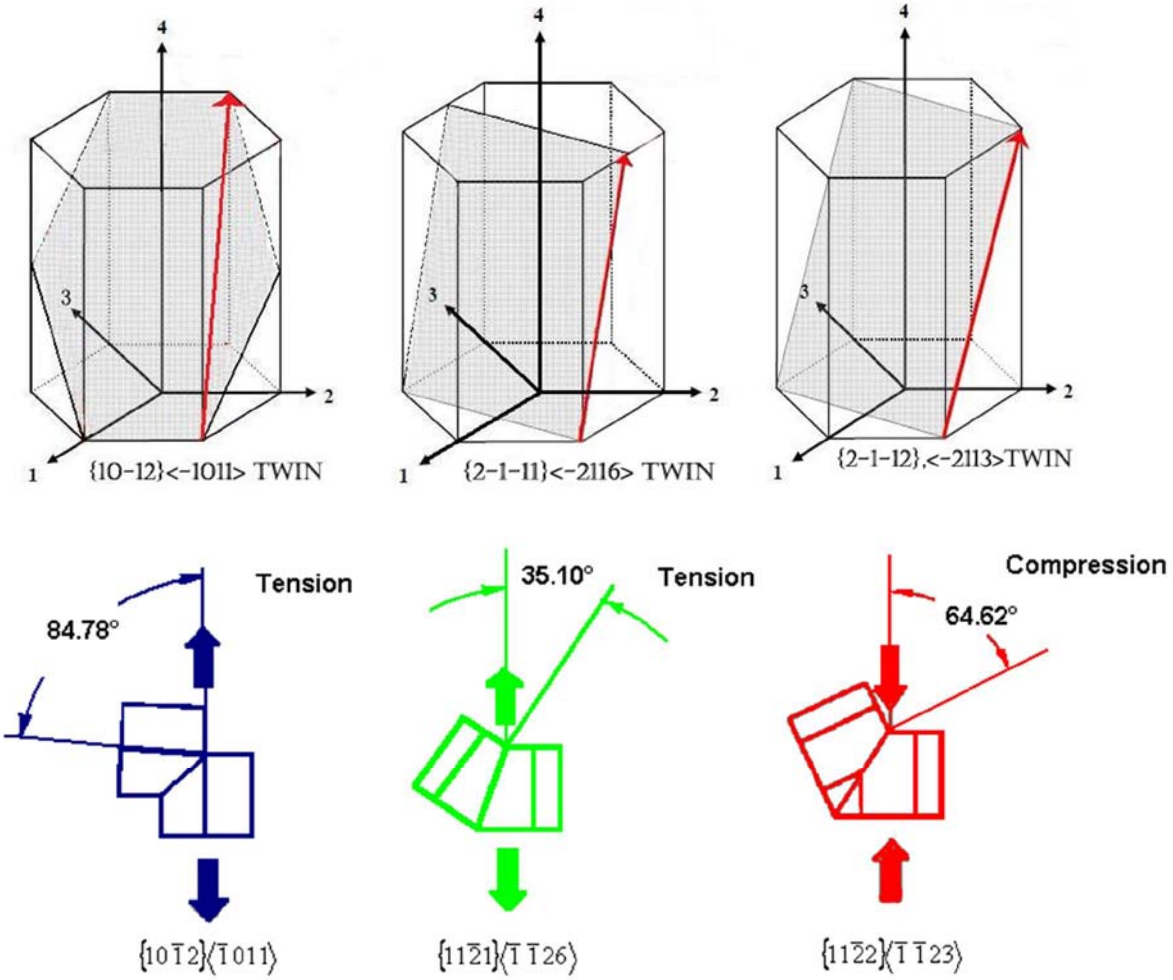

Figure1-4: The {10-12}, {11-21} and {11-22} twins in titanium.

Table 1-1: Types of twinning in hexagonal metals

Metals	c/a	Types of twinning
Cd	1.886	{10-12}
Zn	1.586	{10-12}
Mg	1.624	{10-12}, {11-21}
Zr	1.593	{10-12}, {11-21}, {11-22}
Ti	1.588	{10-12}, {11-21}, {11-22}

The observed type of twinning in hexagonal metals is showed in Table 1-1. Twinning in {10-12} planes occurs in all hexagonal metals, because this twinning has the lowest shear. Titanium, zirconium and hafnium (c/a<1.633) exhibit {10-12} twinning in tension of c axis, {11-22} twinning in compression and in some case, {11-21} twinning in tension (Rosi, Perkins et al. 1956; Chin 1975; Conrad 1981). Magnesium and beryllium (c/a<1.633) shows only {10-12} twinning in tension (Kelley and HOSFORD 1968; Wonsiewicz, Azrin et al. 1972; Mahajan and Williams 1973; Chin 1975). Zinc and Cadmium (c/a>1.633) exhibit {10-12} twinning in compression (Price 1961).

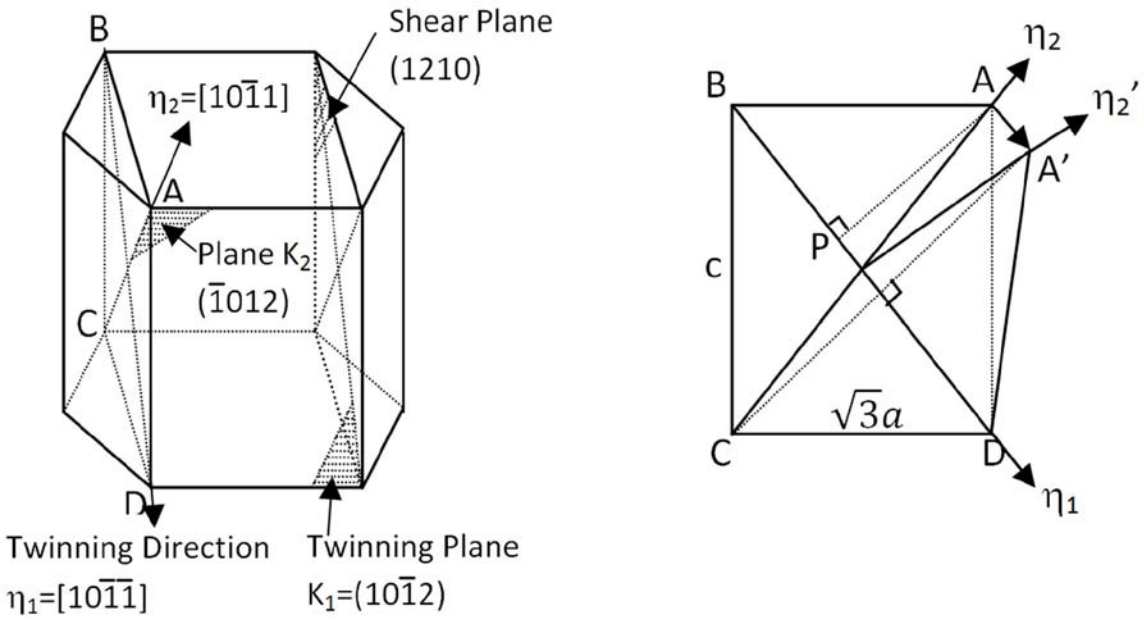

Figure 1-5: Schematic description of twinning in Titanium.

The calculation of shear {10-12} of twinning is illustrated in Figure 1-5, in the schematic figure,

$$AP = \frac{BA \times AD}{BD} = \frac{ac\sqrt{3}}{\sqrt{3a^2+c^2}} \quad \text{1-1}$$

$$AA' = 2OP = \frac{3a^2-c^2}{\sqrt{3a^2+c^2}} \quad \text{1-2}$$

$$S = \frac{AA'}{AP} = \frac{3a^2-c^2}{ac\sqrt{3}} = \frac{3-\gamma^2}{\sqrt{3}\gamma} \quad \text{1-3}$$

Where γ=c/a. The formulas to calculate shear of observed twin mode from (Christian and Mahajan 1995) are given in Table 1-2. The relationship between the shear and the c/a ratio of various types of twinning is illustrated in Figure 1-6. Because the twinning only can provide shear in single direction, the load direction and crystal orientation influence the activation of twinning greatly. The twins with positive slope in Figure 1-6 ({11-22} and {10-11}) only activate under the compression force in the direction of c axis. On the other hand, the twins with negative slope ({10-12} and {11-21}) only activate under the tension force in the direction of c axis.

Table 1-2: Shear of various twin modes [Christian et al. (1995)]

Twin modes	**Shear**
{10-12}<10-1-1>	$(3-\gamma^2)/\sqrt{3}\gamma$
{10-11}<10-1-2>	$(4\gamma^2-9)/4\sqrt{3}\gamma$
{11-21}<11-2-6>	$1/\gamma$
{11-22}<11-2-3>	$\boldsymbol{2(\gamma^2-2)/3\gamma}$

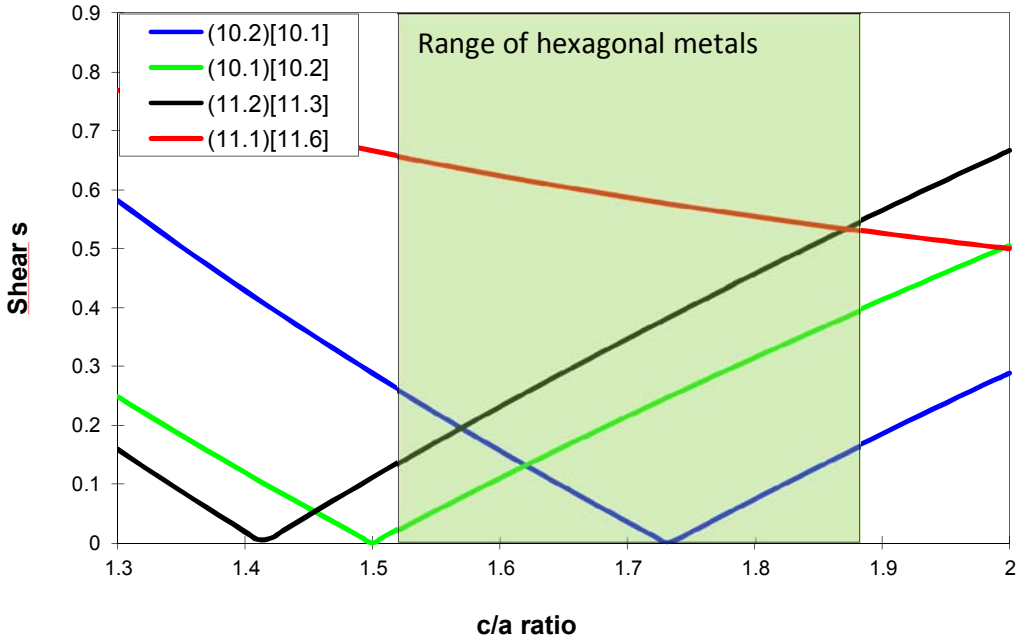

Figure 1-6: The relationship between the shear and the c/a ratio of various types of twinning.

1.2.2 Slip modes

The crystallographic slip is a mechanism that operates in all crystalline materials, metals and metal alloys, calcite or crystalline polymers. This mechanism has already been observed before the twentieth century. Metalworkers observed deformed lines or streaks regular on polycrystals under an optical microscope, and they called them "slip lines". In fact, later observed in the Scanning Electron Microscope, these slip lines were actually steps. The formation of these steps is a direct result of the mechanism of deformation of parts of the crystal (or polycrystal) slide over each other on well defined crystallographic planes (slip systems). This mechanism is due to the movement of dislocations in these slip planes. A dislocation can be

activated when a stress applied to the crystal. Under sufficient stress, the dislocations glide through the crystal. It produces a small displacement (Burgers vector $\vec{b}$) on the surface. When a dislocation slips, the volume of metals remains unchanged, because the shift occurs by shear between parallel planes of the crystal. In the face-centered cubic lattice, the Burgers vectors are in the direction of <110>, and <111> in the bcc. In materials with hexagonal structures, there are several families of slip systems with Burgers vectors of type <a> and <c+a>. A slip system is defined by a glide plane and a direction slip contained in this plan. Table 1-3 and Figure 1-7 below show the different families of slip system operating in hexagonal structures.

Table 1-3: Slip systems in h.c.p. metals

Slip Systems	Slip plane and direction
Basal <a>	{0001}<11-20>
Prismatic <a>	{10-10}<1-210>
Pyramidal <a>	{10-11}<1-210>
Pyramidal <c+a>	{10-11}<11-2-3>
Pyramidal <c+a>	{2-1-12}<-2113>

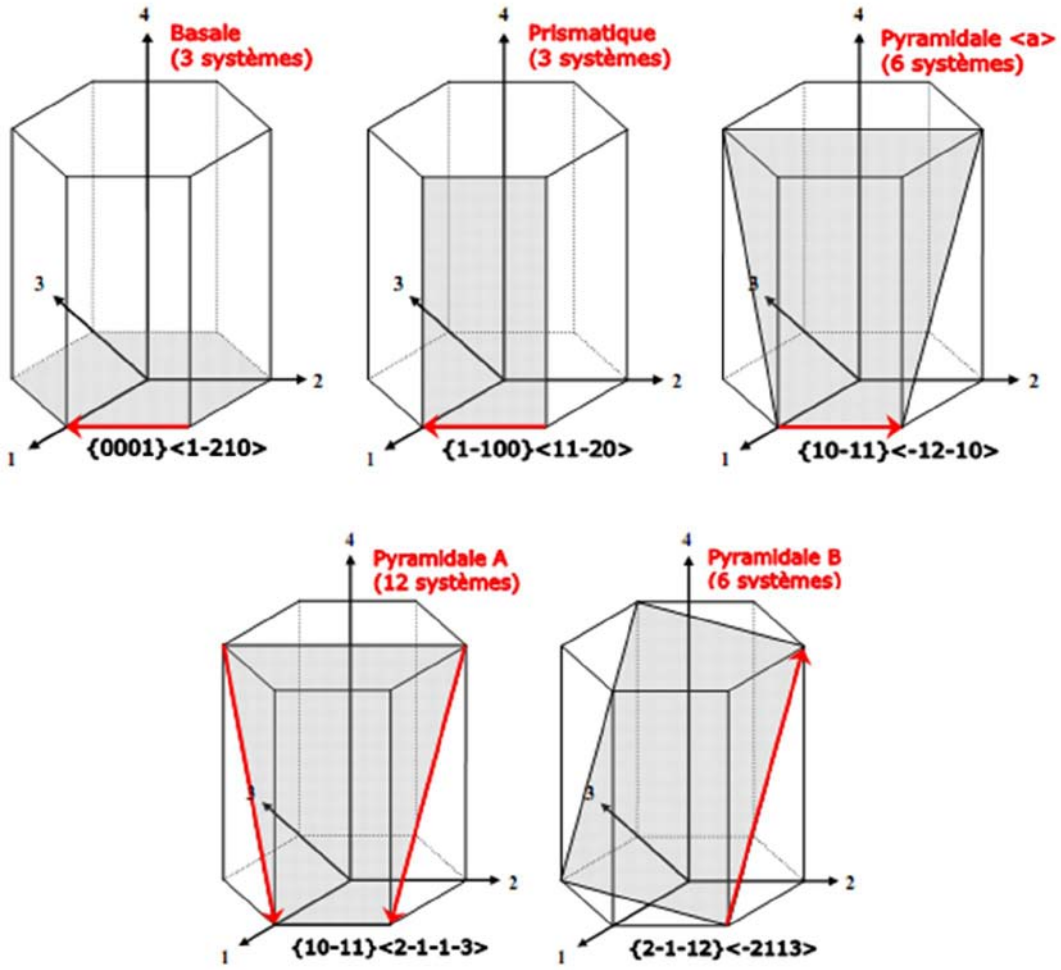

Figure 1-7: The families of slip system operating in hexagonal structures.

2. Hexagonal metals

In this section, we provide a presentation of the main works related to crystal orientation, evolution of texture and different deformation mechanisms in titanium, zirconium, magnesium and zinc.

2.1 Titanium

The plastic deformation in titanium have been studied all the time and especially during rolling (hot and cold). First, it should be mentioned the

published work of Philippe et al. (Philippe, Esling et al. 1988) which reviewed the role of twinning on texture development and plastic deformation of alloys of titanium and zirconium tensile uniaxial, biaxial and rolling, especially highlighted the influence of twinning on the formability. With the help of literature, the analyses were extended to alloy of My, Zn and Be. This work reviewed the conditions for activation of twinning and its effect on the evolution of the texture in various hexagonal materials, and also proved that the modelization of polycrystalline plasticity and texture evolution in hexagonal materials requires an extensive study of the active glide and twinning system by TEM, and taking into account the anisotropy and polarization of possible twinning systems. Koike in 1987 (Koike 1987), Lee et al. (Lee, Esling et al. 1988) and Nourbakhsh et al. (Nourbakhsh and O'Brien 1988) in 1988 did lots of fruitful research in cold rolling. Their results revealed that at low strains, Ti deforms mainly by twinning, whereas at strains > 40%, it deforms solely by slip. Texture measurements indicate that the development of texture in Ti is rapid. Twinning is believed to be responsible for the rapid development of texture and the transitions in texture. The formation of the stable end texture is thought to be due to slip. In 1994, Kailas et al. (Prasad, Biswas et al. 1994) studied the influence of initial texture on the instability of the microstructure of titanium during compression at temperatures between 25 and 400°C. They found that at strain rates $\geq 1\ s^{-1}$, both sets of specimens, in the rolling direction specimens and in the long transverse direction specimens, exhibited adiabatic shear bands, but the intensity of shear bands was found to be higher in the rolling direction specimens than in the long transverse direction specimens. At strain rates $\leq$

$0.1s^{-1}$ the material deformed in a micro structurally inhomogeneous fashion. For the rolling direction specimens, cracking was observed at 100 °C and at strain rates $\leq 0.1\ s^{-1}$. This is attributed to dynamic strain aging. Such cracking was not observed in the long transverse specimens. The differences in the intensity of adiabatic shear bands and that of dynamic strain aging between the two sets of test specimens are attributed to the strong crystallographic texture present in these plates. Subsequently, in 1997, Lebensohn and Canova (Lebensohn and Canova 1997) proposed a self-consistent model to simulate the evolution of texture in titanium and apply to the rolling. This model accounts for crystallographic textures and grain morphologies, as well as for the phase correlation, both in space and orientation. In their experiment, the two phases, (α + β) Ti alloys, exhibit specific morphologic and crystallographic correlations. Their study showed that the model leads to better texture predictions when all these correlations are accounted for. In 1999, Singh et al. (Singh, Bhattacharjee et al. 1999) describe the evolution of texture in titanium alloy Ti-10V-4.5Fe-1.5Al during rolling and annealing. The rolling and re-crystallisation textures obtained in the study are compared with those of other β titanium alloys and bcc metals and alloys such as tantalum and low carbon steel. More recently, Chun et al. in 2005 (Chun, Yu et al. 2005), studied the effect of deformation twinning on microstructure and the evolution of texture during cold rolling. They found that for low to intermediate deformation up to 40% in thickness reduction, the external strain was accommodated by slip and deformation twinning. In this stage, both compressive {11-22} and tensile {10-12} twins, as well as, secondary twins and tertiary twins were activated in the grains of favorable orientation,

and this resulted in a heterogeneous microstructure in which grains were refined in local areas. For heavy deformation, between 60 and 90%, slip overrode twinning and shear bands developed. The crystal texture of deformed specimens was weakened by twinning but was strengthened by slip, resulting in a split-basal texture in heavily deformed specimens. Also in 2005, Bozzolo et al. (Bozzolo, Dewobroto et al. 2005) examined the microstructure and texture in titanium alloy rolled to 80% in order to study the grain enlargement and the effects of dynamic recrystallization. They found that Recrystallization of 80% cold-rolled sheets and subsequent grain growth lead to equiaxed microstructures. The texture obtained at the end of primary recrystallization is very close to that of the cold-rolled state, with the maximum value of the orientation distribution function at {0°, 35°, 0°}. The orientations developing during grain growth correspond to a broad peak centered around {0°, 35°, 30°} which is a minor component in the initial texture. The disappearing orientations are widely scattered throughout orientation space and present two major disadvantages in the growth competition. The grain boundaries remaining after extended grain growth are characterized by an increasing proportion of misorientations below 30° and random rotation axes. In 2001, the work on the behavior of titanium before and after Equal channel angular pressing (ECAP) was made. Stolyarov et al. (Stolyarov, Zhu et al. 2001) interested in the microstructure and properties of ultrafine grain structure in pure titanium past ECAP, which improved mechanical properties: grain size obtained by ECAP alone is about 260 nm. The strength of pure Ti was improved from 380 to around 1000 MPa by the two-step process. It is also reported the microstructures, microhardness,

tensile properties, and thermal stability of these Ti billets processed by a combination of ECAP and cold deformation. In 2002, Shin et al. (Shin, Kim et al. 2002) studied the mechanisms to accommodate the shear induced by titanium in the ECAE. They observed the activity of twinning system and identify them. TEM analysis of the twins revealed that their twin plane is {10-11} and the twins are accompanied with dislocations on non-basal planes. These results suggest that the severe plastic deformation imposed on titanium via ECA pressing is accommodated mainly by the {10-11} twinning, rather than dislocation slips commonly observed in pressing of other metals such as aluminum and steel. The twinning modes that might accommodate the severe strain were proposed based on the dislocation slip systems observed during the pressing. In 2003, Kim et al. also observed deformation twinning in pure titanium during ECAE by means of EBSD measurements. In 2003, Shin et al. (Shin, Kim et al. 2003) analyzed the microstructure of titanium samples after ECAE. They highlight the twinning systems and ensure slip deformation. Transmission electron microscopy (TEM) revealed that the strain imposed by pressing was accommodated mainly by {10-11} deformation twinning. During the second pass, the deformation mechanism changed to dislocation slip on a system which depended on the specific route. For route C (in which the shear is fully reversed during successive passes by 180° rotation of the sample between passes), prism (a) and pyramidal (c+a) slip occurred within alternating twin bands. For route B (in which the sample is rotated 90° after the first pass), prism a slip was the main deformation mechanism. For route A (in which the billet is not rotated between passes), deformation was controlled by basal a slip and micro-twinning in alternating

twin bands. They indicated that the variation in deformation behavior was interpreted in terms of the texture formed during the first pass and the Schmid factors for slip during subsequent deformation. More recently, in 2006, Perlovich et al. (Perlovich, Isaenkova et al. 2006) studied the titanium rods after ECAE at 200°C and 400°C, and they found heterogeneity of deformation, microstructures and textures through the thickness of stem. More generally in 2001, Bache and Evans (Bache and Evans 2001), proposed a study on the influence of texture on the mechanical properties of a titanium alloy. They had the conclusions that highly textured, uni-directionally rolled Ti 6/4 plate demonstrates significantly different in monotonic strength characteristics according to the direction of the principal stress relative to the predominant basal plane texture. Loading in the transverse orientation, perpendicular to basal planes preferentially lying co-incident with the longitudinal-short transverse plane, promotes a relatively high yield stress and ultimate tensile strength (UTS). Under strain controlled fatigue loading, the longitudinal orientation was found to offer the optimum cyclic response. The differences in mechanical behavior have been related to the ability to induce slip in the various plate orientations. In addition, stress relaxation is encouraged under cyclic loading parallel to the longitudinal direction due to the preferential arrangement of {10-10} prismatic planes. In 2003, Zaefferer (Zaefferer 2003) studied the activity of deformation mechanisms in different titanium alloys and its dependence with regard to their compositions. The main results are: in TiAl6V4, <a> basal slip has a lower critical resolved shear stress, τ_c, than prismatic slip. <c+a> pyramidal glide shows a very high τ_c, which is up to two times larger than that for prismatic slip. Nevertheless,

<c+a> glide systems were only rarely activated and twinning systems were never activated. Therefore, deformation with c-components may be accommodated by β-phase deformation or grain boundary sliding. The observed c-type texture is due to the strong basal glide. In T40, τ_c for <c+a> glide is up to 13 times higher than that for prismatic glide. However, <c+a> glide and twinning were strongly activated, leading to the observed t-type texture. In T60, the high oxygen content completely suppressed twinning and strongly reduced <c+a> glide. The less developed t-type texture is due to the combination of <c+a> and basal glide. In 2007, Wu et al. (Wu, Kalidindi et al. 2007) simulate the evolution of texture as well as the behavior of titanium during large plastic deformations. A new crystal plasticity model has been formulated to simulate the anisotropic stress–strain response and texture evolution for α-titanium during large plastic strains at room temperature. The major new features of the model include: (i) incorporation of slip inside twins as a significant contributor to accommodating the overall imposed plastic deformation; and (ii) extension of slip and twin hardening laws to treat separately the hardening behavior of the different slip families (prismatic <a>, basal <a> and pyramidal <c + a>) using hardening parameters that are all coupled to the extent of deformation twinning in the sample. Reasonable agreement between model predictions and experimental measurements has been observed for both the anisotropic stress–strain responses and the evolved deformation textures in three different monotonic deformation paths: (1) simple compression along ND; (2) simple compression along TD; and (3) simple shear in the RD–TD plane.

2.2 Zirconium

In 1991, Tomé et al. (Tome, Lebensohn et al. 1991) propose a new method for modeling grain reorientation due to twinning, they deal with tension and compression in zirconium alloys. This new model, called “Volume Transfer Scheme”, a part of the volume of the crystal transferred to the twinned position directly in the Euler space. Their model predicts the evolution of texture more accurately than traditional models when the twinning is the predominant mechanism of deformation. However, the disadvantage of this model is that you cannot take into account the work hardening. In 1993, Lebensohn et al. (Lebensohn and Canova 1997) present an approach anisotropic viscoplastic self-consistent model for the plastic deformation of polycrystals. This approach is different from that presented earlier by Molinari et al. in his formulation 'stiffness'. The self-consistent model is particularly suitable for highly anisotropic materials such as hexagonal. The authors applied their model to predict the evolution of texture in rolled zirconium and get better results after compared their prediction with experiments. In 1994 and 1995, Philippe et al. (Philippe, Wagner et al. 1994) propose a model of the evolution of texture in hexagonal materials. The authors describe a first step in the evolution of texture and microstructure during cold rolling in zinc, subsequently, Philippe et al. (Philippe, Serghat et al. 1995) extended their studies to titanium and zirconium, taking both the sliding plastic modeling and also twinning into account. The authors performed simulations using models of Sachs and Taylor and compared their results to the available literature. Fortunately, the simulation results were in good agreement with the experiments for reductions between 0 and 80%

reduction. In 1998, et al. (Francillette, Castelnau et al. 1998) performed "channel die" compression tests on polycrystalline zirconium at room temperature, at the plastic deformation of 40%. They tested 5 samples with different initial texture. They simulated the evolution of texture using a crystal plasticity model of self-consistent, the simulation agreed with experiments very well. In 2000, Kaschner and Gray (Kaschner and Gray 2000) studied the influence of texture on the mechanical behavior of zirconium. They evaluate the response of the material in compression according to the predominant orientation of the c-axis of the hexagonal mesh for several test temperatures and strain rate. They found that the compressive-yield responses of both high-purity (HP) crystal-bar and lower-purity (LP) zirconium depend on the loading orientation relative to the c-axis of the hcp cell, the applied strain rate, which varied between 0.001 and 3500 s^{-1}, and the test temperature, which varied between 77 and 298 K. The rate of strain hardening in zirconium was seen to depend on the controlling defect-storage mechanism as a function of texture, strain rate, and temperature. The substructure evolution of HP zirconium was also observed to be a function of the applied strain rate and test temperature. The substructure of HP zirconium was seen to display a greater incidence of deformation twinning when deformed at a high strain rate at 298 K or at 77 K. In 2001, Sanchez et al. (Sanchez, Pochettino et al. 2001) conduct twist tests at high temperature on zirconium alloys in order to study the evolution of the texture. They compared experimental results with those obtained by a self-consistent viscoplastic model and obtain reasonable results. They exhibited particularly that the basal and prismatic slips are necessary to reproduce the main

features of the evolution of texture, and pyramidal slip has little activity in the zirconium. Kim et al. (Kim, Joo et al. 2003) conducted ECAP on pure zirconium to refine the microstructure. They reduce the grain size to 0.2μm without fracture of the material by the imposition of severe plastic straining via ECAP. The results showed that grain size decreased and misorientation between grains increased with increasing number of ECAP passes, using processing route in which the specimen was rotated by 90° in the same direction between each consecutive pass through the ECA pressing die. In 2004, Dewobroto et al. (Dewobroto, Bozzolo et al. 2004) studied the microstructure and texture at different stages of primary recrystallization in sheets zirconium Zr702 previously reduced to 80% by cold rolling. They showed that the new grains after recrystallization have no preferred orientation during static recrystallization, which is due to the growth of sub-grains in the Zr. They considered that, since the global texture change is very slight, recrystallization by subgrain growth is probably one of the most important mechanism during the recrystallization process in zirconium. In 2005, Yu et al. (Yu, Chun et al. 2005) compared textures and microstructures in the zirconium obtained partly by ECAP with them by cold rolling, and they found that ECAP transformed the initial fiber texture to a quite different component, which was also the case for cold rolling. In both cases, the maximum intensity of texture increased with the amount of deformation. Complete recrystallization was realized upon subsequent heat treatment lasting 100 min. at 600°C, and the evolution characteristics of texture and microstructure were also similar for both modes of deformation. These similarities in the microstructure and texture were attributed to the

particular route of ECAP employed in the present study, i.e., route A (in which the billet is not rotated between passes). It is therefore concluded that the deformation and annealing behaviors in this particular route of ECAP are essentially very close to those of cold rolling. In 2006, Perlovich et al. (Perlovich, Isaenkova et al. 2006) examined the evolution of texture in zirconium deformed by ECAE (route B (in which the sample is rotated 90° after the first pass) and C (in which the shear is fully reversed during successive passes by 180° rotation of the sample between passes)) at 350 ° C in a detailed X-ray. The data analysis is based on conceptions of the texture formation theory, connecting features of grain reorientation with activated deformation mechanisms. They note that A degree of reproduction of the same distinctive texture by successive ECAP passes with antecedent rotation of the rod reflects attendant structure changes in material, i.e., the textures have obtained a high degree of similarity of a pass to another. McCabe et al. (McCabe, Cerreta et al. 2006) studied the effects of texture, temperature and deformation on the deformation mechanisem in zirconium during rolling. Orientation imaging microscopy in a scanning electron microscope and defect analysis via transmission electron microscopy are used to characterize the defect microstructures as a function of initial texture, deformation temperature and plastic strain. Finally, they found that the observed deformation mechanisms are correlated with measured mechanical response of the material.

2.3 Magnesium

In this section, we propose a review of literature on textures and their evolution in magnesium. In 2000, Kaneko et al. (Kaneko, Sugamata et al. 2000)

examined the effect of texture on the mechanical properties of AZ31 magnesium. They found that strong texture is observed in magnesium wrought materials in which the basal plane is oriented parallel to the extrusion or rolling direction. As a result, tensile strength of magnesium wrought materials increased by 15 to 20% due to texture hardening at room temperature. The AZ31 alloy sheet is highly anisotropic at room temperature with high r-value above 4, resulting that forming limits in biaxial tension are much lower than those in uniaxial tension. However, this anisotropy decreases with increasing forming temperature and no texture hardening is found at 473 K. In this respect, formability of magnesium alloys sheets in terms of Erichsen and conical cup values is remarkably poor at room temperature but appreciably improves with increasing temperature. Sheet forming of magnesium alloys is practically possible only at the high temperature range where plastic anisotropy disappears. In 2006, Yi et al. (Yi, Davies et al. 2006(Yi, Davies et al. 2006) studied the behavior of magnesium alloy AZ31 under a uniaxial loading (tension and compression). The specimens were cut at 0°, 45° and 90° to the direction of extrusion. They highlight the various modes of deformation acting under the direction of the initial texture. They found that the activity of the basal <a> slip and the tensile twinning exert a significant effect on the mechanical anisotropy during tension, while the importance of the <c + a> slip increases during compression. Helis et al. (Helis, Okayasu et al. 2006) studying the development of texture in the AZ31 for the uniaxial compression at different temperatures and strain rates. Fiber texture was formed in all of the deformation conditions. The main component of the texture varied

depending on deformation conditions; it appeared about 33-38° away from the basal pole after the deformation at higher temperatures and lower strain rates. This can be attributed to the increased activity of the secondary pyramidal slip system. With a decrease in temperatures and an increase in strain rate, the tilting angle of the main component (compression plane) from the basal pole decreased down to about 20°. Construction of a basal fiber texture was detected after deformations at the lowest temperature and high strain rates. In 2005, Kim et al. (Kim, You et al. 2005) studied the texture evolution in AZ31 in asymmetrical rolling. They found that asymmetrically hot rolled AZ31 magnesium alloy sheets exhibited a texture gradient, where the intensity of {0002} basal textures decreased from the upper surface through the center to the lower surface. After subsequent annealing, the intensity of {0002} components was reduced significantly throughout the thickness and the grains were refined possibly by discontinuous recrystallization. Al-Samman et al. (Al-Samman and Gottstein 2005) evaluated the influence of initial texture on one pass hot rolling to different final thicknesses of 5%, 10%, 30%, 50%, 70%, and 90% at 400 ° C in magnesium. The microstructure and macrotexture evolution were examined by optical microscopy (OM) and X-ray diffraction, respectively. Further, microtexture analysis was done by EBSD. Texture modelling with LAPP using an FC Taylor model, based on the expected active slip and twinning modes was performed. The results were compared with the measured textures and obtained a good agreement. Brown et al. (Brown, Agnew et al. 2005) measured in-situ neutron diffraction of a twinned microstructure in rolled magnesium. They observed that 80% of the matrix microstructure is twinned at 8% compression. They found that

elastic lattice strain measurements indicate that the stress in the newly formed twins (daughters) is relaxed relative to the stress field in the surrounding matrix. However, since the daughters are in a plastically “hard” deformation orientation, they quickly accumulate elastic strain as surrounding grains deform plastically. Polycrystal modeling of the deformation process provides insight about the crystallographic deformation mechanism involved. Singh et al. (Singh and Schwarzer 2005) describes the development of texture in cast pure magnesium during unidirectional rolling, multi-step reverse rolling and multi-step cross rolling at different temperatures. And they found that the unidirectionally and the multi-step reverse hot-rolled plates exhibit mainly an asymmetric R-type texture with basal-pole split. In 2006, Watanabe et al. (Watanabe, Mukai et al. 2007) studied the texture evolution in AZ31 magnesium and ductility in different conditions of rolling symmetrical. They found that the strain rate was inversely proportional to the square of the grain size and to the second power of stress. The activation energy was close to that for grain boundary diffusion at 523-573 K, and was close to that for lattice diffusion at 598-673 K. From the analysis of the stress exponent, the grain size exponent and activation energy, it was suggested that the dominant diffusion process was influenced by temperature and grain size. It was demonstrated that the notion of effective diffusivity explained the experimental results. In 2005, Hartig et al. (Hartig, Styczynski et al. 2005) measured the texture of the rolled AZ31 and perform simulations by the crystal plasticity model self-consistent viscoplastic. They considered that anisotropy of plastic flow stresses can be explained by the off-basal character of the texture and the activation of the

prismatic slip in addition to the basal, pyramidal slip and the (01-1-2) <011-1> twinning system, discussed the results obtained by comparing the simulation with the experience. Gehrmann et al. (Gehrmann, Frommert et al. 2005) studied the texture on the plastic deformation of magnesium AZ31 in compression flat at 100 and 200 ° C. The measured flow curves and the microstructure investigation reveal that plastic deformation of magnesium at these temperatures is generally inhomogeneous and dominated by the appearance of shear bands. However, if the initial texture is chosen such that the formation of a basal texture is slowed down or even suppressed, substantial ductility can be achieved at temperatures as low as 100 °C. The texture development due to crystallographic slip can be reasonably modelled by a relaxed constraints Taylor simulation and yields information on the activated slip systems. Walde et al. (Walde and Riedel 2005; Walde and Riedel 2007) simulated the texture evolution during rolling of AZ31 with finite element code ABAQUS / Explicit, in which they have implemented a model self-consistent viscoplastic. This model is able to describe the softening behavior of the magnesium alloy AZ31 during hot compression and allows us to simulate the development of the typical basal texture during hot rolling of this alloy. Their simulations are quite consistent with experimental measurements of texture.

3. References

Al-Samman, T. and G. Gottstein (2005). "Influence of starting textures on the development of texture and microstructure during large strain hot rolling of pure magnesium." Solid State Phenomena **105**: 201-206.

Bache, M. and W. Evans (2001). "Impact of texture on mechanical properties in an advanced titanium alloy." Materials Science and Engineering A **319**: 409-414.

Barrett, C. and T. Massalski (1966). Structure of metals, New York: McGraw-Hill.

Bozzolo, N., N. Dewobroto, et al. (2005). "Texture evolution during grain growth in recrystallized commercially pure titanium." Materials Science and Engineering A **397**(1-2): 346-355.

Brown, D., S. Agnew, et al. (2005). "Internal strain and texture evolution during deformation twinning in magnesium." Materials Science and Engineering: A **399**(1-2): 1-12.

Chin, G. (1975). "On the microstructure of extruded rods and drawn wires of beryllium." Metallurgical and Materials Transactions A **6**(1): 238-240.

Christian, J. W. (1965). The theory of transformation in metals and alloys, Pergamon Press, Oxford.

Christian, J. W. and S. Mahajan (1995). "Deformation twinning." Progress in Materials Science **39**(1-2): 1-157.

Chun, Y. B., S. H. Yu, et al. (2005). "Effect of deformation twinning on microstructure and texture evolution during cold rolling of CP-titanium." Materials Science and Engineering A **398**(1-2): 209-219.

Conrad, H. (1981). Mechanisms of fatigue in metals under coal liquefaction conditions, North Carolina State Univ., Raleigh (USA). Dept. of Materials Engineering. **26:** 199-210.

Dewobroto, N., N. Bozzolo, et al. (2004). Experimental investigations of recrystallization texture development in Zirconium (Zr702), Trans Tech Publ.

Francillette, H., O. Castelnau, et al. (1998). Experimental and predicted texture evolutions in zirconium alloys deformed in channel die compression, Trans Tech Publ.

Gehrmann, R., M. M. Frommert, et al. (2005). "Texture effects on plastic deformation of magnesium." Materials Science and Engineering A **395**(1-2): 338-349.

Hartig, C., A. Styczynski, et al. (2005). Plastic anisotropy and texture evolution of rolled AZ31 magnesium alloys, Trans Tech Publ.

Helis, L., K. Okayasu, et al. (2006). "Microstructure evolution and texture development during high-temperature uniaxial compression of magnesium alloy AZ31." Materials Science and Engineering: A **430**(1-2): 98-103.

Hume-Rothery, W. and G. V. Raynor (1962). The structure of metals and alloys, Institute of metals.

Kaneko, J., M. Sugamata, et al. (2000). "Effect of texture on the mechanical properties and formability of magnesium wrought materials." Nippon Kinzoku Gakkaishi **64**(2): 141-147.

Kaschner, G. and G. Gray (2000). "The influence of crystallographic texture and interstitial impurities on the mechanical behavior of zirconium." Metallurgical and Materials Transactions A **31**(8): 1997-2003.

Kelley, E. and W. HOSFORD (1968). "The deformation characteristics of textured magnesium." TRANS MET SOC AIME **242**(4).

Kim, H. S., D. H. Joo, et al. (2003). "Grain refinement of commercial purity zirconium by equal channel angular pressing." Materials science and technology **19**(3): 403-405.

Kim, S. H., B. S. You, et al. (2005). "Texture and microstructure changes in asymmetrically hot rolled AZ31 magnesium alloy sheets." Materials Letters **59**(29-30): 3876-3880.

Koike, M. (1987). "Hot-rolling texture in titanium sheet." Tetsu to Hagane-Journal of the Iron and Steel Institue of Japan **73**.

Lebensohn, R. A. and G. R. Canova (1997). "A self-consistent approach for modelling texture development of two-phase polycrystals application to titanium alloys." Journal Name: Acta Materialia; Journal Volume: 45; Journal Issue: 9; Other Information: PBD: Sep 1997: 3687-3694.

Lee, H., C. Esling, et al. (1988). "Development of rolling texture in titanium." Textures and Microstructures **7**: 317-337.

Mahajan, S. and D. F. Williams (1973). "Deformation twinning in metals and alloys." International Metallurgical Reviews **18**: 43-61.

McCabe, R., E. Cerreta, et al. (2006). "Effects of texture, temperature and strain on the deformation modes of zirconium." Philosophical Magazine **86**(23): 3595-3611.

Nourbakhsh, S. and T. D. O'Brien (1988). "Texture formation and transition in Cold-rolled titanium." Materials Science and Engineering **100**: 109-114.

Perlovich, Y., M. Isaenkova, et al. (2006). Features of texture and structure development in zirconium under equal channel angular pressing, Trans Tech Publ.

Philippe, M. J., C. Esling, et al. (1988). "Role of Twinning in Texture Development and in Plastic Deformation of Hexagonal Materials." Textures and Microstructures **7**: 265-301.

Philippe, M. J., M. Serghat, et al. (1995). "Modelling of texture evolution for materials of hexagonal symmetry--II. application to zirconium and titanium [alpha] or near [alpha] alloys." Acta Metallurgica et Materialia **43**(4): 1619-1630.

Philippe, M. J., F. Wagner, et al. (1994). "Modelling of texture evolution for materials of hexagonal symmetry--I. Application to zinc alloys." Acta Metallurgica et Materialia **42**(1): 239-250.

Prasad, Y., S. Biswas, et al. (1994). Influence of Initial Texture on the Microstructural Instabilities During Compression of Commercial Alpha-Titanium at 25 Degrees to 400 Degrees INDIAN INST OF SCIENCE BANGALORE.

Price, P. (1961). "On dislocation loops formed in zinc crystals during low temperature pyramidal glide." Philosophical Magazine **6**: 449-451.

Reed-Hill, R. E. and R. Abbaschian (1964). "Physical metallurgy principles."

Rosi, F. D., F. C. Perkins, et al. (1956). "Mechanism of plastic flow in titanium at low and high temperatures." J. Metals; Journal Volume **8**: 115-122.

Sanchez, P., A. Pochettino, et al. (2001). "Torsion texture development of zirconium alloys." Journal of Nuclear Materials **298**(3): 329-339.

Schmid, E. and W. Boas (1950). "Plasticity of Crystals, FA Hughes and Co." Ltd, London: 271–277.

Shin, D., I. Kim, et al. (2003). "Microstructure development during equal-channel angular pressing of titanium." Acta Materialia **51**(4): 983-996.

Shin, D. H., I. Kim, et al. (2002). "Shear strain accommodation during severe plastic deformation of titanium using equal channel angular pressing." Materials Science and Engineering A **334**(1-2): 239-245.

Singh, A., A. Bhattacharjee, et al. (1999). "Microstructure and texture of rolled and annealed [beta] titanium alloy Ti-10V-4.5 Fe-1.5 Al." Materials Science and Engineering A **270**(2): 225-230.

Singh, A. and R. Schwarzer (2005). "Evolution of texture in pure magnesium during rolling." Zeitschrift für Metallkunde **96**(4): 345-351.

Stolyarov, V. V., Y. T. Zhu, et al. (2001). "Microstructures and properties of ultrafine-grained pure titanium processed by equal-channel angular pressing and cold deformation." Journal of Nanoscience and Nanotechnology **1**(2): 237-242.

Taylor, A. (1961). X-ray Metallography, Wiley.

Tome, C., R. Lebensohn, et al. (1991). "A model for texture development dominated by deformation twinning: application to zirconium alloys." Acta Metallurgica et Materialia **39**(11): 2667-2680.

Walde, T. and H. Riedel (2005). "Modeling texture evolution during rolling of magnesium alloy AZ31." Solid State Phenomena **105**: 285-290.

Walde, T. and H. Riedel (2007). "Modeling texture evolution during hot rolling of magnesium alloy AZ31." Materials Science and Engineering: A **443**(1-2): 277-284.

Watanabe, H., T. Mukai, et al. (2007). "Effect of temperature of differential speed rolling on room temperature mechanical properties and texture in an AZ31 magnesium alloy." Journal of materials processing technology **182**(1-3): 644-647.

Wonsiewicz, B., M. Azrin, et al. (1972). "Analysis of local necking in a biaxially stretched sheet." Metallurgical and Materials Transactions B **3**(5): 1322-1324.

Wu, X., S. R. Kalidindi, et al. (2007). "Prediction of crystallographic texture evolution and anisotropic stress-strain curves during large plastic strains in high purity [alpha]-titanium using a Taylor-type crystal plasticity model." Acta Materialia **55**(2): 423-432.

Yi, S. B., C. Davies, et al. (2006). "Deformation and texture evolution in AZ31 magnesium alloy during uniaxial loading." Acta Materialia **54**(2): 549-562.

Yu, S., Y. Chun, et al. (2005). "Comparison of equal channel angular pressing and cold rolling in the evolution of microstructure and texture in zirconium." Metals and Materials International **11**(2): 101-111.

Zaefferer, S. (2003). "A study of active deformation systems in titanium alloys: dependence on alloy composition and correlation with deformation texture." Materials Science and Engineering A **344**(1-2): 20-30.

Chapter 2: Materials, Equipment and Techniques

This chapter is devoted to introducing the materials, samples preparation, equipment and experimental techniques used in the present work, especially the SEM/EBSD technique and analysis. Then, we provide a detailed description of the interrupted "in situ" experiment arrangement used in rolling and channel die compression tests.

1. Materials and samples preparation

1.1 Materials

The as-received material was hot-rolled and then annealed commercial pure titanium sheet (mean grain size is 10 μm) of 1.5 mm thickness with the composition given in table 2-1.

Table Ⅱ-1: Chemical composition of commercially pure titanium T40

Elements	H	C	N	O	Fe	Ti
Composition ppm (wt.)	3	52	41	1062	237	Balance

1.2 Heat treatment

In order to obtain a coarse grain microstructure with equiaxed grains, a grain growth annealing was performed on so some samples at 800°C for 2 hours, and then the grain had grown to 200 μm after the annealing treatment.

1.3 Samples preparation

The samples were firstly mechanically polished with silicon carbide sandpaper (600#, 1200#, 2400# until 4000# sandpaper (Struers standard)) and then electrolytically-polished in a solution of 200 ml perchloric acid in 800 ml methanol at 17V (30 seconds) at a temperature of 20°C .

2. Electron Back Scattered Diffraction (EBSD)

This part introduces our most important experimental methods and equipment -Electron Back Scattered Diffraction (EBSD) in detail. We will

explain how an EBSD system works, describes the experiments that can be performed and how to undertake them, and finally outlines the basic crystallography needed for EBSD.

In this work, A Field emission JEOL-6500F FEG-SEM with EBSD camera and HKL CHANNEL5 software is used to perform EBSD measurement and analysis.

HKL CHANNEL5 uses a modular approach to its various. All software modules interact seamlessly with one another and form a powerful and expressive suite with which to perform microstructural characterization. Therefore the HKL CHANNEL5 Flamenco allows image collection, versatile EBSD analysis and phase identification all within a single program.

2.1 Introduction

EBSD is a technique which allows crystallographic information to be obtained from samples in the scanning electron microscope (SEM). In EBSD a stationary electron beam strikes a tilted crystalline sample and the diffracted electrons form a pattern on a fluorescent screen. This pattern is characteristic of the crystal structure and orientation of the sample region from which it was generated. The diffraction pattern can be used to measure the crystal orientation, measure grain boundary misorientations, discriminate between different materials, and provide information about local crystalline perfection. When the beam is scanned in a grid across a polycrystalline sample and the crystal orientation measured at each point, the resulting map will reveal the constituent grain morphology, orientations, and boundaries. This data can also be used to show the preferred crystal

orientations (texture) present in the material. A complete and quantitative representation of the sample microstructure can be established with EBSD.

2.2 Basics of EBSD

The principal components of an EBSD system are shown in Figure2-1, which includes a phosphor screen which is fluoresced by electrons from the sample to form the diffraction pattern, a sensitive charge coupled device (CCD) video camera for viewing the diffraction pattern on the phosphor screen. And a computer to control EBSD experiments, analyze the diffraction pattern and process and display the results.

For EBSD, a beam of electrons is directed at a point of interest on a tilted crystalline sample in the SEM. The mechanism by which the diffraction patterns are formed is complex, but the following model describes the principal features. The atoms in the material inelastically scatter a fraction of the electrons, with a small loss of energy, to form a divergent source of electrons close to the surface of the sample. Some of these electrons are incident on atomic planes at angles which satisfy the Bragg equation:

$$n\lambda = 2d \sin\theta \qquad 2\text{-}1$$

where n is an integer, λ is the wavelength of the electrons, d is the spacing of the diffracting plane, and θ is the angle of incidence of the electrons on the diffracting plane. These electrons are diffracted to form a set of paired large angle cones corresponding to each diffracting plane. When used to form an image on the fluorescent screen, the regions of enhanced electron

intensity between the cones produce the characteristic Kikuchi bands of the electron back scattered diffraction pattern.

The center lines of the Kikuchi bands correspond to the intersection of the diffracting planes with the phosphor screen. Hence, each Kikuchi band can be indexed by the Miller indices of the diffracting crystal plane which formed it. The intersections of the Kikuchi bands correspond to zone axes in the crystal and can be labeled by zone axis symbols. The semi-angle of the diffracted cones of electrons is (90 - θ) degrees. For EBSD this is a large angle so the Kikuchi bands approximate to straight lines. The width ω of the Kikuchi bands close to the pattern center is given by:

$$\omega \approx {}^{2}/_{\theta} \approx \frac{n/\lambda}{d} \qquad 2\text{-}2$$

In Figure 2-2, l is the distance from the sample to the screen. Hence, planes with wide d-spacings give thinner Kikuchi bands than narrow planes. Because the diffraction pattern is bound to the crystal structure of the sample, as the crystal orientation changes the resultant diffraction pattern also changes. The positions of the Kikuchi bands can therefore be used to calculate the orientation of the diffracting crystal.

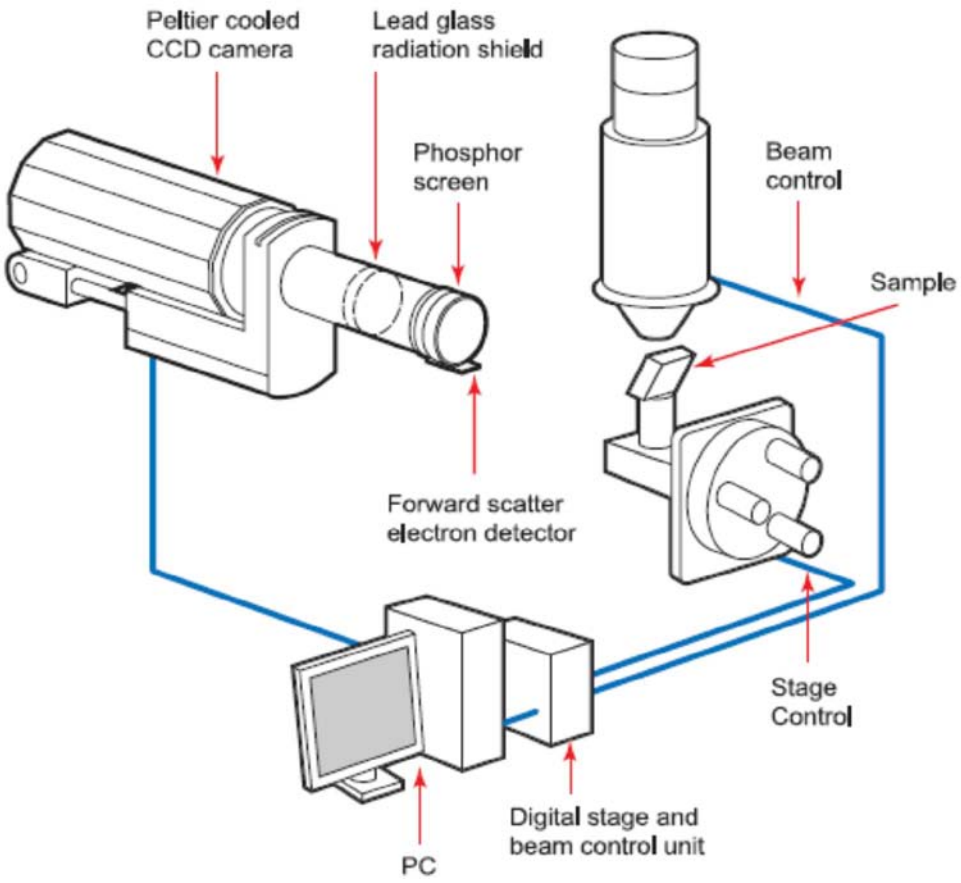

Figure 2-1: Components of an EBSD system.

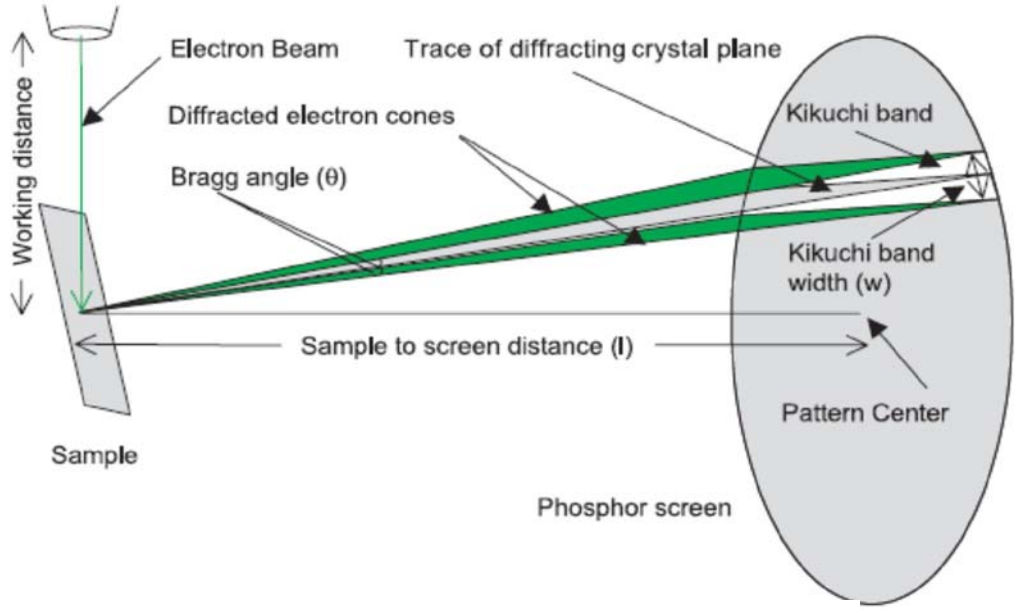

Figure 2-2: EBSD geometry.

The crystal orientation is calculated from the Kikuchi band positions by the computer processing the digitized diffraction pattern collected by the CCD camera. The Kikuchi band positions are found using the Hough transform. The transform between the coordinates (*x, y*) of the diffraction pattern and the coordinates (ρ,θ) of Hough space is given by:

$$\rho = x\cos\theta + y\sin\theta \qquad 2\text{-}3$$

A straight line is characterized by ρ, the perpendicular distance from the origin and θ the angle made with the x-axis and so is represented by a single point (ρ,θ) in Hough space. Kikuchi bands transform to bright regions in Hough space which can be detected and used to calculate the original positions of the bands. Using the system calibration, the angles between the planes producing the detected Kikuchi bands can be calculated. These are compared with a list of inter-planar angles for the analyzed crystal structure to allocate Miller indices to each plane. The final step is to calculate the orientation of the crystal lattice with respect to coordinates fixed in the sample. His whole process takes less than a few milliseconds with modern computers.

2.3 Basic crystallography for EBSD

2.3.1. Crystal orientation

A crystal orientation is measured with respect to an orthogonal coordinate system fixed in the sample. The sample system is normally aligned with

directions used in texture measurements on rolled sheet materials. The x axis is parallel to the rolling direction of the sample (RD), the y axis parallel to the transverse direction (TD) and the z axis parallel to the normal direction (ND) (Figure 2-3).

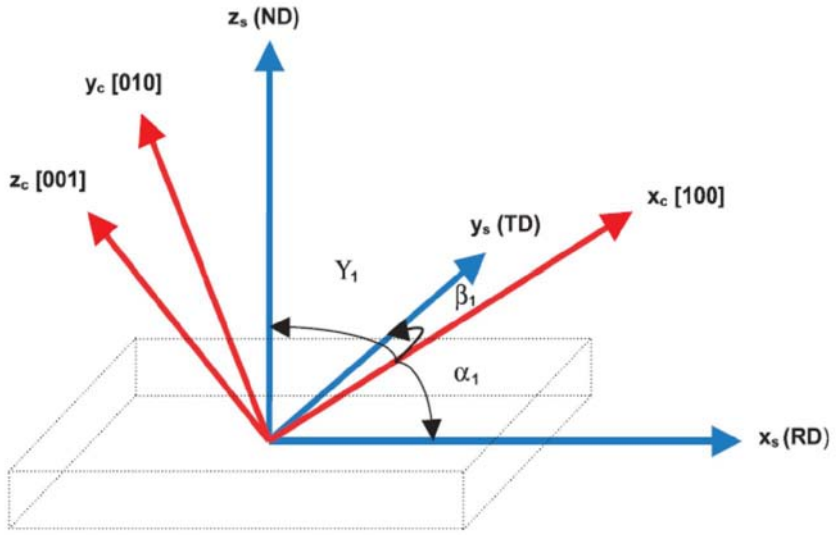

Figure 2-3: Relationship between crystal and sample coordinate systems. α_1, β_1 and γ_1 are the angles between the crystal direction [100] and RD, TD and ND respectively.

The relationship between a crystal coordinate system and the sample system is described by an orientation matrix G. A direction measured in the crystal system r_c is related to the same direction measured in the sample system r_s by:

$$r_c = Gr_s \qquad 2\text{-}4$$

The rows of the matrix **G** are the direction cosines of the crystal system axes in the coordinates of the sample system.

$$G = \begin{bmatrix} \cos\alpha_1 & \cos\beta_1 & \cos\gamma_1 \\ \cos\alpha_2 & \cos\beta_2 & \cos\gamma_2 \\ \cos\alpha_3 & \cos\beta_3 & \cos\gamma_3 \end{bmatrix} \qquad 2\text{-}5$$

Figure 2-3 shows how the angles α_1, β_1 and γ_1 are defined. α_2, β_2, γ_2 and α_3, β_3, γ_3 are similarly defined as the angles between the [010] and [001] crystal directions and the three sample axes.

2.3.2. Misorientation

The orientation between two crystal coordinate systems can also be defined by the angle-axis pair θ[uvw]. One coordinate system can be superimposed onto the other by rotating by an angle θ around the common axis [uvw] (Figure 2-4). Because it is an axis of rotation, the direction [uvw] is the same in both coordinate systems. The angle-axis pair notation is normally used to describe grain boundary misorientations.

The orientation between two coordinate systems can also be defined by a set of three successive rotations about specified axes. These rotations are called the Euler angles ϕ_1, Φ, ϕ_2 and are shown in Figure 2-5, which shows the rotations necessary to superimpose the crystal coordinate system (red) onto the sample system (blue). The first rotation ϕ_1 is about the z axis of the crystal coordinate system. The second rotation is Φ about the new x-axis. The third rotation is ϕ_2 about the new z-axis. The dotted lines show the positions of the axis before the last rotation. Note that the orientation can also be defined by an equivalent set of Euler angles which superimpose the sample coordinate system onto the crystal coordinate system.

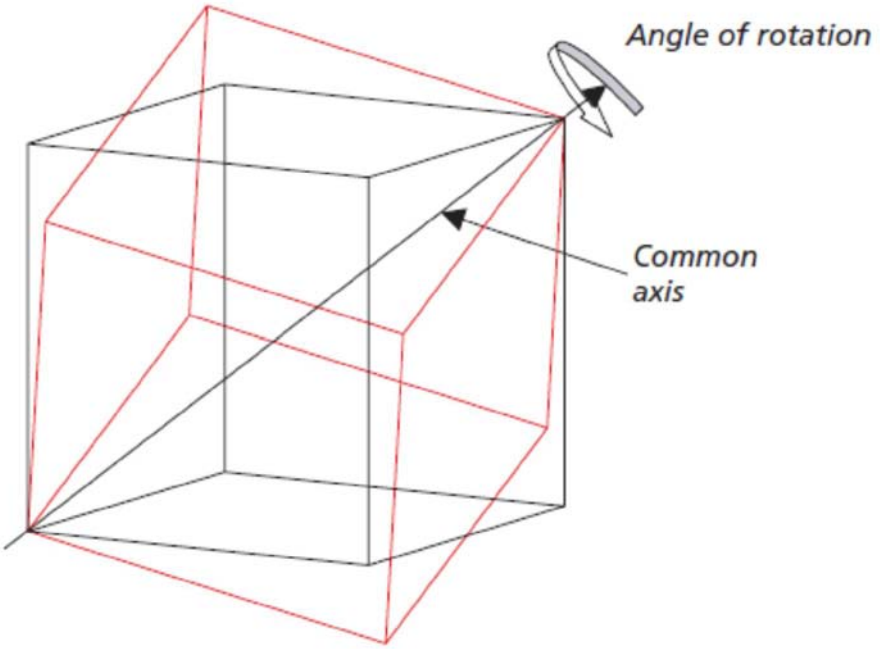

Figure 2-4: Two interpenetrating lattices can be realigned by a single rotation about a common axis [uvw] by an angle θ. In the figure the axis is the common [111] direction and the rotation angle 60°.

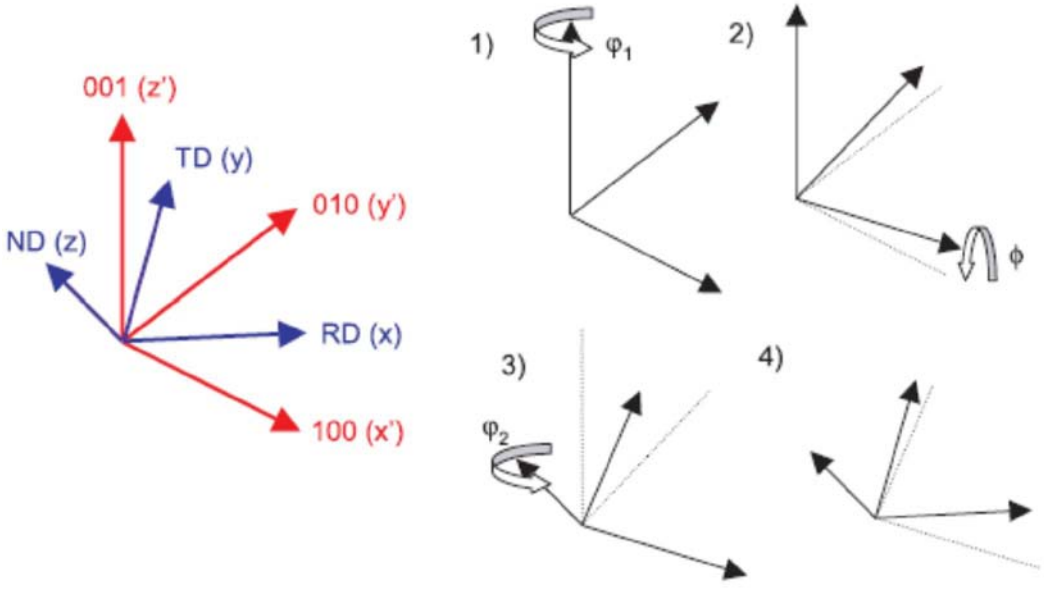

Figure 2-5: Definition of the Euler angles.

3. In-situ EBSD test and interrupted “in-situ” EBSD test

After automated EBSD systems are used in combination with other equipment within the scanning electron microscope (SEM), it is possible to perform in-situ tension test in the sample chamber of SEM and apply EBSD measurements simultaneously. While a changes in a single EBSD pattern could be observed during in-situ deforming of a sample, so much greater insight can be gained by EBSD scan data during an experiment. This chapter briefly introduces in-situ EBSD tension test and interrupted “in-situ” EBSD test used in this study.

3.1 In-situ EBSD test

The arrangement of an in-situ EBSD test is illustrated in Figure 2-9, including mini tensile testing machine installed in the chamber of SEM, a load and displacement recording for controlling the tensile speed, loading, unloading and recording the force and displacement data, an automated EBSD systems to collect Kikuchi patterns, a computer to save Kikuchi patterns collected and index them with special software.

The EBSD measurement are taking during the in-situ experiment． In order to get high quality Kikuchi patterns, the sample must be maintained at the standard 70° tilt during the experiment. This requires good compatibility between the SEM，EBSD camera and deformation stage.

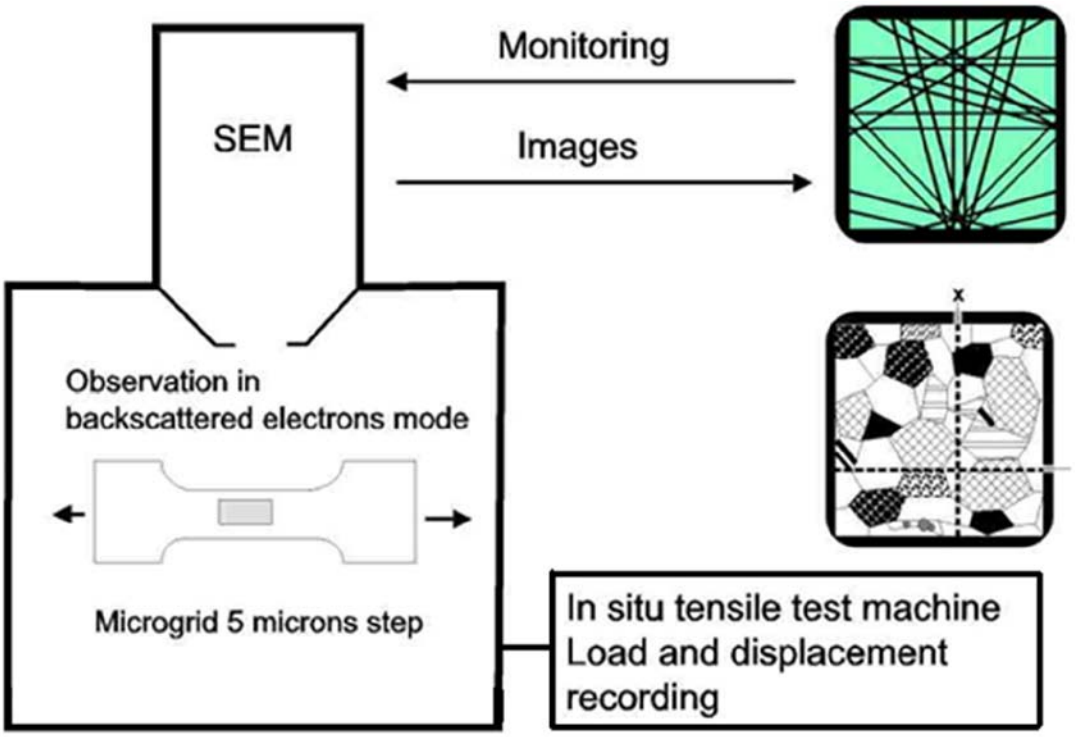

Figure 2-6: An in-situ EBSD tension test

3.2 Interrupted “in-situ” EBSD test

Although in-situ EBSD test is an excellent method in collecting orientation data of grains during deformation, it requests some strict conditions such as low deformation speed, small measure area and so on; most important is that tension test is the only deformation mode it can provide. Therefore, an interrupted “in situ” EBSD investigation method was proposed and applied. In this method, we concentrate on sufficient amount of grains and perform EBSD measurement prior and after the deformation in the same zone, therefore, we can acquire the detailed orientation information of these grains in the interrupted step of deformation and identify the deformation

modes during the deformation process. This method can be applied in rolling, tension, compression and some other deformation modes.

3.3 Experiment arrangement

The samples were cold rolled or compressed in channel die in several passes respectively, first to a certain amount of deformation and then to a further amount of deformation, and continue to more and more deformation.

To perform interrupted “in situ” measurement, a 500×300 mm^2 area was carefully polished and marked out with four micro-indentations. The orientation of all the grains in this polished area was measured by SEM/EBSD before and after each deformation step. The rolling and channel die compression layout is illustrated in Figure 2-12. Both sheets of the sandwich were firmly stuck together to avoid any surface sliding during the deformation in order to maintain a good surface quality. The evolution of grain orientation during deformation will be presented later both by pole figures and orientation flow fields.

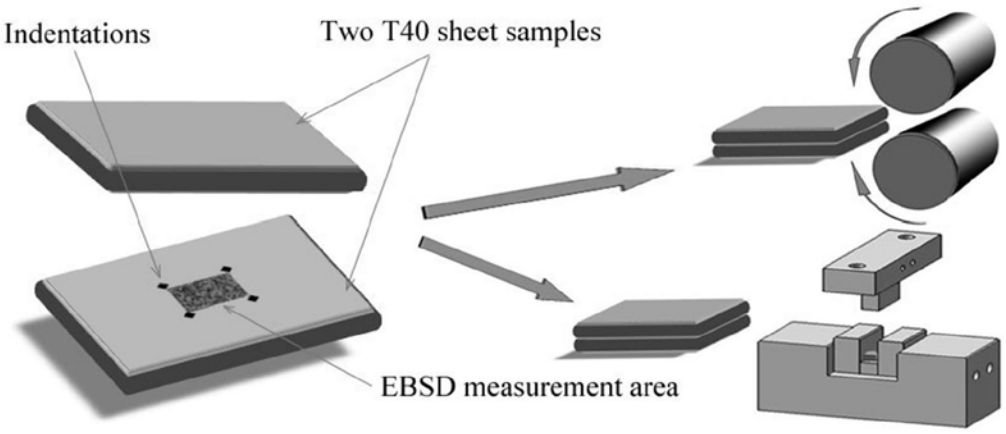

Figure 2-7**:** The preparation of samples and arrangement of the rolling and channel die compression tests.

Chapter 3: Deformation twinning in rolling and channel die compression

According to former studies on titanium, in the deformation at room temperature, three different types of twin systems were activated: {10-12} tensile twinning, {11-22} compression twinning and- to a small extent - {11-21} tensile twinning, depending on the grain orientation.

In this chapter, we continued this study on the deformation modes in rolling and channel die compression at room temperature, to provide information on the lattice rotation in the course of the deformation. The role of twinning, the formation and the evolution of mechanical twins is studied with the method of interrupted "in situ" SEM/EBSD measurements.

Study of deformation mechanisms in titanium by interrupted rolling and channel die compression tests

Lei Bao[a,b], Christophe Schuman[a], Jean-sébastien Lecomte[a], Marie-Jeanne Philippe[a], Xiang Zhao[b], Liang Zuo[b], Claude Esling[a]

[a] *LEM3 - UMR CNRS 7239 Université Paul Verlaine-Metz - Île du Saulcy - 57045 METZ Cedex 1 - FRANCE*

[b] *Key Lab for Anisotropy and Texture of Materials (Ministry of Education), Northeastern University, Shenyang, 110004 China*

***Abstract*:** The mechanisms of small plastic deformation of titanium (T40) during cold rolling and channel die compression by means of "interrupted in situ" EBSD orientation measurements were studied. These interrupted EBSD orientation measurements allow determining the rotation flow field which leads to the development of the crystallographic texture during the plastic deformation. Results show that during rolling, tension twins and compression twins occur and various glide systems are activated, the number of grains being larger with twins than with slip traces. In channel die compression, only tension twins are observed in some grains, whereas slip traces can be spotted in almost all observed grains. The different stress conditions and different strain rates existing under the two modes of deformation lead to the activation of different deformation mechanisms.

***Keywords*:** *titanium, deformation mechanism, twinning, gliding, orientation, EBSD*

Introduction

The mechanism of plastic deformation has been studied in some detail in the past [Yoo (1981); McDarmaid, Bowen and Partridge (1984); Vedoya, Pochettino and Penelle (1988); Philippe, Serghat, Houtte, and Esling (1995); Panchanadeeswaran, Doherty and Becker (1996); Kalidindi, Bhattacharyya and Doherty (2004); Prasannavenkatesan, Li, Field and Weiland (2005); Merriman, Field and Trivedi (2008); Skrotzki, Toth, Kloden, Brokmeier and Arruffat-Massion (2008); Quey, Piot and Driver (2010)]. Many efforts have been made in studying deformation twinning and gliding in single and polycrystalline metals [Akhtar (1975); Akhtar, Teghtsoonian and Cryst (1975); Kalidindi (1998); Field, True, Lillo and Flinn (2004); Jiang, Jonas,

Mishra, Luo, Sachdev and Godet (2007); Jiang and Jonas (2008)]. The mechanical response of titanium, like other HCP metals, is strongly dependent on the combination of active deformation modes: gliding and twinning. The specific deformation mechanisms depend on the c/a ratio, the available deformation modes, the critical resolved shear stress (CRSS) for gliding, the twin activation stress as well as the imposed deformation relative to the crystallographic texture. According to previous work, $\{10\bar{1}2\}$ tension twins, $\{11\bar{2}1\}$ tension twins and $\{11\bar{2}2\}$ compression twins are activated during plastic deformation at room temperature. Due to the compacity ratio c/a <1.633 in titanium, prismatic glide is the easiest one at room temperature but basal and pyramidal glide were also observed [Pochettino, Gannio, Edwards and Penelle (1992)].

However the previous studies concerning the texture and deformation modes were mostly performed after a certain amount of deformation either by of X-ray diffraction XRD or by transmission electron microscopy (TEM). Therefore the initial orientation of the individual grains and the evolution of the orientation flow during deformation were not documented. Moreover, after a certain amount of deformation, twinning and gliding were both active and interacted with each other. Thus it was difficult to resolve the specific orientation condition to activate each deformation mode (either twinning or gliding). Therefore, the present work is devoted to these aspects, providing the lack of information in the literature. In order to follow the evolution of individual orientations during the deformation and to determine the effect of initial orientation on the deformation modes, an interrupted “in situ” EBSD investigation method was proposed. In this

method, we follow a sufficient number of grains and perform EBSD measurement in the same area, prior to and after the deformation. Thus it is possible to acquire detailed orientation information of these grains in the interrupted step of deformation and identify the active deformation modes.

Experimental

The as-received material was hot-rolled and then annealed commercial purity titanium sheet of 1.5 mm thickness with the composition given in table 1.

Table 1 Chemical composition of commercially pure titanium T40

Element	H	C	N	O	Fe	Ti
Composition (ppm (wt.))	3	52	41	1062	237	Balance

In order to obtain a twin-free microstructure with equiaxed grains, a grain growth annealing was performed at 750°C for 2 hours. After the annealing, the samples were mechanically and then electrolytically-polished in a solution of 200 ml perchloric acid in 800 ml methanol at 17V (30 seconds) and at a temperature of 5°C before deformation. Then, the samples were cold rolled or compressed in channel die in two passes respectively, first to 10 % and then to 20% reduction. To perform interrupted “in situ” measurement, a 500×300 mm^2 area was carefully polished and marked out with four micro-indentations. The orientation of all the grains in this polished area was measured by SEM/EBSD before and after each deformation step. The rolling and channel die compression layout is illustrated in Fig. 1. Both sheets of the sandwich were firmly stuck together

to avoid any surface sliding during the rolling in order to maintain a good surface quality. EBSD measurements were performed with a JEOL-6500F SEM with a step size of 0.4 µm. The evolution of grain orientation during deformation will be presented later both by pole figures and orientation flow fields.

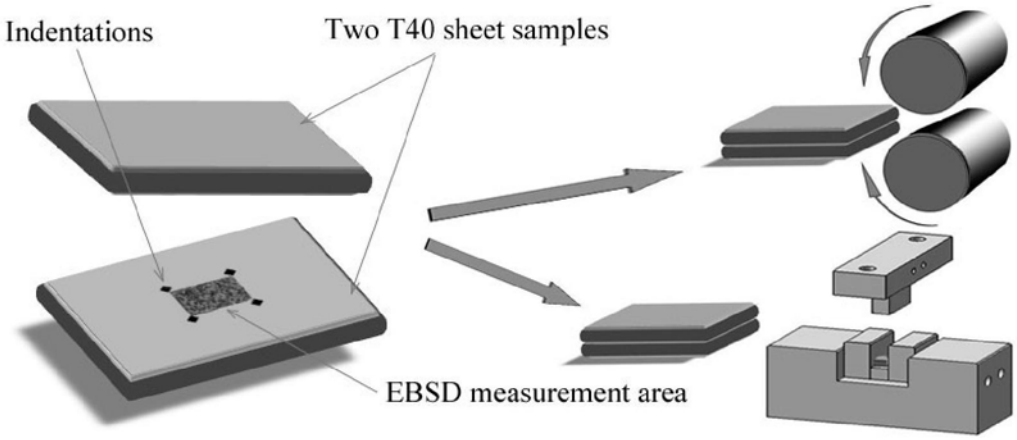

Fig. 1: The preparation of samples and arrangement of the rolling and channel die compression tests.

Deformation in rolling

The orientation map of the grain growth annealed sample shown in Fig. 2 (a) reveals a completely recrystallized microstructure with an average grain size of 10 µm. The {0002}-pole figure (PF) in Fig. 2 (b) shows two strong maxima at ±30° tilted from ND towards TD, whereas the $\{10\bar{1}0\}$ PF displays the maximum pole densities parallel to RD. In this work, the setting of the coordinate systems and the Euler angles $\{\phi1,\Phi, \phi2\}$ are defined according to Bunge's convention, see Bunge, Esling and Muller (1980).

The lattice rotation was studied after each rolling pass. The orientation of each individual grain was carefully determined, so that the lattice rotation of each grain could be brought in relation to its own orientation as well as to that of its neighbouring grains. It was found that $\{11\bar{2}2\}$ compression twins (the misorientation between the twin and its matrix corresponds to a 65° rotation about their common $<10\bar{1}0>$ axis) and $\{10\bar{1}2\}$ tension twins (85° about $<1\bar{2}10>$ axis [Philippe, Esling and Hocheid(1988)]) were most frequently observed (Fig 3). The respective amount of these two types of twinning was further presented by means of the misorientation-angle distributions in Fig. 4. It is seen that after 10% rolling (Fig. 4 (b)), 65° misorientation occurs most frequently, suggesting that $\{11\bar{2}2\}$ twinning was predominant at this stage of deformation. This result is reasonable considering that the initial orientation favors the activation of this compression twin. Whereas when rolling continues to 20%, $\{10\bar{1}2\}$ tension twinning was remarkably increased (Fig. 4 (c)). The orientation analysis could be studied from the microscopic point of view of the crystal reorientation step by step, in terms of the rotation flow field. A small arrow is plotted in the Euler space between the initial grain orientation and the final grain orientation. This field of small arrows offers a graphical representation of the rotational flow field. The flow field can be defined and plotted in the Euler space, and represents an efficient tool to describe the texture evolution through modeling, e.g. Clement and Coulomb (1979), Bunge and Esling (1984), Knezevic, Kalidindi and Fullwood(2008).

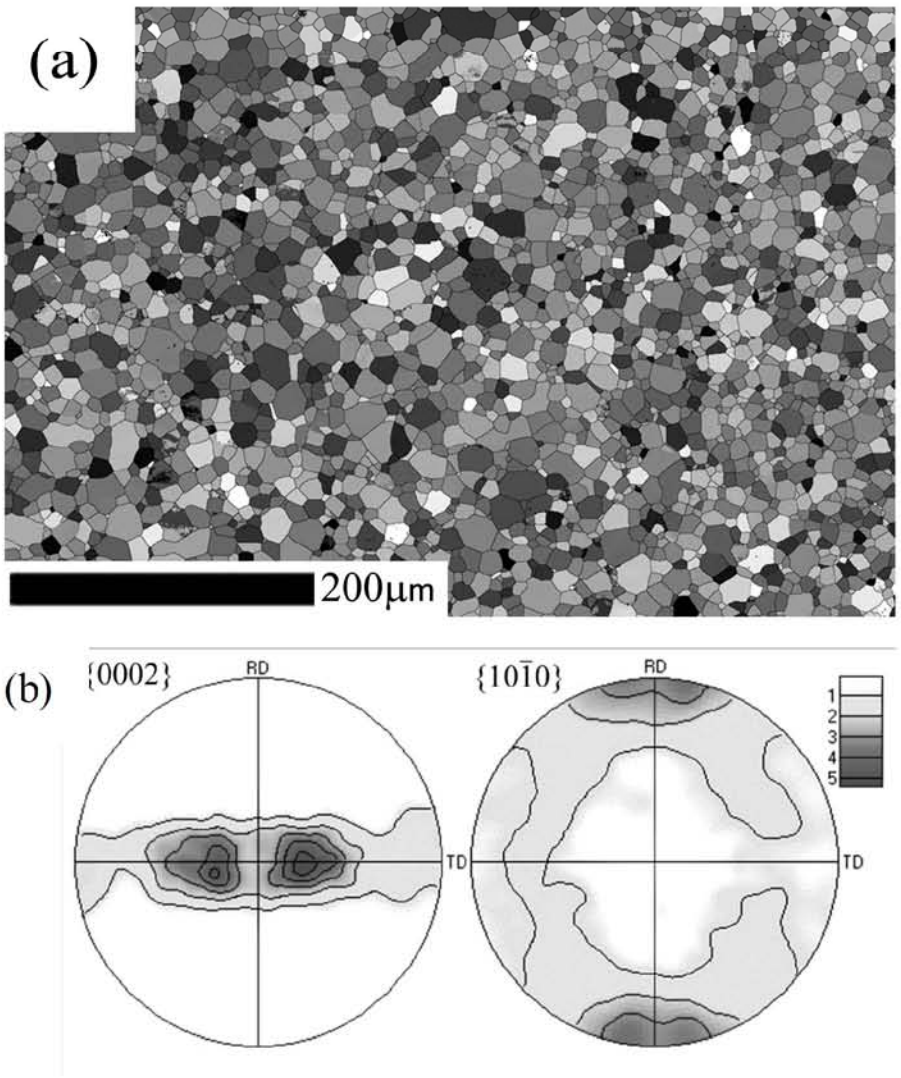

Fig. 2: EBSD orientation mapping (a) and {0002}, {10-10} pole figures (b).

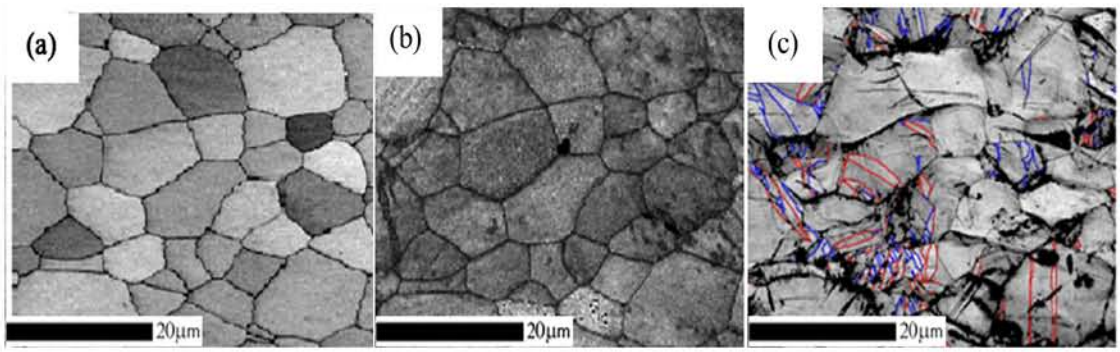

Fig. 3: Orientation micrograph of one selected area, before rolling (a), after 10% (b) and 20% (c) rolling. Blue lines: {10-12} twin boundaries; red lines: {11-22} twin boundaries.

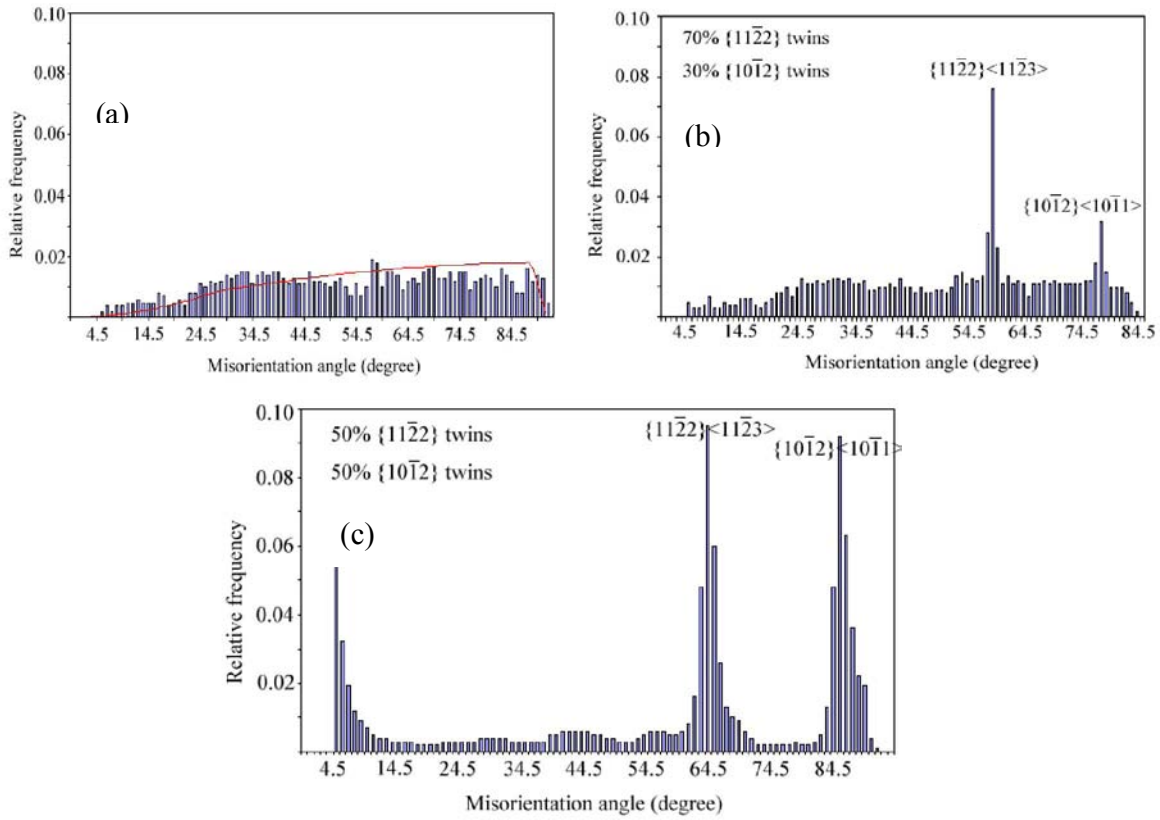

Fig. 4: Misorientation-angle distributions of samples deformed to 0% (a), 10% (b) and 20% (c) reduction.

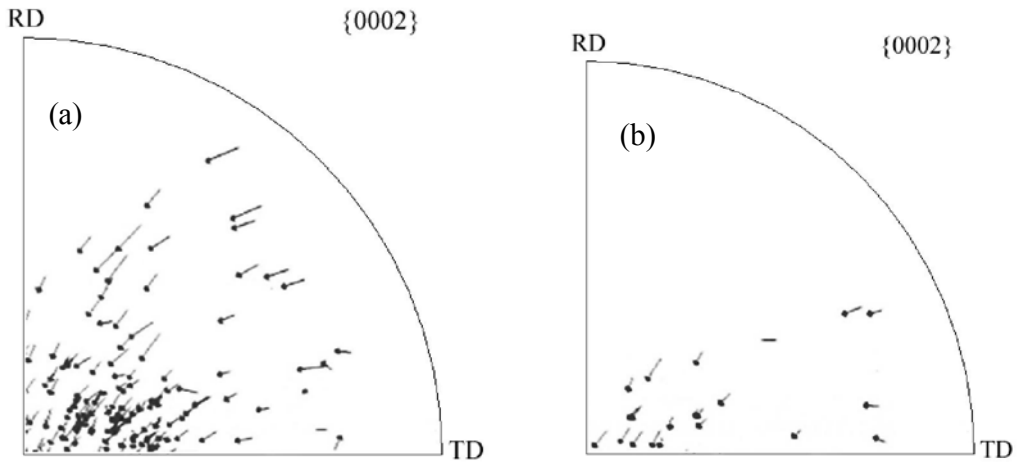

Fig. 5: Rotational flow field in grains showing no twins (a). Lattice rotation field in untwinned part (or matrix) of grains showing twins (b).

In the present case of hexagonal material, due to the particular importance of the c-axes, we choose to plot the small arrows linking the initial orientation and the final orientation in the two dimensional [0001] pole figures. For further discussion, it was of interest to plot separately the rotation flow field of the grains without twins on the one hand (Fig.5 (a)) and the rotation flow field of the matrix of the grains with twins (Fig. 5 (b)). It is seen from Fig 5 that both orientation flow fields are similar, but for a smaller amplitude of the rotation of the matrix of twinned grains, as compared with that of the grains without twins.

Thanks to the interrupted "in situ" method used in the present work, we can follow the evolution of the twins (from nucleation to growth) in each grain. Fig. 6 shows one selected grain before and after each rolling pass. In the figure, the blue lines represent the $\{10\bar{1}2\}$ twin boundaries and the red lines the $\{11\bar{2}2\}$ twin boundaries. It is interesting to find that $\{11\bar{2}2\}$ compression twin appears in the grains with c-axes close to ND. The twinned part grows during the deformation process and the c-axes of the twinned part, reoriented 65° to those of the matrix, are in an orientation favorable for the activation of the $\{10\bar{1}2\}$ tension twin. Subsequently, $\{10\bar{1}2\}$ tension twin activates inside this "new grain" formed by the primary compression twin, and this new secondary twin builds a double twin. So two types of twins, tension and compression twins can form in one and the same grain, compression twins as first order and tension twins as second order twins. In other words, the $\{11\bar{2}2\}$ twinning brings the c-axis of the twinned part out of the stable orientation. The twinned part is favorably oriented to initiate a tension twin. Then the $\{10\bar{1}2\}$

tension twin forms, reorienting the c-axis of the newly twinned part into a stable orientation.

Slip traces are observed in some grains in the post-deformation EBSD map. In order to identify the activated glide systems corresponding to the traces observed, the possible traces of all possible glide planes [Partridge (1967)] are calculated in the crystal coordinate system, using the orientation data of the related grains and comparing with the observed traces. Consequently, basal <a>, prismatic <a> and pyramidal <a> or <c+a> glide systems are identified in this work.

Deformation in channel die compression

In channel die compression, only one type of twin - $\{10\bar{1}2\}$ tension twin is observed and the amount of twinned grains is very low, only 1.07% of the observed grains, which cannot be clearly resolved from the misorientation-angle distribution diagram in Fig. 7.

Compared with rolling, numerous slip traces are observed in a great number of grains in EBSD maps after channel die compression. Using the above trace comparison method, basal <a>, prismatic <a> and pyramidal <a> or <c+a> glide are identified. A statistical set of 100 randomly selected grains with slip traces is studied. The occurrence of various glide systems in the studied grains is listed in Table 2**.** It is seen that among the activated glide systems, 11% are basal <a>, 51% are prismatic <a> and 38% are pyramidal <c+a> or <a>. The Schmid factors for the three glide systems were calculated, and the calculation indicated that most grains have high Schmid factors for pyramidal <c+a> glide system but low Schmid factors for

basal <a> and prismatic <a>. This is due to the strong texture which means a majority of grains belong to one main orientation mode.

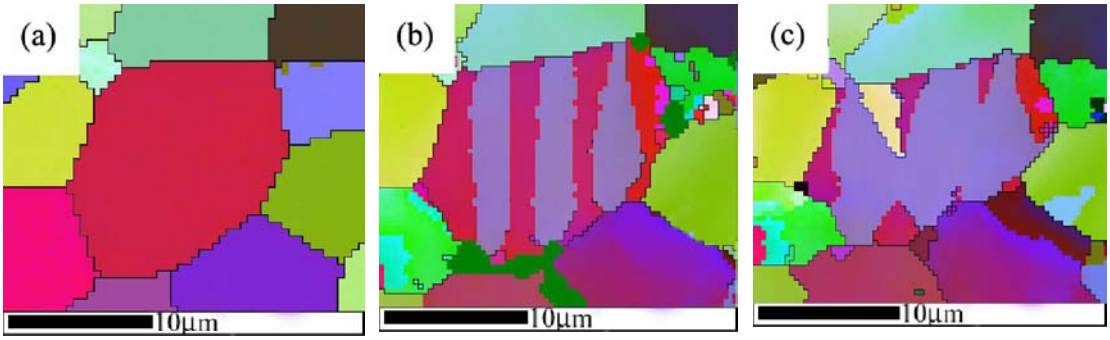

Fig. 6: Initial grain with c axis close to the ND (dark red) (a); 10% deformation: $\{11\bar{2}2\}$ compression twins outlined by red lines (b); 20% deformation: a part of $\{11\bar{2}2\}$ twins undergoes secondary $\{10\bar{1}2\}$ tension twinning, (c). outlined by blue twinning boundaries delimiting the tension twin (in yellow colour).

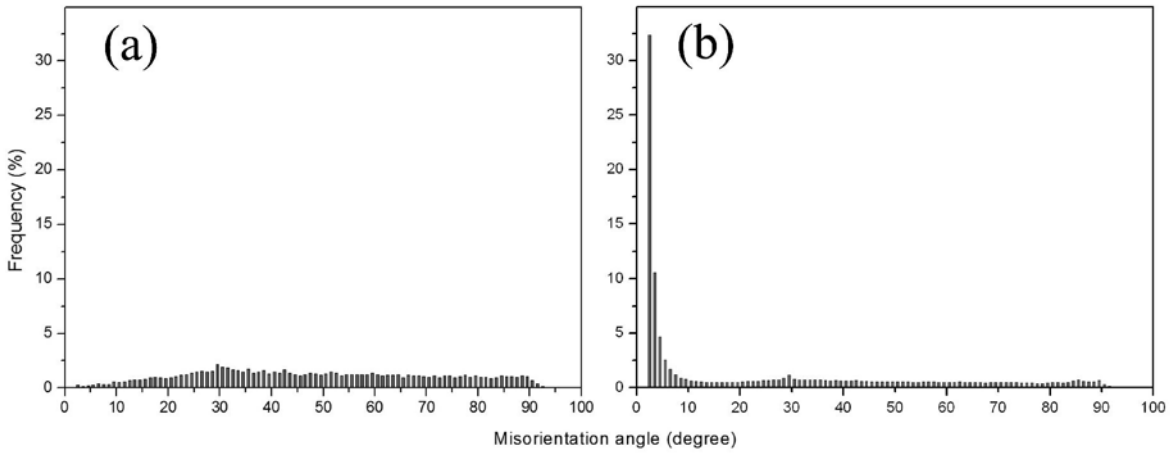

Fig. 7: Misorientation-angle distribution, before compression (a) and after 20 % compression (b).

Table.2 Activated glide systems in 100 randomly selected grains.

Activated glide system	frequency
Basal <a>	11%
Prismatic <a>	51%
Pyramidal <a> or <c+a>	38%

Discussion

Orientation analysis indicates that at 10% reduction, the c-axis of the grains with $\{10\bar{1}2\}$ twins (tension along c-axis) is oriented close to the rolling direction, as shown in Fig. 8 (a), whereas that of the grains with $\{11\bar{2}2\}$ twins (compression along c-axis) is oriented close to the sample normal direction, as shown in Fig. 8 (b). These results are coherent with the theoretical expectations (Fig. 9). The c-axis of the $\{10\bar{1}2\}$ and $\{11\bar{2}1\}$ twinned part in each grain is systematically oriented close to a stable orientation belonging to the rolling texture component, however, the $\{11\bar{2}2\}$ twinning leads the c-axis of the twinned part oriented close to the rolling direction i.e. to an unstable orientation. As shown in Fig. 10, the $\{10\bar{1}2\}$ twinning reorientates the c-axis by 84.78°as schematized with the blue arrow in the figure. Likewise, the $\{11\bar{2}2\}$ twinning reorientates the c-axis by 64.62° as schematized with the red arrow. The green area is delimiting the stable orientation belonging to the rolling texture (characterized by c axes tilted about 30° from ND to TD). From the figure, we can see clearly that the $\{10\bar{1}2\}$ twinning reorientates the matrix to the stable orientation whereas $\{11\bar{2}2\}$ twinning acts reversely.

An interesting result of this study is that the effect of twinning on strain accommodation is to create a newly oriented zone (a new grain) and does not induce additional deformation mechanisms in the remaining matrix part of the grain. In other words, the deformation mechanisms in the matrix part of the twinned grains remain the same as those in the untwinned grains. The $\{11\bar{2}1\}$ and $\{10\bar{1}2\}$ twinning tend to reorientate the c-

axes close to stable orientations. Thus, there is no tendency for secondary twinning to occur within such primary twins.

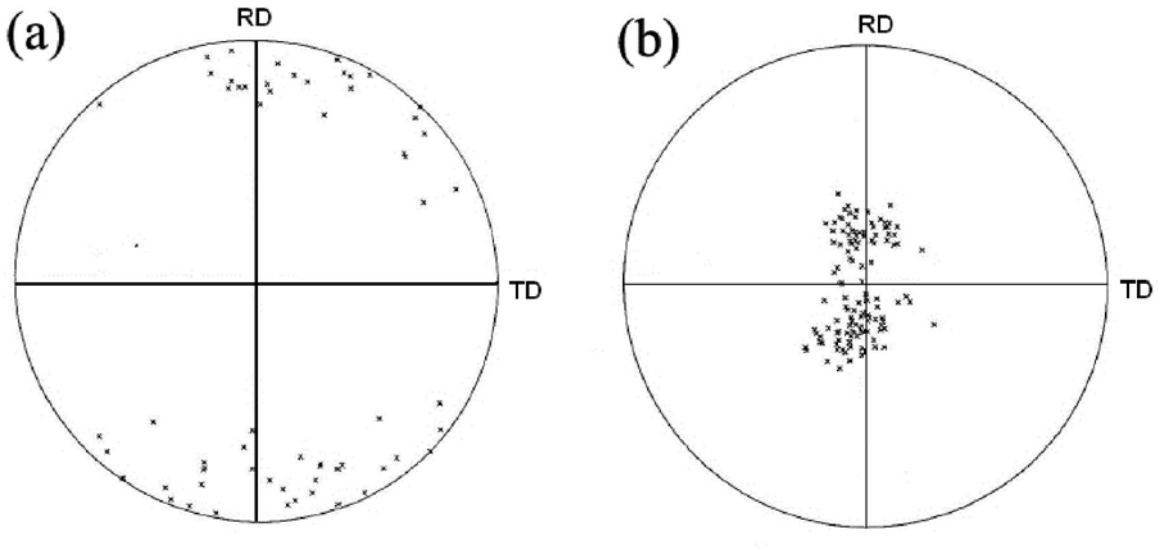

Fig. 8: Initial {0002}-Pole figure of grains having $\{10\bar{1}2\}$ twin (a) and Initial {0002}-Pole Figure of grains having $\{11\bar{2}2\}$ twin (b) after 10% deformation.

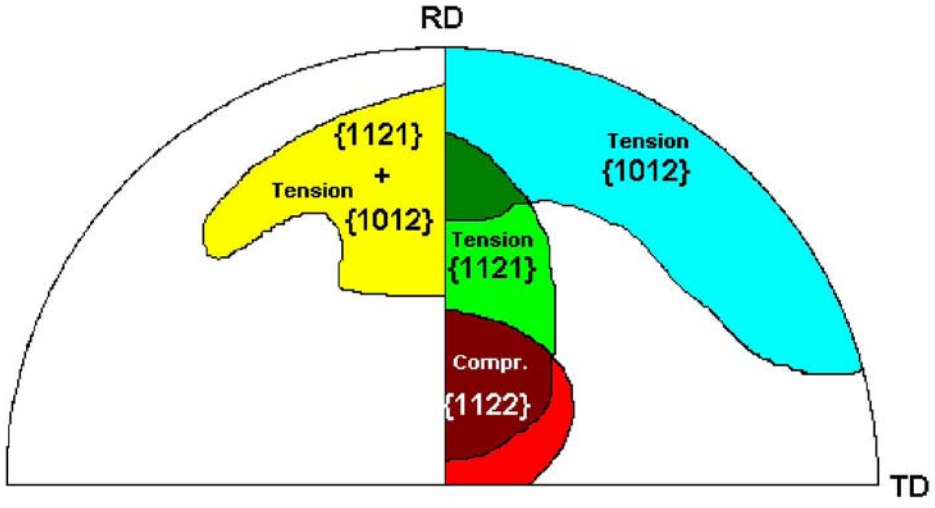

Fig. 9: (0002) Pole Figure delimitating schematically the orientation domains of the c-axes of the grains in which the indicated twinning is expected to be activated (theoretical expectations)

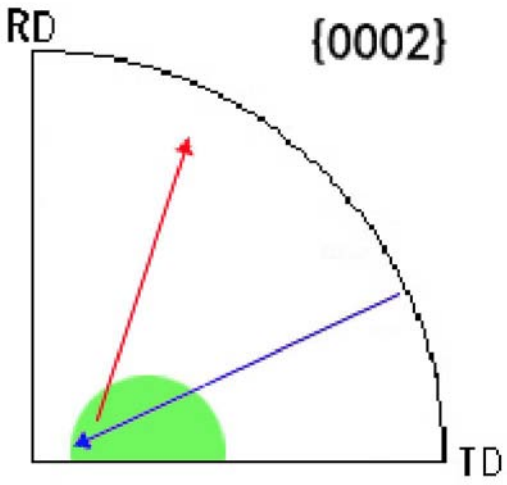

Fig. 10 Schematical reorientation of c axes by $\{10\bar{1}2\}$ twinning (blue) and $\{11\bar{2}2\}$ twinning (red arrow).

Secondary twinning only takes place in the $\{11\bar{2}2\}$ compression twins whose c-axes are orientated far away from the stable texture orientation. In such a case, the new and major twins appearing inside the $\{11\bar{2}2\}$ twins are $\{10\bar{1}2\}$ tension twins. This explains why when deformation is increased from 10% to 20% the amount of $\{10\bar{1}2\}$ tension twin dramatically increases. The c-axis of this secondary twin orientates towards the stable orientation. We could hardly observe the presence of any third-order twin, even after much higher deformation.

This can be easily understood by the relation between the geometrical and energetical characteristics of twinning. Several models have been developed to describe the nucleation of twin [Eshelby, J.D. (1957); Christian, J.W. (1958)]. These models are based on a “pole mechanism” i.e. a dislocation whose Burgers vector has a component normal to the twin planes equal to their spacing and a partial dislocation connected to this

pole. The pole can be seen as a dislocation source and the partial dislocations are produced continuously in the planes parallel to the twin plane during deformation. If the path in which the partial dislocations move is short, the dislocations will easily be blocked, pile up and react to the source disabling it. Deformation twins always have a lenticular shape, since the interface can deviate from the twinning plane without greatly increasing the twin-interface energy [Partridge (1967)]. In addition, the strain energy increase should also be taken into account, approximately equal to $(c/r)\mu S^2$, where c and r represent the thickness and length of the twin, μ the shear modulus and S the twinning shear. Hence, secondary twins are already confined in a small volume due to the lenticular shape and cannot provide enough free path to develop a higher order twinning. In fact, in titanium alloys it is difficult to induce twinning at room temperature once the size of the matrix drops below the range of about 10 µm.

A major benefit of the interrupted "in situ" method is that we can follow the deformation process step by step. For example, in the grains having their initial c-axis close to ND for which secondary twinning occurs inside the primary twins, we can clearly discriminate the initial matrix from the primary twins thanks to the in-situ orientation information. In this case the primary twinned area is much larger than the remaining matrix and thus represents the “new matrix” for possible subsequent secondary twinning.

The effect of the neighboring grains slightly modifies the orientation in the vicinity of the grain boundary. This leads to a larger spread in the orientation measured in the vicinity of the grain boundary when the

neighboring grain is strongly misoriented with respect to the considered grain.

Compared with rolling, channel die compression showed a simple deformation mode including only $\{10\bar{1}2\}$ tension twinning and various gliding. The primary reason is the simple stress condition applied in channel die compression. Therefore, we used the channel die compression results to clarify the effect of grain size on twinning.

357 grains with orientation favorable to the activation of $\{10\bar{1}2\}$ twinning were selected and divided into three groups according to their diameter. Group 1: 0 to 10 μm (221 grains); Group 2: 10 to 20 μm (129 grains); Group 3: 20 to 30 μm (7 grains). The calculated percentage of grains with twins for the three groups is shown in Fig.11. It is clear that with the similar orientation (c axis tilted 70º～90º from normal direction ND), no twin occurs in the grains smaller than 10μm. With the increase of the grain size, the occurrence of the twin increases. Hence, grain size is an important factor affecting twin activation. The reason can be understood from geometrical and energetical considerations we introduced above.

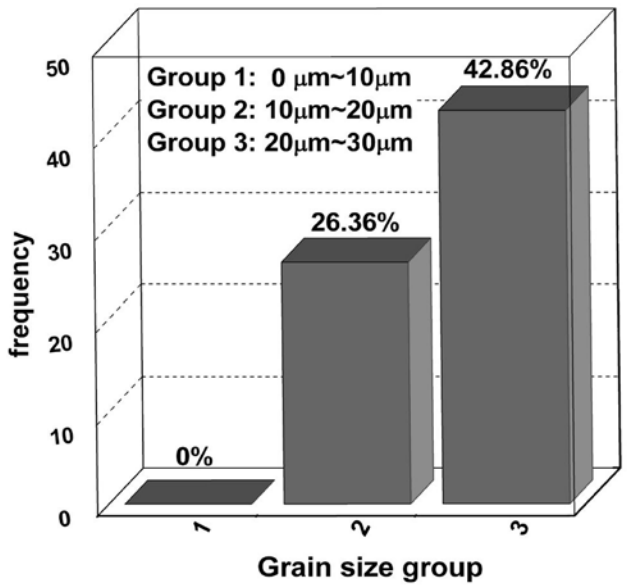

Fig.11: Percentage of twinned grains in the three different grain-size groups.

Conclusion

Twinning occurs in grains having specific orientations. Generally, the reorientation induced by twinning aligns the c-axis of the twinned part to the stable rolling texture orientation, so that no further secondary twinning can be induced. Secondary twinning occurs only when the primary twinning orientates the c-axis of the primary twins far away from the stable orientations (this is generally the case for the $\{11\bar{2}2\}$ twinning). The formation of the $\{10\bar{1}2\}$ secondary twin inside the $\{11\bar{2}2\}$ primary twin results in a reorientation of the c-axis of the secondary twin to a stable orientation. Only a little amount of second order twin could be observed and twinning of higher than second order was not found.

The rotation of the matrix-part of the grains having twins is similar to that of the non-twinned grains with similar orientation. The twinned part of a grain can be considered as a new grain. When twins grow within the grain,

they can consume almost the whole matrix. Special attention should be paid when determining the twinned volume fraction. With the EBSD measurement, a strong increase of the twinned volume could be demonstrated. This contradicts the conventional judgement that the twinned part is always the smallest part in a twinned grain, as concluded by optical microscopy. Only step by step EBSD orientation mapping allows an unambiguous determination of the twinned volume fraction. The confirmation that the order of twinning never exceeds the second order is very useful for the modeling polycrystalline plasticity in metals, such that the order allowed for twins should be restricted to only the first and second order (also called double twins).

Prismatic glide is the predominant glide system (51%), basal and pyramidal glide take 11% and 38% respectively. The relatively higher amount of pyramidal glide can related to the initial transverse or T-texture.

References

Akhtar, A. (1975): Basal slip and twinning in α-titanium single crystals *Metallurgical and Materials Transactions A*. vol. 6 pp. 1105-1113.

Akhtar, A.; **Teghtsoonian**, E. (1975): Dislocation sub-structure in α-Ti single crystals. *Journal of Crystal Growth.* Vol. 28 pp. 227-230.

Bunge, H.J.; **Esling**, C. (1984): Texture development by plastic deformation. *Scripta Metallurgica*. Vol. 18 pp. 191-195.

Bunge, H.J.; **Esling**, C.; **Muller**, J. (1980): *Journal of Applied Crystallography.* vol. 13 pp. 544-554

Christian, J.W. (1958): Accommodation strains in martensite formation, and the use of a dilatation parameter *Acta Metallurgica*.Vol. 6 pp. 377-379.

Clement, A.; **Coulomb**, P. (1979): Eulerian simulation of deformation textures. *Scripta Metallurgica*. Vol. 13 pp. 899-901.

Eshelby, J.D. (1957): The Determination of the Elastic Field of an Ellipsoidal Inclusion, and Related Problems. *Proceedings of the Royal Society of London. Series A.* Vol. 241 pp. 376-396.

Field, D.P.; **True,** B.W.; **Lillo,** T.M.; **Flinn,** J.E. (2004): Observation of twin boundary migration in copper during deformation Matls. *Materials Science and Engineering A*. Vol. 372 pp. 173-179.

Jiang, L.; **Jonas**, J.J. (2008): Effect of twinning on the flow behavior during strain path reversals in two Mg (+Al, Zn, Mn) alloys. *Scripta materialia.* Vol. 58 pp. 803-806.

Jiang, L.; **Jonas**, J.J.; **Mishra**, R.K.; **Luo** A.A.; **Sachdev**, A.K.; **Godet**, S. (2007): Twinning and texture development in two Mg alloys subjected to loading along three different strain paths. *Acta Materialia.* Vol. 55 pp. 3899-3910.

Kalidindi, S.R. (1998): Incorporation of deformation twinning in crystal plasticity models. *Journal of the Mechanics and Physics of Solids*, Vol. 46 pp. 267-284.

Kalidindi, S.R.; **Bhattacharyya,** A.; **Doherty,** R.D. (2004): Detailed analyses of grain-scale plastic deformation in columnar polycrystalline aluminium using orientation image mapping and crystal plasticity models. *Proc. Royal Society of London Series A*, Vol. 460 pp. 1935-1956.

Knezevic, M.; **Kalidindi**, S. R.; **Fullwood**, D. (2008): international jornal of plasticity. Vol. 24 pp. 1264-1276.

McDarmaid, D.S.; **Bowen**, A.W.; **Partridge**, P.G. (1984): Tensile properties of strongly textured Ti-6Al-4V after superplastic deformation. *Materials Science and Engineering*. Vol. 64 pp. 105-111.

Merriman, C.C.; **Field,** D.P.; **Trivedi,** P. (2008): Orientation dependence of dislocation structure evolution during cold rolling of aluminum. *Materials Science and Engineering A*. Vol. 494 pp. 28-35.

Panchanadeeswaran, S.; **Doherty,** R.D.; **Becker,** R. (1996): Direct observation of orientation change by channel die compression of a polycrystalline aluminum - Use of a split sample. *Acta Materialia*. Vol. 44 pp. 1233-1262.

Partridge, P.G.(1967): The crystallography and deformation modes of hexagonal close-packed metals. *Metallurgical, Review*. Vol. 12 pp. 169-194.

Philippe, M.J.; **Esling**, C.; **Hocheid**, B. (1988): Role of twinning in texture development and in plastic deformation of hexagonal materials. *Textures and Microstructures*. Vol. 7 pp. 265-301.

Philippe, M.J.; **Serghat**, M.; **Van Houtte,** P.; **Esling**, C. (1995): Modelling of texture evolution for materials of hexagonal symmetry-II. Application to zirconium and titanium α or near α alloys. *Acta Metallurgica et Materialia*. Vol. 43 pp. 1619-1630.

Pochettino, A.A.; **Gannio**, N.; **Edwards**, C Vial.; **Penelle**, R. (1992): Texture and pyramidal slip in Ti, Zr and their alloys. *Scripta Metallurgia et Materialia* Vol. 27 pp. 1859-1863.

Prasannavenkatesan, R.; **Li,** B.Q.; **Field,** D.P,; **Weiland,** H. (2005): A parallel macro/micro elastoplasticiy model for aluminum deformation and comparison with experiments, *Metall. Mater. Trans A*, Vol. 36 pp. 241-256.

Quey, R.; **Piot,** D.; **Driver,** J.H. (2010): Microtexture tracking in hot-deformed polycrystalline aluminium: Experimental results. *Acta Materialia* Vol. 58 pp.1629-1642.

Skrotzki, W.; **Toth,** L.S.; **Kloden,** B.; **Brokmeier,** H.G.; **Arruffat-Massion,** R. (2008): Texture after ECAP of a cube-oriented Ni single crystal *Acta Materialia*. Vol. 56 pp. 3439-3449.

Vedoya, P.; **Pochettino**, A.; **Penelle**, R. (1988): Plastic Anisotropy of Titanium, Zirconium and Zircaloy 4 Thin Sheets. *Textures and Microstructures.*Vol. 8 pp. 601-610.

Yoo, M.H. (1981); Slip, twinning, and fracture in hexagonal close-packed metals. *Metallurgical and Materials Transactions A*. vol. 12 pp. 409-418.

Study of plastic deformation in hexagonal metals by interrupted in-situ EBSD measurement

Lei Bao [a,b], Jean-Sébastien Lecomte [a], Christophe Schuman [a], Marie-Jeanne Philippe [a], Xiang Zhao [b], Claude Esling [a *]

[a] *LETAM, CNRS FRE 3143 (former UMR 7078) University of Metz, 57045 Metz, France*
[b] *Key Lab for Anisotropy and Texture of Materials (Ministry of Education), Northeastern University, Shenyang, 110004 China*

Abstract: The present work was undertaken to provide information, lacking in the literature, on the lattice rotation and the role of twinning during cold rolling of commercial purity titanium (T40). The proposed method consists of determining the individual rotation of the grains induced by low to intermediate deformation (up to 30% in thickness reduction) and following the rotation field using electron backscattered diffraction (EBSD) measurements in a high resolution FEG SEM at different steps of deformation (10 and 20 %). We have especially studied the formation, the evolution and the role of mechanical twins.

According to the former research, during the deformation at room temperature, three different types of twin systems were activated: $\{10\bar{1}2\}$ tensile twinning, $\{11\bar{2}2\}$ compression twinning and - to a small extent - $\{11\bar{2}1\}$ tensile twinning, depending on the grain orientation. Secondary twins (often $\{10\bar{1}2\}$ within $\{11\bar{2}2\}$ twins) were activated in the grains oriented favourably for this secondary twinning. This resulted in a heterogeneous microstructure in which grains were refined in some areas. It also induced re-orientation of the c-axes to stable orientations. No twins of higher order than the second order twins could be found.

The rotation flow field was measured by following the rotation of 800 grains. It was possible to determine the individual grains rotations as well as the average flow field. For grains having twinned parts, the lattice rotation of the matrix is similar to that of the grains having a similar crystallographic orientation but without any twin. Twins form in grains having specific orientations with respect to the macroscopic stress field; they can grow in the grain with increasing strain and may consume almost the whole matrix.

Keywords*: Titanium; Rolling; Rotation flow field; Gliding; Twinning; Texture.*

Introduction

Introduction

The titanium textures observed at room temperature in the hexagonal close-packed (HCP) structure are inherited to some extent from their prior texture in the body centred cubic (BCC) structure [1]. However most of the

research effort concentrated on the strong deformation textures that Titanium [2-4], like other HCP metals, develops during the rolling at room temperature, that lead to a pronounced plastic anisotropy of the polycrystalline materials [5]. The mechanical response of HCP metals is strongly dependent on the combination of active deformation modes: slip and twinning. The specific deformation mechanisms depend on the c/a ratio, the available deformation modes, the critical resolved shear stress (CRSS) for slip and the twin activation stress, as well as the imposed deformation relative to the crystallographic texture. For pure titanium, $\{10\bar{1}0\}<1\bar{1}20>$ slip is the primary deformation mode. This slip mode alone, however, cannot accommodate the imposed strain in the grains of a polycrystalline aggregate, because it cannot provide 5 independent slip systems [4, 6-9]. Additional deformation mechanisms such as pyramidal planes with <c+a> Burger's vector or twinning usually have to be activated. The observed ductility has been attributed essentially to the occurrence of twinning on the $\{11\bar{2}1\}$ and $\{11\bar{2}2\}$ planes.

Chun et al. [10] studied the effect of deformation twinning on microstructures during cold rolling of commercially pure (CP) titanium. The primary twinning systems activated were $\{11\bar{2}2\}<1\bar{1}23>$ compressive twins and $\{10\bar{1}2\}<10\bar{1}1>$ tension twins. Secondary twins, mainly of the tensile type, were also activated.

In order to describe the texture evolution, different models of polycrystalline plasticity are used. Polycrystal plasticity models are routinely employed to predict deformation textures. Wu et al. [11] employed a new

Taylor type of crystal plasticity model to predict the texture evolution and anisotropic stress-strain curves in α-titanium. The main features of this model include: (i) incorporation of slip inside twins as a significant contributor to accommodating the overall imposed plastic deformation; and (ii) extension of slip and twin hardening laws to treat separately the hardening behaviour of the different slip families (prismatic <a>, basal <a> and pyramidal <c+a>) using hardening parameters that are all coupled to the extent of deformation twinning in the sample. Proust et al. [12] developed a model which takes into account the texture evolution associated with twin reorientation and the effect of the twin barriers on dislocation propagation. The role of the twins as barriers to dislocations was explicitly incorporated into the hardening description via geometrically necessary dislocations (GNDs) and a directional Hall-Petch mechanism. However, with these complex models, the lack of direct experimental information on slip and twinning systems imposes difficulties for the related modelling practices.

The present work was undertaken to provide information, lacking in the literature, on the lattice rotation and the role of twinning during cold rolling of commercial purity titanium (T40). The method proposed consists of determining the individual rotation of the grains induced by low to intermediate deformation (up to 30% in thickness reduction) and to following the rotation field using electron backscattered diffraction (EBSD) measurements in a high resolution FEG SEM at different steps of deformation (10 and 20 %). We have especially studied the formation, the evolution and the role of mechanical twins. Additional work on

identification of slip systems by two different approaches (deformation experiments on single crystals as well as numerical *ab initio* and molecular dynamics calculations) are being developed in parallel.

Experimental

The as-received material was hot-rolled and then annealed commercial pure titanium sheet of 1.5 mm thickness with the composition is given in table 1.

Table 1 Chemical composition of commercially pure titanium T40

Element	H	C	N	O	Fe	Ti
Composition (ppm (wt.))	3	52	41	1062	237	Balance

In order to obtain a microstructure with a mean grain size of 30 μm, a grain growth anneal was performed at 750°C for 2 hours. After annealing, the samples were mechanically ground and then electrolytically-polished in a solution of 20 ml perchloric acid in 80 ml methanol at 17V (30 seconds) and a temperature of 5°C before the cold rolling. Then, the samples were cold rolled in two passes, first to 10 % and then to 20% reduction. The cold rolling was performed in the transverse direction of the former hot rolling in order to induce significant reorientations of the C- axes of the grains. To follow the rotation of the individual grains during the deformation, a 500×300 μm^2 area was carefully polished and marked out with four micro-indentations. The orientation of all the grains in this polished area (about 800 grains) was measured by SEM/EBSD before and after each deformation step. The rolling layout is illustrated in Fig. 1. Both sheets of the sandwich were firmly stuck together to avoid any surface sliding during the rolling in

order to maintain a good surface quality. EBSD measurements were performed with a JEOL-6500F SEM with a step size of about 0.77 µm. The evolution of grain orientation during deformation will be presented later both by pole figures and lattice rotation fields.

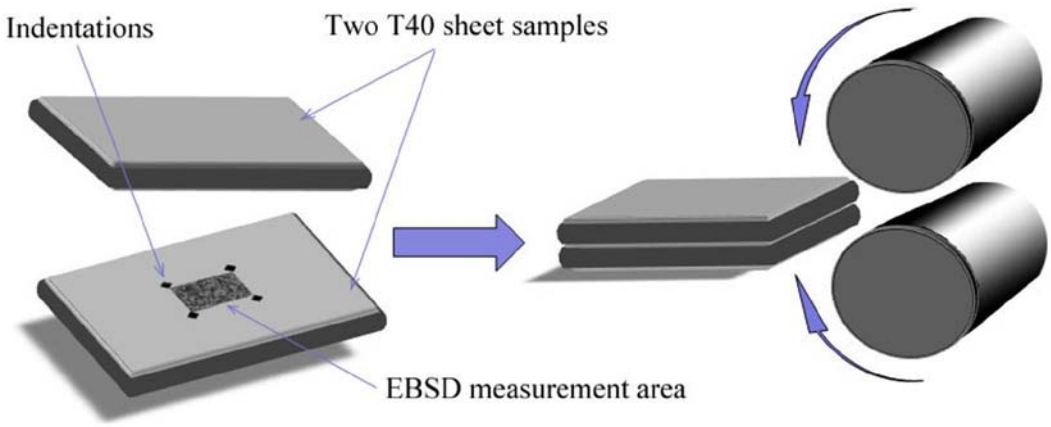

Fig. 1 Successive cold-rolling was performed on sandwich samples. The inner surface was initially polished and the orientation of the grains was measured by EBSD before and after each rolling step.

Results

Initial microstructure and texture

The orientation map of the grain growth annealed sample shown in Fig. 2 reveals a completely recrystallized microstructure. No twins were observed as metals with HCP structure do not undergo recrystallization twinning. The{0002}-pole figure (PF) in Fig. 3 shows two strong maxima at ±35° tilted from ND towards TD, the setting of the coordinate systems, and the definition of the Euler angles being in accordance to Bunge's convention (see e.g., Ref.[13]). The $\{10\bar{1}0\}$ PF displays the maximum pole densities parallel to RD.

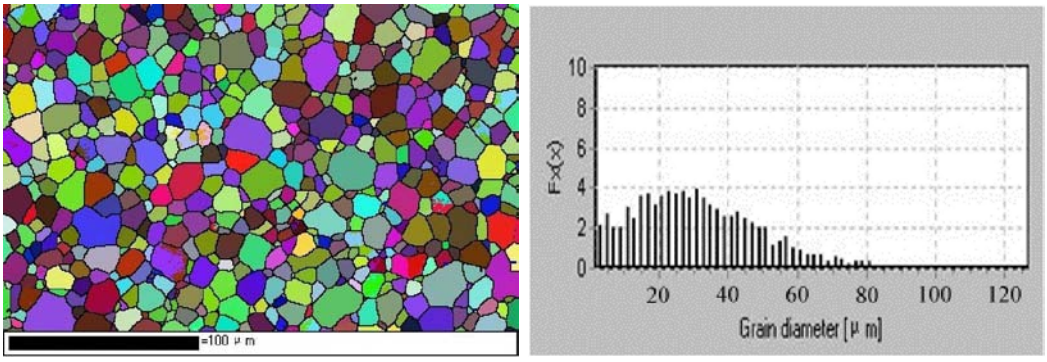

(a) (b)

Fig. 2 (a) Orientation micrograph of the microstructure prior to deformation for the CP-titanium and (b) its grain size distribution.

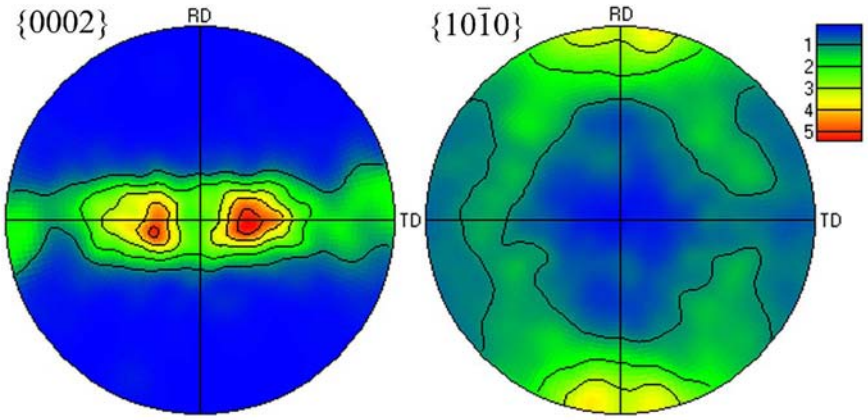

Fig. 3 Pole figures of the CP-Ti sheet after the grain growth annealing. The texture is dominated by the orientation E ($\phi1$ = 0°, Φ=30°, $\phi2$=30°) characterized by {0002}<$1\bar{1}20$> tilted 30° from ND towards TD.

Evolution of the microstructure during cold rolling: effect of twinning

The lattice rotation was studied after each deformation pass. The orientation of each individual grain was carefully determined, so that the lattice rotation of each grain could be brought in relation to the orientation to its own orientation as well as to that of its neighbouring grains. It was found that {$11\bar{2}2$}<$1\bar{1}\bar{2}3$> compression twins (the misorientation between

the twin and its matrix corresponds to 65 ° rotation about their common <$10\bar{1}0$> axis) and {$10\bar{1}2$}<$10\bar{1}\bar{1}$> tension twins (85° about <$11\bar{2}0$>) were most frequently observed. The respective amount of these two twinning modes was further presented by means of the misorientation-angle distributions in Fig. 4. It is seen that at 10% deformation (Fig. 4 (b)), 65° misorientation occurs most frequently, suggesting that {$11\bar{2}2$} twinning was predominant at this deformation stage. This result is reasonable considering that the initial orientation favors the occurrence of this compression twin. Whereas when deformation continues to 20%, ($10\bar{1}2$) tension twinning was remarkably increased (Fig. 4 (c)).

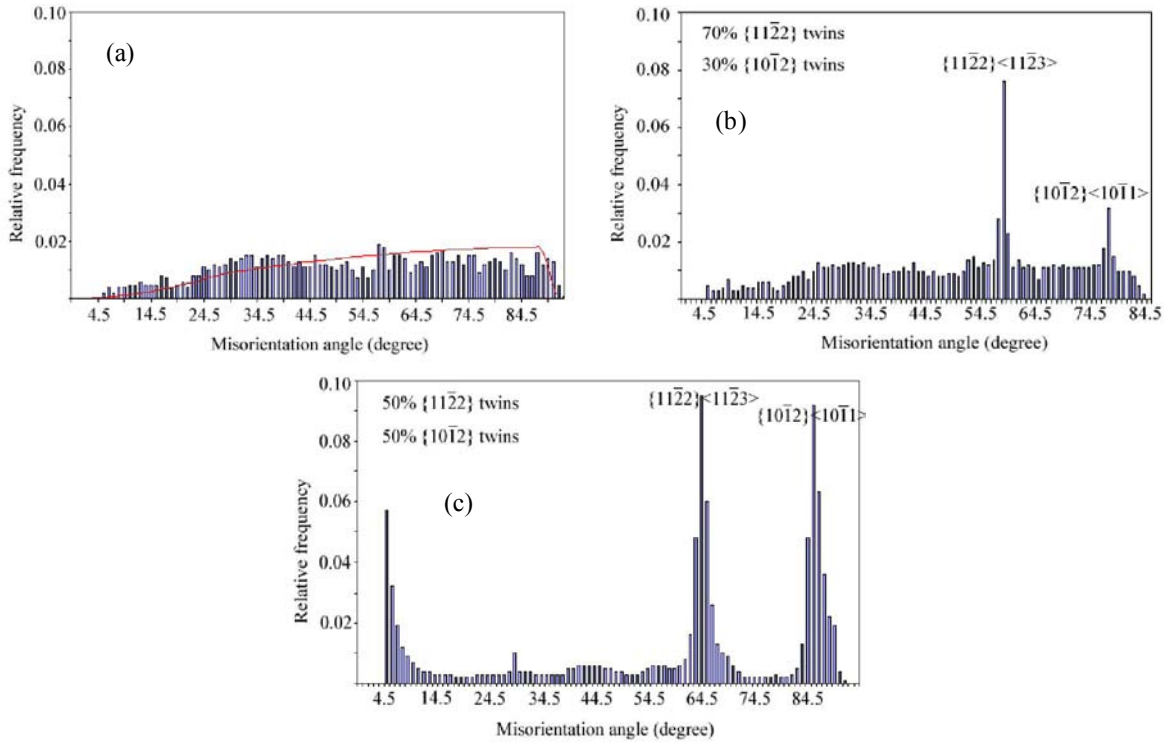

Fig. 4 Misorientation-angle distributions of samples deformed to (a) 0%, (b) 10% and (c) 20% reduction.

Lattice rotation fields and texture development

The orientation analysis could be studied from the microscopic viewpoint of the crystal reorientation step by step, in terms of the lattice rotation flow field. A small arrow is plotted between the initial grain orientation and the final grain orientation. This field of small arrows offers a graphical representation of the flow field. The orientation flow field can be defined and plotted in the Euler space, and represents an efficient tool to describe the texture evolution through modeling, e.g. Clement and Coulomb (1979) [13], Bunge and Esling (1984) [14]. In the present case of hexagonal material, due to the particular importance of the c-axes, we choose to plot the small arrows linking the initial orientation and the final orientation in the two dimensional pole figures of the c-axes. For the further discussion, it was of interest to plot separately the rotation flow field of the grains having no twinned part on the one hand (Fig.5 (a)) and the rotation flow field of the matrix part of the grains presenting twinned parts inside the grains (Fig. 5 (b)). Both orientation flow fields are similar, but for a smaller amplitude of the rotation of the matrix of twinned grains, as compared to the grains without twins.

The orientation analysis could be also studied from the macroscopic viewpoint of development of crystallographic texture, and presented in the classical representation of pole figures.

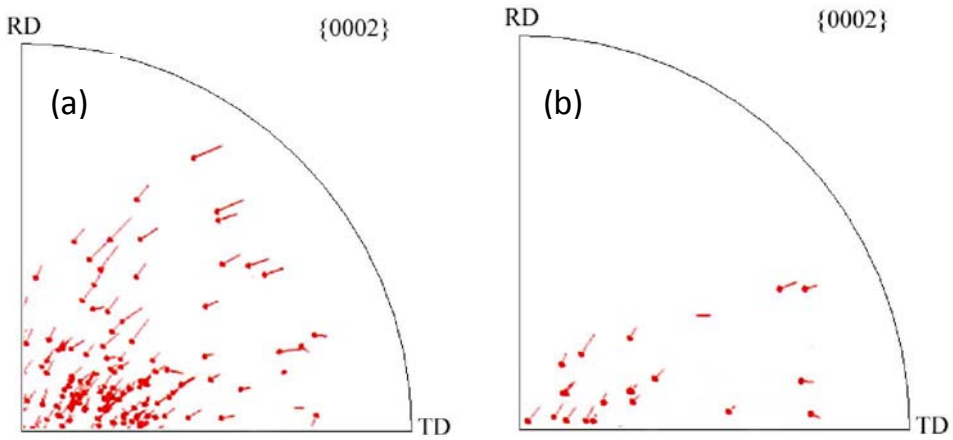

Fig. 5 (a) Lattice rotation field in grains showing no twins. (b) Lattice rotation field in untwinned part or matrix of grains showing twins.

Orientation analysis indicates that at 10% reduction, the c-axis of the grains with $\{10\bar{1}2\}$ twins (tension along c-axis) is oriented close to the rolling direction, as shown in Fig. 6 (a); whereas that of the grains with $\{11\bar{2}2\}$ twins (compression along c-axis) is oriented close to the sample normal direction, as shown in Fig. 6 (b). These results are coherent with the theory (Fig. 7). The c-axis of the $\{10\bar{1}2\}$ and $\{11\bar{2}1\}$ twinned part in each grain is systematically oriented close to a stable orientation belonging to the rolling texture component, however, the $\{11\bar{2}2\}$ twinning leads the c-axis of the twinned part oriented close to the rolling direction i.e. to an unstable orientation. As shown in Fig. 8, the $\{10\bar{1}2\}$ twinning gives an 84.78°misorientation of c-axis and illustrated with blue arrow in this figure. Likewise, the $\{11\bar{2}2\}$ twinning gives a 64.62°misorientation of c-axis and shown with red arrow. Green area delimits the stable orientation belongs to the rolling texture (characterized by c axes tilted 30 from ND to TD). Form the figure, we can see clearly that the $\{10\bar{1}2\}$ twinning transfer the

orientation of matrix to the stable orientation and $\{11\bar{2}2\}$ twinning acts reversely.

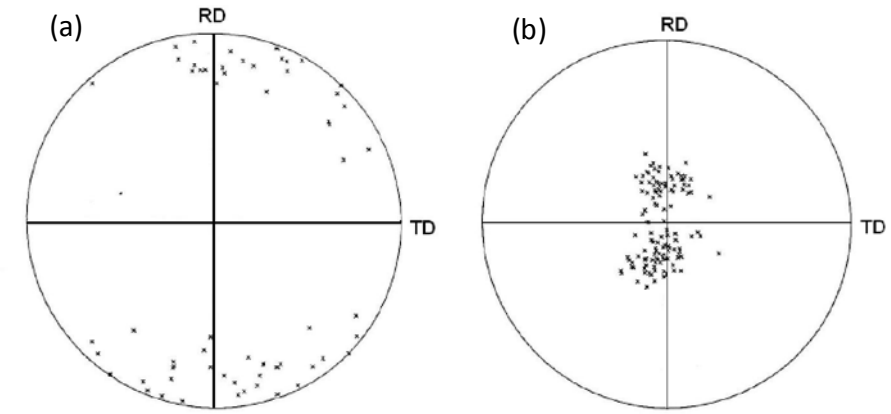

Fig. 6 (a) {0002} -Pole figure of grains having $\{10\bar{1}2\}$ twin and (b) {0002} Pole Figure of grains having $\{11\bar{2}2\}$ - Twin (10% deformation).

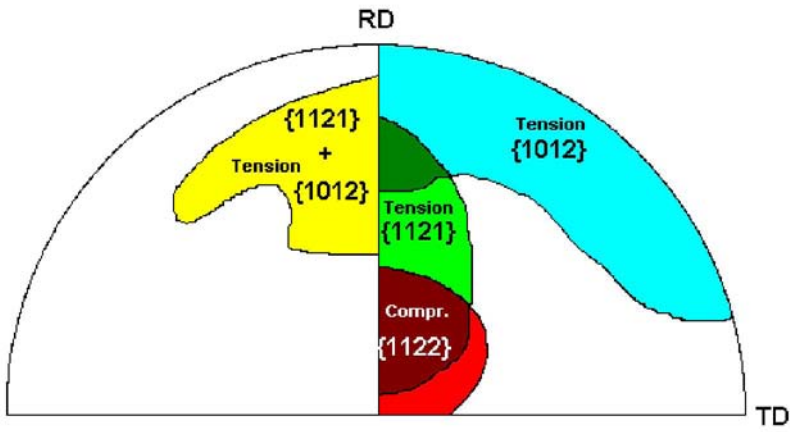

Fig. 7 (0002) Pole Figure showing schematically the orientation domains of the c-axes of the grains in which the indicated twinning is expected to be activated (theoretical).

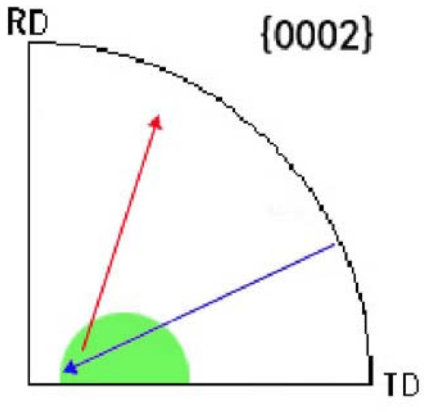

Fig. 8 Misorientation of c axes caused by $\{10\bar{1}2\}$ twinning (blue arrow) and $\{11\bar{2}2\}$ twinning (red arrow).

Secondary twinning

Due to the technique used in the present work, we can follow the evolution of the twins in each grain. Fig. 9 shows one selected sample area before and after each deformation pass. In the figure, the blue lines represent the $\{10\bar{1}2\}$ twin boundaries and the red lines the $\{11\bar{2}2\}$ twin boundaries. Interestingly it is found that tension twins and compression twins can coexist in one and the same grain (Fig. 9). From studies of the literature, we could not find an explanation for this coexistence which was initially unexpected.

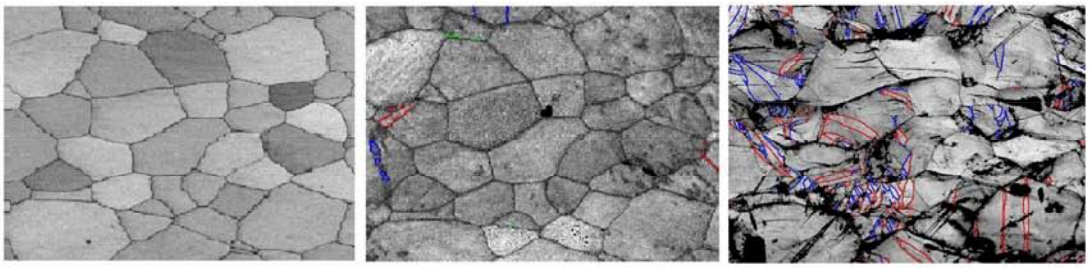

(a) (b) (c)

Fig. 9 Orientation micrograph of one selected area (a) before rolling, after (b) 10% and (c) 20% rolling. Blue lines: $\{10\bar{1}2\}$ twin boundaries; red lines: $\{11\bar{2}2\}$ twin boundaries.

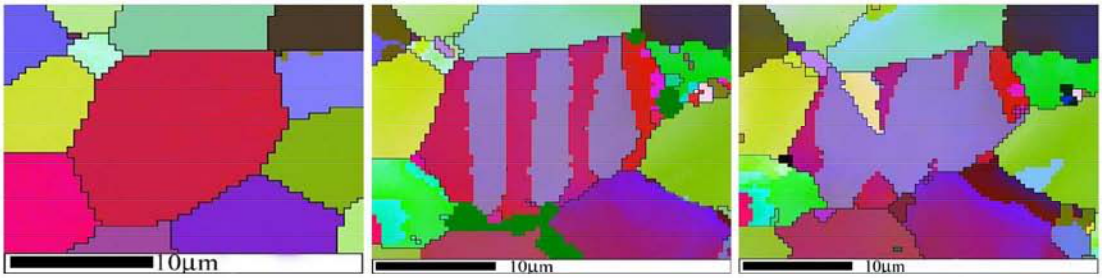

(a) (b) (c)

Fig. 10 (a) Initial grain with c axis oriented close to the normal direction (red); (b) 10% deformation: $\{11\bar{2}2\}$ compression twins outlined by red lines; (c) 20% deformation: a part of $\{11\bar{2}2\}$ twins undergoes secondary $\{10\bar{1}2\}$ tension twinning, as outlined by blue twinning boundaries delimiting the tension twin (in yellow colour).

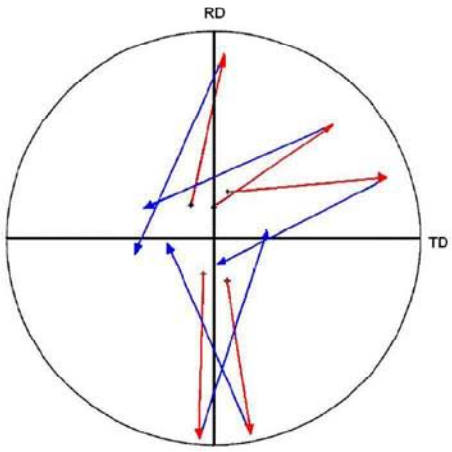

Fig. 11 Trajectory of the reorientation by $\{10\bar{1}2\}$ secondary twinning in $\{11\bar{2}2\}$ primary twins. Red: reorientation by $\{11\bar{2}2\}$ compression twins; blue: reorientation by $\{10\bar{1}2\}$ tension twins.

Fig. 10 shows a grain with its c-axis oriented close to the sample normal direction (ND). The $\{11\bar{2}2\}$ compression twins appear when the deformation reaches 10% (Fig. 10(b)). However, when deformation reaches 20%, the $\{11\bar{2}2\}$ twin spreads to merge across almost the entire grain and then the $\{10\bar{1}2\}$ tension twin is activated in the interior of the $\{11\bar{2}2\}$ twin. This occurrence of second order twins can be observed in all such oriented grains. Without the initial orientation information of the grain, we could not easily have distinguished the initial matrix from the twins. In fact after 10% deformation, the initial matrix shrinks considerably; with residues remaining just between the compression twins such that the large twinned area becomes the "new matrix" for the further tension twins.

This appearance of the $\{10\bar{1}2\}$ tension twin inside the $\{11\bar{2}2\}$ compression twin is the so-called secondary twinning. In fact, as we have indicated, the formation of $\{11\bar{2}2\}$ twinning brings the c-axis of the twinned part far out of the stable orientation range. The twinned part is favorably oriented to initiate a tension twin. Then the $\{10\bar{1}2\}$ tension twin forms, bringing the c-axis of the newly twinned part to a stable orientation. The trajectory of the c-axes orientation evolution during these twinning processes is indicated in the {0002} pole figure, Fig. 11.

Effect of the orientation of the neighbouring grains: heterogeneous deformation

In large grains, different domains in the one and the same grain may undergo different lattice rotations. Fig. 12 presents a large grain (green color) in which several parts have experienced different lattice rotations.

The numbers inside the small neighboring grains give the misorientations of the c-axes with respect to the c-axis corresponding to the mean orientation of the large green grain. We can study here the respective rotations of the domains inside the large green grain, notably in the neighbourhood of the grain boundary, and thus estimate the influence of the neighbouring grains. In any case the rotation of the grain interior is smaller than that of the part close to the grain boundary, especially when the neighbouring grains are highly misoriented with respect to the investigated domain.

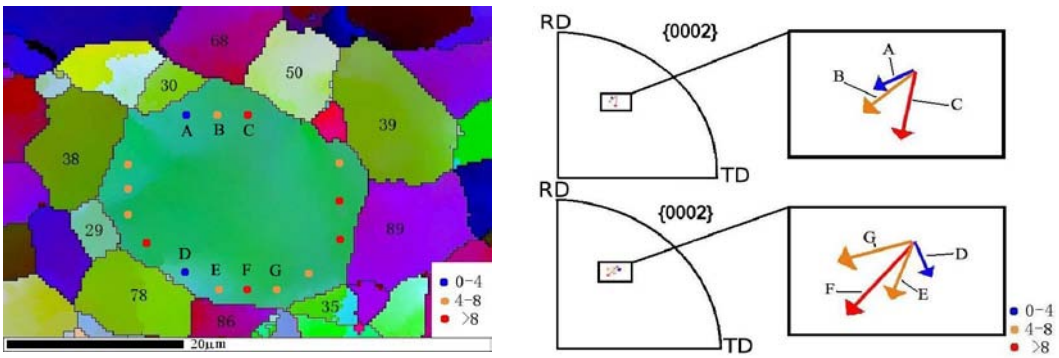

(a) (b)

Fig. 12 Effect of the neighboring grains on the lattice rotation. (a) Misorientation of the c-axes of neighboring grains (numbers inside the neighboring grains) with respect to the large grain they surround and reorientation of the c-axis in the regions A, B…in the neighborhood of the grain boundary (color code in the inset). (b) Illustration of the reorientation of the c axes in the various boundary regions A, B…of the large green grain.

Discussion

Comparison of the rotation of the matrix part of the grains containing twins with the rotation of the untwinned grains indicates that the lattice rotation in the two cases are similar, even if the amplitude of the rotation in the non-twinned part of the twinned grains is relatively smaller.

This tends to show that the main effect of twinning is to create a newly oriented zone (a new grain) and does not induce additional deformation mechanisms in the remaining matrix part of the grain. In other words, the deformation mechanisms in the matrix part of the twinned grains remain the same as those in the untwinned grains. The reorientation induced by $\{11\bar{2}1\}$ and $\{10\bar{1}2\}$ twinning tends to orientate the c-axes close to stable orientations. Thus, there is no tendency for secondary twinning to occur within such twins.

The secondary twinning only takes place in the $\{11\bar{2}2\}$ compression twins whose c-axes are orientated far away from the stable texture orientation. In such a case, the new and major twins appearing inside the $\{11\bar{2}2\}$ twins are $\{10\bar{1}2\}$ tension twins. This explains why when deformation is increased from 10% to 20% the amount of $\{10\bar{1}2\}$ tension twin drastically increases. The c-axis of this secondary twin orientates towards to the stable orientation. We could hardly observe the presence of any third-order twin, even after much higher deformation. This can be easily understood by the relation between the geometrical and energetical characteristics of twinning (and by the mean free path necessary for the formation of a twin). In fact, in titanium alloys it is difficult to induce twinning once the grain size in the matrix drops below the range of about 10 µm.

The great benefit of the present method is that we can follow the deformation process step by step. For example, in the grains having their initial c-axis close to ND for which secondary twinning occurs inside the primary twins, we can clearly discriminate the initial matrix from the

primary twins thanks to the in-situ orientation information. In this case the primarily twinned area is much larger than the remaining matrix and thus represents the “new matrix” for the subsequent secondary twinning.

The effect of the neighboring grains slightly modifies the orientation in the vicinity of the grain boundary, and leads to a larger spread in orientation when the neighboring grain is strongly misoriented with respect to the considered grain. The detailed experimental study of the complex twinning conditions in hexagonal materials may be helpful to the implementation of mechanical twinning in models and codes of polycrystalline plasticity. A thorough study of the implementation of mechanical twinning in a Grain Interaction Model and the application to magnesium alloys [16] can be read with interest in this special volume of AEM.

Conclusion

Twinning occurs in grains that have particular orientations. Generally, the reorientation induced by twinning aligns the c-axis of the twinned part to the stable rolling texture orientations, so that no further secondary twinning can be induced. Secondary twinning occurs only when the primary twinning orientates the c-axis of the primary twins far away from the stable orientations (this is generally the case for the $\{11\bar{2}2\}$ twinning). The formation of the $\{10\bar{1}2\}$ secondary twin inside the $\{11\bar{2}2\}$ primary twin results in a reorientation of the c-axis of the secondary twin to a stable orientation. Only a little amount of second order twinning could be observed and twinning of higher than second order was never found.

The rotation of the matrix-part of the grains having twins is similar to that of the non-twinned grains with similar orientation. The twinned part of a grain can be considered as a new grain. When twins grow within the grain, they can consume almost the whole matrix. Special attentions should be paid when determining the twinned volume fraction. Thanks to the EBSD measurement, a strong increase of the twinned volume could be demonstrated. This contradicts the conventional judgement that the twinned part is always the smaller part in a twinned grain, as concluded by optical microscopy. Only step by step EBSD orientation mapping allows an unambiguous determination of the twinned volume fraction. The confirmation that the order of twinning never exceeds the second order is very useful for the modelling of plasticity in polycrystalline metals, such that the order allowed for twins should be restricted to only the first and second order (also called double twins).

References

[1]. N. Gey, M. Humbert, M. J. Philippe, Y, Combres, Mater. *Sci. Eng. A.* **1997**, *230*, 68.

[2]. H. P. Lee, C. Esling, H. J. Bunge, *Textures and Microstructures*. **1988**, *7*, 317.

[3]. M. J. Philippe, C. Esling, B. Hocheid, *Textures and Microstructures*. **1988**, *7*, 265.

[4]. M. J. Philippe, M. Serghat, P. V. Houtte, C. Esling, *Acta Metall*. **1995**, *43*, 1619.

[5]. J. J. Fundenberger, M. J. Philippe, F. Wagner, C. Esling, *Acta Mater.* **1997,** *45*, 4041.

[6]. A. Akhtar, *Metall. Mater. Trans. A.* **1975**, *6*, 1105.

[7]. P. G. Partridge, *Metall Rev*. **1967,** *12*, 169.

[8]. G. W. Groves, A. Kelly, *Phil Mag*. **1963,** *8*, 877.

[9]. D. R. Thornburg, H. R. Piehler, *Titanium Sci. Technol*, *Plenum Press.* **1973**, *2*, 1187.

[10]. Y. B. Chun, S. H. Yu, S. L. Semiatin and S. K. Hwang, Mater. *Sci. Eng. A.* **2005**, *398*, 209.

[11]. X. Wu, S. Kalidindi, C. Necker, A. Salem, *Acta Mater*. **2007**, *55*, 423.

[12]. G. Proust, C. Tomé, G. Kaschner, *Acta Mater*. **2007**, *55*, 2137.

[13]. H. J. Bunge, C. Esling, J. Muller, *J. Appl. Crystallogr.* **1980**,13, 544

[14]. A. Clement, P. Coulomb, *Scripta Metall.* **1979**, *13*, 899.

[15]. H. J. Bunge, C. Esling, *Scripta Metall.* **1984**, *18*, 191.

[16]. S. Mu, T. Al-Samman, V. Mohles, G. Gottstein, *AEM.* **2010**, DOI:10.1002.

Chapter 4: Variant selection in primary twins, secondary twins and double twins

In this chapter, with the purpose of studying the mechanisms governing the selection of specific twin variants, we performed some calculations of Schmid factor SF, deformation energy factor and some geometrical factors in primary and secondary twins. We came to the conclusion that the Schmid and energy factor plays an important role in variant selection during primary and secondary twinning. It is suggested that rank (or level) of the deformation energy of each variant should be adopted as the main criterion in predicting the variant selection, and the Schmid factor used as an additional second criterion. We also extended our discussion to the various twinning behaviors of {11-22} and {10-12} primary twins. The {11-22} twin shows a behaviour of multiply twin variants system (MVS) and the {10-12} twin shows predominant variant system (PVS) and these mainly result from the orientation relationship between stress components and the parent grain.

A Study of Twin Variants Selection and Twin Growth in Titanium

Lei Bao[a,b], Christophe Schuman[a], Jean-sébastien Lecomte[a], Marie-Jeanne Philippe[a], Xiang Zhao[b], Claude Esling[a]

[a] *LEM3 - UMR CNRS 7239 Université Paul Verlaine-Metz - Île du Saulcy - 57045 METZ Cedex 1 - FRANCE*

[b] *Key Lab for Anisotropy and Texture of Materials (Ministry of Education), Northeastern University, Shenyang, 110004 China*

Abstract: An in depth analysis on twin variant selection and twin growth character during compression by means of "interrupted in situ" EBSD orientation measurement is carried out. An experimental verification of the use of Schmid's law as a criterion for selecting twin variants is performed and the result is positive. Twin variants having Schmid factors higher than 0.4 have a good chance to be activated. Twin growth exhibits two modes: {11-22} twin shows a tendency to multiple variants system (MVS) and {10-12} twin shows predominant variant system (PVS). Schmid factor also plays an important role in MVS and PVS.

Keywords*: Twin; Twin variants; Twin growth; Schmid factor; Titanium.*

Introduction

Twinning is a particularly important deformation mode in α titanium [1-6]. Twinning process strongly depends on the crystallographic orientation of the matrix. The simple Schmid factor allows to calculate the resolved shear stress on the twin system from the applied macroscopic stress. Titanium exhibits two major twinning systems at room temperature, {10-12} twin and {11-22} twin. The {10-12} system is referred to as tension twin ({11-22} as a compression twin) because it only activates under tension (compression) load along the c axis of the matrix [7]. Hence, Schmid's law loses effectiveness of selecting twin type because of the directionality of twinning, and it is not clear whether Schmid's law is an applicable criterion in the selection of twin variants. The development of an efficient activation criterion is essential when employed to model the deformation behavior of

materials with twinning as their important deformation mechanism, such as HCP metals.

This work is concerned with experimental verification of Schmid' law as a criterion for selecting twin variants, and extend to a study of the twin growth as well. In order to trace the evolution of individual orientations during the deformation and the growth of twin, an interrupted "in situ" EBSD investigation method [8] was proposed and applied. In this method, we concentrate on a sufficient amount of grains and perform EBSD measurement on these grains in each step of the deformation. Therefore, we can acquire the detailed orientation information of these grains in the interrupted deformation step.

Experimental

The material used in this investigation is a cold-rolled commercially pure titanium T40 sheet with 1062 ppm (wt.) oxygen. The sheet was annealed at 800°C for 2 hours to allow the deformed microstructure to be fully recrystallized. The final average grain size is 200μm. A four-stepped compression test was performed at room temperature at the rate of 0.5mm/min. The total thickness reduction after each step is 8%, 16%, 24% and 35%, respectively. The EBSD orientation measurement was performed on the same sample area after each deformation step with a JEOL 6500F field-emission-gun SEM equipped with EBSD acquisition camera and HKL channel 5 software.

In order to obtain statistically representative results, 100 twinned grains are randomly selected to analyze the twin variant selection role and twin

growth behaviors. To eliminate the effect of grain size, the selected grains have a similar size.

Results

Initial texture

Figure 1 shows the {0002} and {10-10} pole figures (PFs) of the as-annealed Ti40 sheet. It is seen that the initial texture is characterized by two strong maxima at ±30° tilted from ND towards TD in the {0002} PF and the maximum density of poles in RD in the {10-10} PF. It means that the majority of grains have their c axes close to the compressive force direction, i.e. the normal direction (ND) of the sample. Clearly, the orientation of these grains is quite favorable for the activation of {11-22} compression twin.

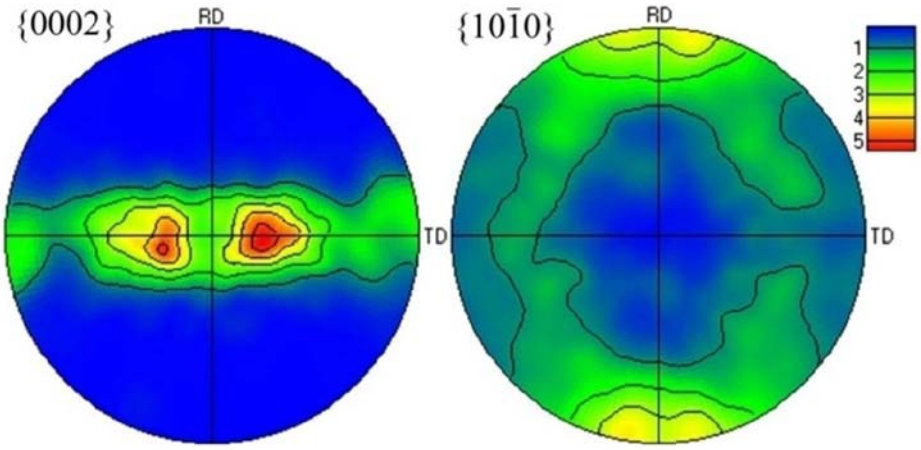

Figure. 1: The initial texture presented in the pole figures of {0002} and {10-10}.

The selection of twin variants

In the present study, after 8% deformation, both {10-12} tension twin and {11-22} compression twin are spotted in some grains but {11-22}

compression twin is more frequent. This result is coherent with the initial texture. Theoretically, there are six twin variants in each twin family [1], but in one initially un-deformed grain, only a limited number of variants are active in each twinning mode. Due to the crystallographic symmetry, the maximum number of variants for the {10-12} tension twin is two, whereas that for the {11-22} compression twin can reach four, depending on the proximity of the c-axis to the applied force. With the increase of the amount of deformation, twinning occurs in more grains.

The growth of twin

Figure 2 shows the EBSD maps of two typical grains at the initial state, 8% and 16% deformation, one containing {11-22} compression twin (Figure 2 (a)) and the other {10-12} tension twin (Figure 2 (c)). Figure 2 (b) and (d) indicate the SF for each twin variant (active variants are highlighted in red). It appears that the growth of {11-22} compression twin variants and {10-12} tension twin variants exhibit different features. After {11-22} compression twin lamellae form, they grow and expand rapidly along the shear direction. Subsequently, the rapid expansion causes the growing variants to intersect with each other. The collision between lamellae of different variants blocks the respective growth of one another. The subsequent deformation progressed by the formation of new twin lamellas of the same variants (or repeated twin nucleation) in the un-deformed matrix contoured by the already formed twin lamellae with the progress of the deformation (Figure 2(a)).

However, for the {10-12} tension twin, repeated twin nucleation occurs at the very beginning of the deformation. The twin lamellae also rapidly grow in the shear direction until they intersect the grains boundaries. Different from the compression twinning, it accommodates the subsequent deformation mainly by thickening the already formed twin lamellae, which transforming the whole initial grain into twin, as shown in Figure 2 (c).

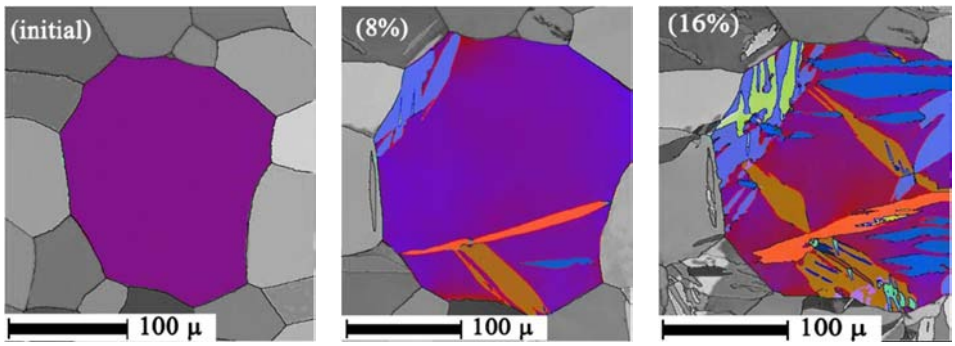

(a)

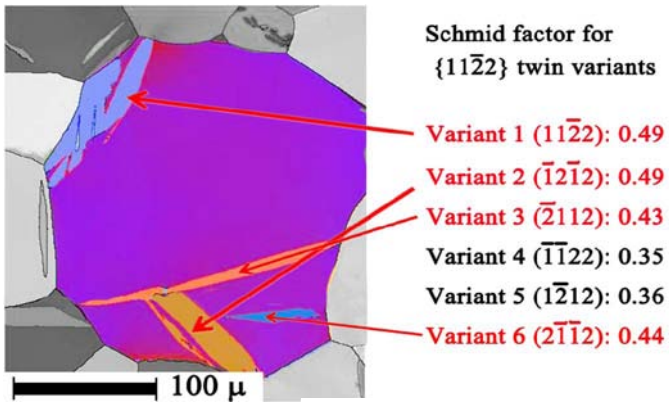

(b)

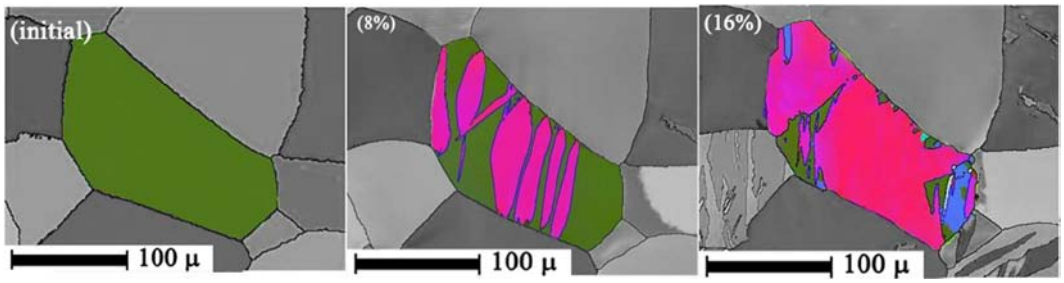

(c)

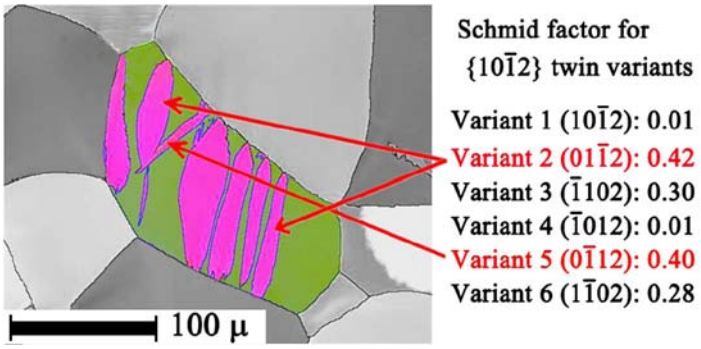

(d)

Figure 2 (a) and (c) show EBSD maps of two grains at the deformation steps of initial, 8%, 16% , (a) with {11-22} compression twin variants and (c) with {10-12} tension twin variants. (b) and (d) indicate the Schmid factors for each twin variant (active variants are highlighted in red).

Discussion

In this study, {11-22} compression twinning and {10-12} tension twinning show quite different twin variant selection and growth characters. {11-22} twin always exhibits three or four variants in one grain and these variants possess large misorientation with respect to each other. We call this multiply variants system (MVS), as shown in Figure 2 (a). However, {10-12} twin exhibit only one or two variants. We call it predominant variant system (PVS), as shown in Figure 2 (c). After growth, they consume almost the whole volume of the initial grain.

In order to study the mechanisms that lead to the selection of specific twin variants, the misorientation between the variants of the respective {11-22} and {10-12} twins is calculated and listed in Table 1. Figure 3 shows the schematic presentation of orientation of {11-22} and {10-12} twin variants with respect to the matrix. As a compression twin, {11-22} twin forms under the resolved compressive force that is parallel to the c axis of the matrix. Since all the six {11-22} twin variants have symmetrical relations by 60° rotation around c axis, the six variants should have the same Schmid factor under a resolved compressive force which is parallel to the c axis. In our experimental observations, for the grains with {11-22} compression twin, the applied compressive force always slightly deviates from the c axes, therefore usually three or four variants have relatively high Schmid factors and these variants are activated simultaneously. In Table 1, it is can be seen that the misorientation angles between the {11-22} compression twin variants range from 51.2°to 77.29°, so in one grain, {11-22} twin lamellae belonging to different variants are always at large angles to each other.

In the case of {10-12} tension twin, it forms under the resolved compressive force that is perpendicular to the c axis of the matrix. In this situation, only two variants have high Schmid factors. The twin planes of these two variants are related by a 180° rotation symmetry around the c axis (V1 and V4, V2 and V5, V3 and V6 in Table1 and Figure 3 (b)) and the misorientation between the two variants is only 9.98°. Hence, in one grain, {10-12} twin lamellae belonging to these two variants are always parallel or near parallel.

Normalized Schmid factor (*NSF*) [9] is used in the present work to study whether Schmid factor is decisive for the variant selection. In a given grain,

the NSF of this grain equals to the SF of the active variants (SF_a) divided by the highest SF (SF_h) of the six possible variants. Figure 4 (a) show the normalized SF (NSF) versus SF_a. Note that the {10-12} and {11-22} twins are studied separately and represented by different colors: blue for {10-12} and red for {11-22}. If NSF=1, the active twin variant is the one with the highest SF; if NSF<1, an additional or another twin variant is active instead of the one with the highest SF. The frequency of the normalized Schmid factor is displayed in Figure 4 (b). The interest of Figure 4 is that it provides the information to what extent the SF of the active variants deviate from the highest SF in the case of an active variant with non-highest SF. As shown in Figure 4, the Schmid factors of all the active variants SF_a lie in the range from 0.32 to 0.5 (X axis in Figure 4 (a)) and the NSF that is equal to one has the highest occurrence. The average Schmid Factor of all active twins (SF_a) in the studied grains is 0.43 and the minimum is 0.32. From the results above, it can be deduced that Schmid law is determinant for the activation of the twin variants. However, still in some cases, variants with non-highest SF (NSF<1) are activated. Their activation may be attributed to the microscopic local stress that is deviated from the macroscopic load. In these cases, the Schmid factor of the active twin system with respect to the local stress may be the highest.

Table 1 The misorientation angle and axis between each pair of variants of respectively {11-22} twin and {10-12} twin.

{11-22} twin						
	variant (11-22)	variant (-12-12)	variant (-2112)	variant (-1-122)	variant (1-212)	variant (2-1-12)
variant (11-22)	0°	60.00° [11-21]	77.29° [1-870]	51.20° [1-100]	77.29° [8-1-70]	60.00° [-1-12-1]
variant (-12-12)		0°	60.00° [-12-1-1]	77.29° [8-7-10]	51.20° [10-10]	77.29° [1780]
variant (-2112)			0°	60.00° [-2111]	77.29° [71-80]	51.20° [01-10]
variant (-1-122)				0°	60.00° [-1-121]	77.29° [-18-70]
variant (1-212)					0°	60.00° [1-211]
variant (2-1-12)						0°

{10-12} twin						
	variant (10-12)	variant (01-12)	variant (-1102)	variant (-1012)	variant (0-112)	variant (1-102)
variant (10-12)	0°	60.00° [-1010]	60.75° [71-80]	9.98° [-12-10]	60.75° [-8170]	60.00° [10-10]
variant (01-12)		0°	60.00° [0-110]	60.75° [-18-70]	9.98° [-2110]	60.75° [-1-780]
variant (-1102)			0°	60.00° [0-110]	60.75° [-18-70]	9.98° [-2110]
variant (-1012)				0°	60.00° [10-10]	60.75° [-7-180]
variant (0-112)					0°	60.00° [01-10]
variant (1-102)						0°

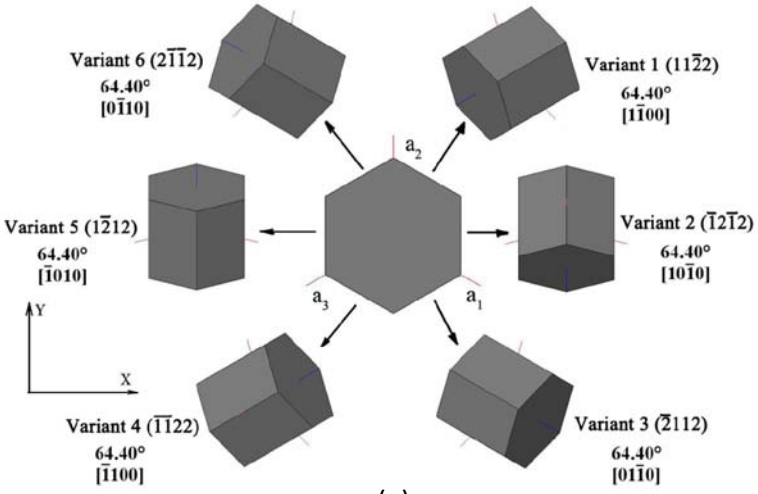

(a)

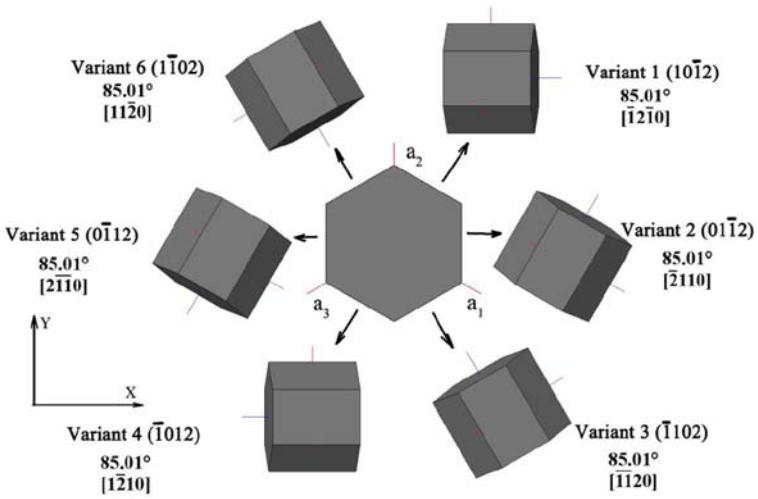

(b)

Figure 3 Schematic presentation of twin variants of {11-22} twin (a) and {10-12} twin (b).

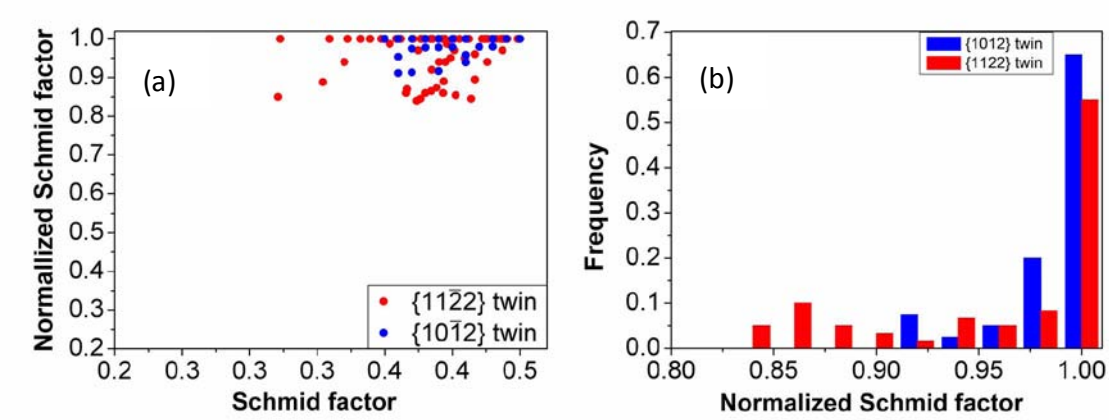

Figure 4 Distribution of NSFs (a) and their frequency (b).

Conclusions

In this work, we performed an analysis on twin variant selection and twin growth in polycrystalline titanium during small reduction compression by "interrupted in situ" EBSD measurement. The following results can be concluded:

1. Schmid' law is an appropriate criterion for twin variants selection. Twin variants with Schmid factors higher than 0.4 have a good chance to be activated.
2. In compression, when the c-axis of the initial grain is close to the compression load, the SFs of the six variants are close and high, showing MVS.
3. In contrast, {11-22} twin always exhibit only one variant per grain. This predominant twin variant grows fast until almost no matrix is left, showing PVS.

Acknowledgement

This work was supported by the Federation of Research for Aeronautic and Space (Fédération de Recherche pour l'Aéronautique et l'Espace Thème Matériaux pour l'Aéronautique et l'Espace : project OPTIMIST (optimisation de la mise en forme d'alliage de titane).

References

[1] P. G. Partridge, *International Materials Reviews*. **1967**, 12, 169.
[2] U. F. Kocks, D. G. Westlake, *AIME MET SOC TRANS.* **1967**, 239, 110.
[3] H. Conrad, G. London, V. Damiano, *Plenum,* New York, **1968**, 153.
[4] M. H. Yoo, *Metallurgical and Materials Transactions A,* **1981**, 12, 1543.

[5] M. J. Philippe, C. Esling, B. Hocheid, *Textures and Microstructures,* **1988**, 7, 265.

[6] M. J. Philippe, M. Serghat, P. Houtte-Van, C. Esling, *Acta Metallurgica et Materialia,* **1995**, 43, 1619

[7] F. D. Rosi, F. C. Perkins, S. S. Seigle, *Trans. Met. Soc. AIME,* **1956**, 8, 115.

[8] L. Bao, C. Schuman, J. S. Lecomte, M. J. Philippe, X. Zhao, L. Zuo, C. Esling, *Computers, Materials & Continua*, **2010**, 15, 113.

[9] L. Capolungo, P. E. Marshall, R. J. McCabe, I. J. Beyerlein, C. N. Tomé, *Acta Materialia,* **2009**, 57, 6047.

A study of variant selection during double twinning in titanium

Lei Bao[a, b], Christophe Schuman[a], Jean-Sébastien Lecomte[a], Marie-Jeanne Philippe[a], Xiang Zhao[b], Claude Esling[a]

[a] *LEM3 - UMR CNRS 7239 Université Paul Verlaine-Metz - Île du Saulcy - 57045 METZ Cedex 1 - FRANCE*

[b] *Key Lab for Anisotropy and Texture of Materials (Ministry of Education), Northeastern University, Shenyang, 110004 China*

Abstract*:* The double twinning in commercial pure titanium (T40) was studied in channel die compression by means of "interrupted in situ SEM/EBSD orientation determination". Particular attention was paid to the twin variant selection during double twinning. All possible misorientations corresponding to the double twin combination of {10-12}, {11-21} and {11-22} twins were calculated with respect to the sample coordinate system. This approach leads to a method for establishing the crystallographic identity of each double twin variant. All the double twin variants are classified into 10 groups according to the crystallography equivalence of the misorientation angle and axis. However, taking the order of the twins into account, double twin variants are classified into 15 rather than 10 groups, since 5 of them depend of the order of the twins.

A new variant selection criterion based on the plastic energy was proposed and it proved an outstanding accuracy up to 85% for predicting the primary twin variant selection and 95% for the secondary twin variant selection. The Schmid factor also gave a fair accuracy of about 50% for the primary twin and 40% for secondary twin variant selection. The twins in the adjacent grains were found to induce the activation of the same variants near the grain boundary in the case the angle between the two twin planes are below 20°. No influence of geometric features was found on the variant selection in double twins.

Keywords: *Titanium; Twinning; Double twinning; Variant selection; interrupted in situ SEM/EBSD orientation determination.*

Introduction

Mechanical twinning is a particularly important deformation mode in α titanium [Vedoya et al. (1988); Philippe et al. (1995); Fundenberger et al. (1997); Zaefferer, (2003)]. It also offers a means to control the properties of titanium such as ductility and fracture strength [Kocks and Westlake (1967); Partridge (1967); Mahajan and Williams (1973)]. At room temperature, three major twinning systems are commonly observed in titanium: the {10-12} twin, the {11-21} twin and the {11-22} twin [Philippe et al. (1988)]. The

{10-12} and {11-21} systems are referred to as tension twin ({11-22} as a compression twin) because it is only activated under tension (compression) load along the c axis of the parent crystal [Rosi et al. (1956)]. Once a twin forms, the crystal lattice of the twin has a misorientation with respect to the former parent crystal lattice, misorientation which is represented by a rotation depending on the twin systemThis orientation change accelerates the occurrence of the secondary twinning inside the primary twin due to a more favorable orientation. The combination of primary and secondary twins is called double twin. In other words, a double twin can be regarded as the structure of a secondary twin inside a pre-existing primary twin [Barnet et al. (2008); Martin et al. (2010)]. In titanium, the double twins combined of the {10-12} tension twin and the {11-22} compression twin are commonly observed in rolling and compression deformation [Bao et al (2010a)]. At present, it is well established that the variant selection in the primary twin generally follow Schmid law [Lebensohn and Tome (1993)], which indicated that the variants with higher resolved shear stress are more likely to be selected. However in the case of secondary twinning, Barnet [Barnet et al. (2008)] have shown that the variant selection does not follow Schmid's law. [Martin et al. (2010)] have shown that in magnesium, Schmid's law is not the only criterion controlling the variant selection, shared volumes and primary to secondary accommodation shears are prevalent.

In this paper, some calculations of Schmid factors, crystallographic geometry, and plastic energy associated with double twinning were performed to investigate the variant selection in double twinning and

reveal the relevant microscale features responsible for the formation of secondary twins. A study on the influences of the twinning on the texture evolution was also carried out. Moreover, an “interrupted in situ SEM/EBSD orientation determination” [Bao et al (2010b)] was adopted. This approach allows to obtain the time resolved information on the appearance of the twin variants, their growth, the interaction between them and the interaction with the grain boundaries or twin boundaries.

Experimental

The material used was a commercial pure titanium T40 sheet of 1.5 mm thickness with the composition given in table 1. First, the sheet was annealed at 800°C for 2 hours to allow the deformed microstructure to be fully recrystallized with a final average grain size of about 200μm.

Table 1 Chemical composition of commercially pure titanium T40

Element	H	C	N	O	Fe	Ti
Composition (ppm (wt.))	3	52	41	1062	237	Balance

The samples with the dimension of 15mm×10mm were prepared, mechanically polished and further electrolytically polished at a temperature of 5°C in a solution of 200 ml perchloric acid in 800 ml methanol at 17V (30 seconds) for subsequent SEM/EBSD measurements. On the polished surface, a 1250×950 μm^2 area was selected and delimited by four micro-indentations. The microstructure and OIM of this selected area was measured by SEM/EBSD before and after each channel die compression step (0, 8, 16, 24 and 35% reduction). The surface with the selected area

was firmly stuck with another polished sample (sandwich like) to avoid any surface sliding during the compression, in order to maintain a good surface quality. The channel die compression layout is illustrated in Fig. 1. SEM/EBSD measurements were performed with a JEOL 6500F field-emission-gun SEM equipped with EBSD acquisition camera with a step size of 0.6 μm at 15KV. The data were acquired and processed with the HKL Channel 5 software from HKL technology.

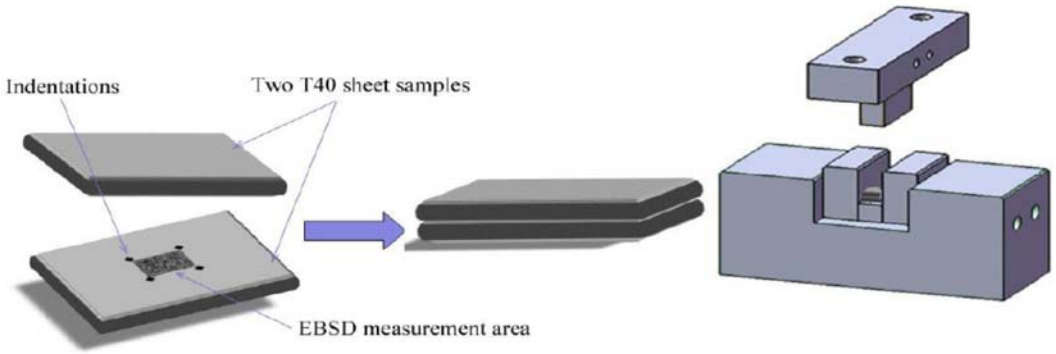

Fig 1: Schematic description of the channel-die set-up used.

In order to obtain statistical representation of the results, 100 twinned grains were randomly selected to analyze the twin variant selection. To eliminate the effect of the grain size, only the grains having similar sizes ranging from 180μm to 220μm were selected.

Results

1. Microstructure and texture

The OIM of the initial sample shown in Fig. 2 (a) reveals a completely recrystallized microstructure. From the pole figures (PF) in Fig. 2 (c), it can be found that the initial texture is characterized by two strong maxima at

±30° tilted from ND (normal direction) towards TD (transverse direction) in the {0002} PF and the maximum pole density in the RD (rolling direction) in the {10-10} PF. It means that the majority of grains have their c axes close to the compressive load direction, i.e. ND of the sample. Clearly the orientation of these grains is quite favorable for the {11-22} compression twinning [Akhtar (1975)].

Fig. 2 (b) exhibits the same area selected as shown in Fig. 2 (a), but after 8% reduction. The boundaries of {10-12} tension twins were marked in blue and the boundaries of {11-22} compression twins in red. Two types of primary twins and two types of double twins were spotted: the {10-12} tension twin (T1 twin) and the {11-22} compression primary twin (C twin), the primary {11-22} compression with the secondary {10-12} tension twin inside (C-T1 double twin) and the primary {10-12} tension with the secondary {11-22} compression twin inside (T1-C double twin).

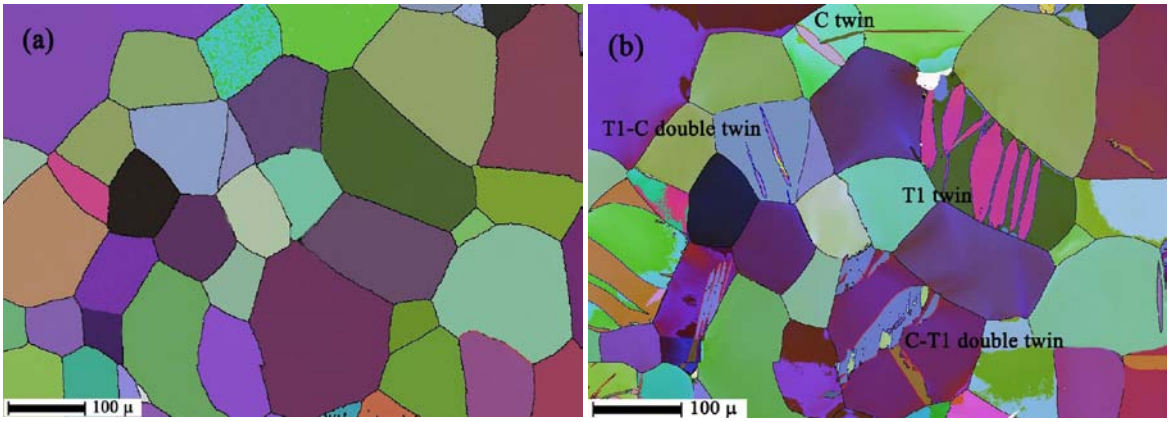

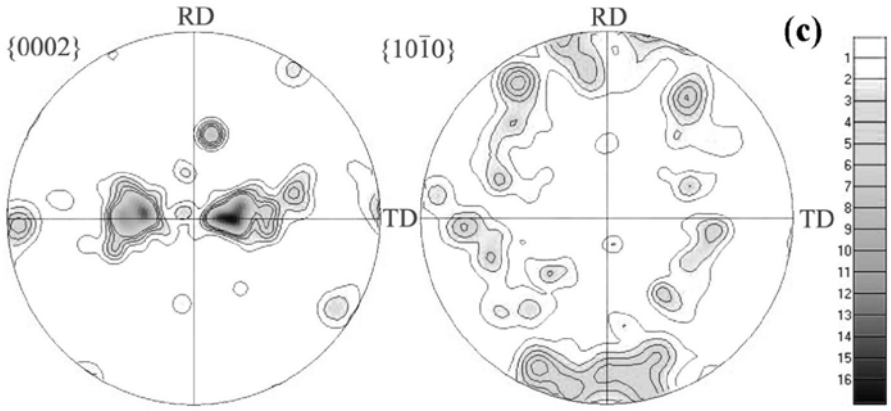

Fig. 2. (a). OIM of the initial microstructure of the T40 titanium. (b). OIM of the microstructure after 8% deformation. Red line represents {11-22} twin boundaries and blue line represents {10-12} twin boundaries. (c). {0002} and {10-10} pole figures of the initial texture.

2. Theoretical misorientations of variants of double twins with respect to the matrix

From the literature [Partridge (1967); Philippe et al. (1988)], it is known that in Ti at room temperature there also exists another {11-21} tension twin (T2 twin), which was not found in the present work. Therefore, in total, 6 types of double twins combined of C, T1 and T2 twins could possibly be expected, , namely C-T1 (a T1 tension twin forms inside a pre-existing C compression twin), T1-C, C-T2, T2-C, T1-T2 and T2-T1. As we know, six variants are possible for each twin system. In the case of double twinning, one double twinning combination could create 36 possible variants with respect to the initial parent grain and thus, the six double twin combinations create 216 possible variants in total. Variants are usually described by the minimum misorientation angle and the corresponding axis with respect to the parent crystal. In addition to the minimum angle-axis parameterization, variants can also be distinguished in the pole figure. In

this study, we made the calculations for all the possible double twins and gave the variants in both representations above, minimum angle-axis and pole figure.

In Table 2, the variants were presented in the minimum angle-axis (ω, d) parameterization. It could be deduced that the misorientation of the 216 variants of double twin can be divided into 10 groups with the same misorientation angle and crystallographic equivalent axes, namely three groups for the combination of C and T1 twins, four groups for the combination of C and T2 twins and three groups for the combination of T1 and T2 twins. Consequently, these 10 variant groups were called geometric variants in this paper.

Table 2. (a) Double twins combined of C and T1 twin.

Group	Minimum angle-axis pair	Affected by the order of twins
A	41.3°<1 -5 4 3>	Yes
B	48.4°<5 -5 0 3>	No
C	87.9°<4 -7 3 0>	No

(b) Double twins combined of C and T2 twin.

Group	Minimum angle-axis pair	Affected by the order of twins
D	29.5°<1 -1 0 0>	No
E	55.0°<5 -10 5 3>	No
F	80.6°<1 -1 0 0>	No
G	86.8°<5 -15 10 3>	Yes

(c) Double twins combined of T1 and T2 twin.

Group	Minimum angle-axis pair	Affected by the order of twins
H	56.9°<4 -14 10 3>	Yes
I	66.5°<5 -15 10 3>	Yes
J	89.4°<4 -12 8 3>	Yes

Another method was employed to represent each individual variant by its c-axis in the {0002} pole figure. Each variant was plotted in the {0002} pole figure with a symbol and a color code corresponding to every set of double twin (Fig. 3). Note that this is a pole figure referenced in a XYZ coordinate frame, i.e. it is not used to describe an orientation with respect to the sample frame, but to represent the misorientation with respect to the parent grain. This is a direct and effective way to study the texture evolution induced by the double twinning. In this representation, the 216 variants could be classified into 15 groups instead of the 10 geometric variants by the minimum angle-axis, because the variants with the misorientation angles of 41.3°, 86.8°, 56.9°, 66.5° and 89.4° are affected by the sequence of the twinning. For instance, although the double twinning in C-T1 respectively T1-C sequence both produce a 41.3° misorientation about a <1-543> axis, they induce a different rotation with respect to the sample coordinate, thus resulting in a different texture evolution by the double twinning (Fig. 3). Hence, the number of double twin variant groups is increased from 10 to 15, and these 15 variant groups were called orientation variants in this paper.

The pole figure provides a clear schematic representation about the misorientation induced by the double twinning. It also demonstrates that, for some specific double twins, the twinning sequence has an effect although these double twins are classified into the same group since they have the same misorientation angle about axes belonging to a same family equivalent by the point symmetry group of the crystal lattice. This should

be noted in particular when simulating the evolution of the texture induced by the double twinning.

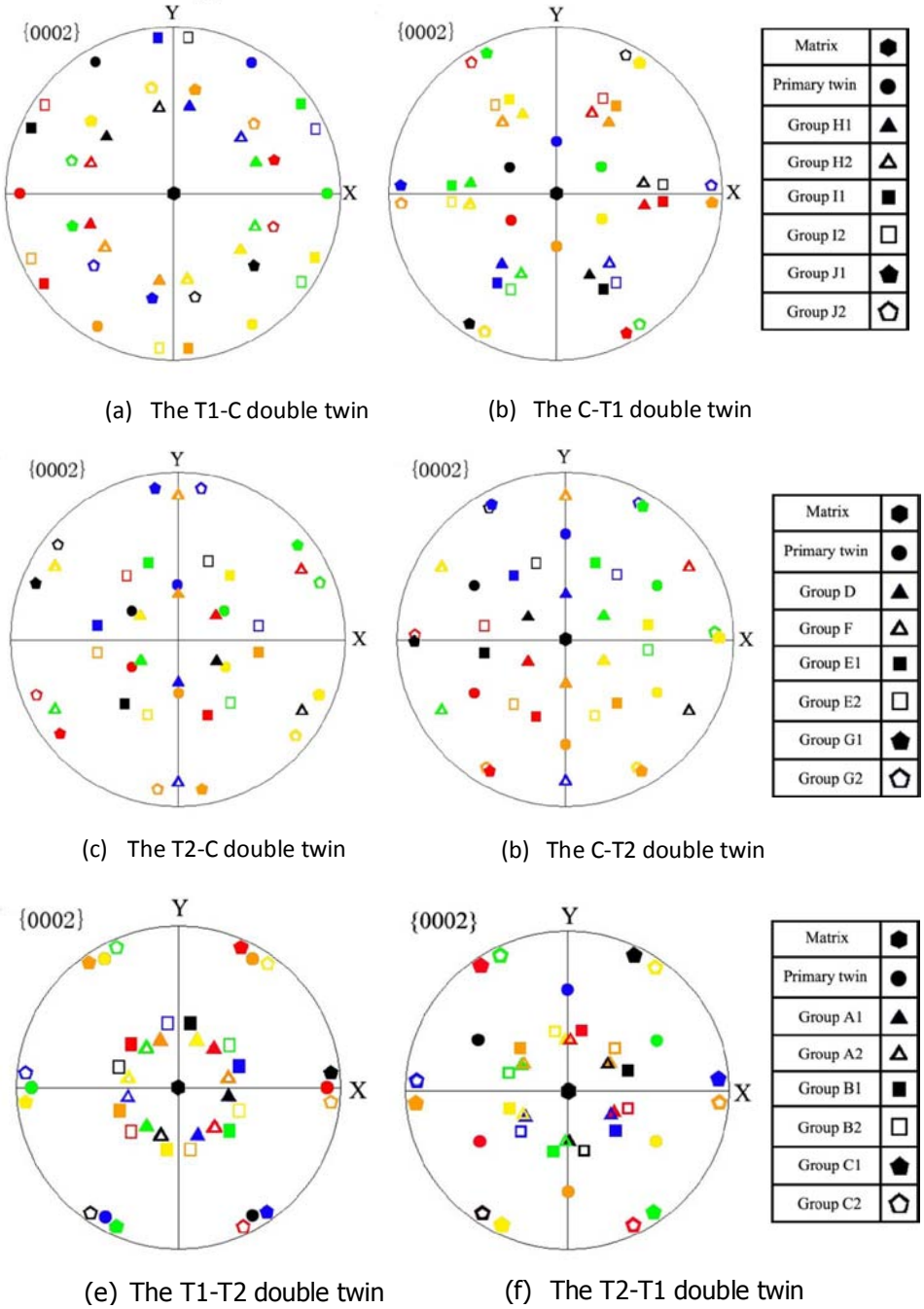

(a) The T1-C double twin (b) The C-T1 double twin

(c) The T2-C double twin (b) The C-T2 double twin

(e) The T1-T2 double twin (f) The T2-T1 double twin

Fig. 3. The {0002} pole figure of all possible double twin variants. The color code relates the secondary twin variants (six symbols) to their respective primary twin variants (filled circle). Each primary twin variant and the six possible secondary twin variants inside are presented with a same color.

3. Variant selection of the double twinning

Since the T2 twin (the {11-21} tension twin) was not found in this study, only the combination of T1 and C was investigated in the experimental study on variant selection for double twinning. To perform a statistical analysis, 100 grains with double twins were systematically studied. C-T1 and T1-C double twins were analyzed separately despite they induce the same misorientation by symmetrically equivalent rotations, namely Group A (41.3° about <1-543>), Group B (48.4° about <5-503>) and Group C (87.9° about <4-730>).

The frequency of the occurrence of each variant group in both C-T1 and T1-C double twins was presented in Fig. 4. It could be seen that the Group B (78.9% in the frequency) predominated over the other two in C-T1 double twin, the Group A was 20% and the Group C was nearly inactivated (1.8%). In the case of the T1-C double twin, the dominant variant group was the Group C (66.7% in the frequency), whereas Group A was 33.3%.

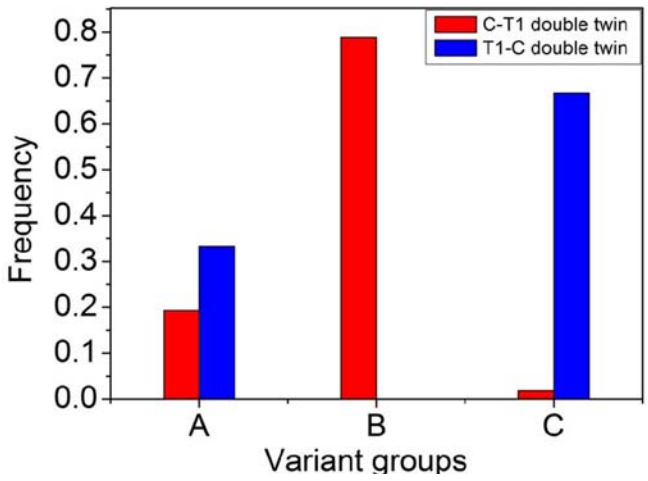

Fig. 4. Frequency of occurrence of double twin variant group A, B and C.

3.1.Schmid factor analysis

Since the Schmid factor (SF) plays an important role in twin variant selection [Lebensohn et al. (1993)], this study first examined the effect of the Schmid factor on the variant selection in the primary and secondary twinning, respectively. For each selected grain, the geometric SF was calculated to examine the resolved stress applied on the twin plane and along the twin shear direction, given the applied macroscopic compressive stress.

Primary twinning

The ranking of the SF corresponding to the active variants of primary twins was shown in Fig. 5 (a) in the form of a histogram. Normalized Schmid factor (*NSF*) [Capolungo et al. (2009)] was adopted in the present work to investigate whether the Schmid's law is conclusive for the variant selection. In a given grain, the NSF of this grain equals to the SF of the active variants (SF_a) divided by the highest SF (SF_h) of the six possible variants. If NSF=1, it means that the active twin variant is the one with the highest SF; if NSF<1, another twin variant is activated instead of the one with the highest SF. The frequency of the NSF was displayed in Fig. 5 (b). The interest of NSF is that it provides the information to what extent the SF of the active variants deviate from the highest SF in the case of an active variant with non-highest SF. As shown in Fig. 5, it can be seen that Schmid's law gives a 50% accuracy in predicting variants selection of the primary twinning. The majority of the primary twins form on the variants with the first or second rank of SF.

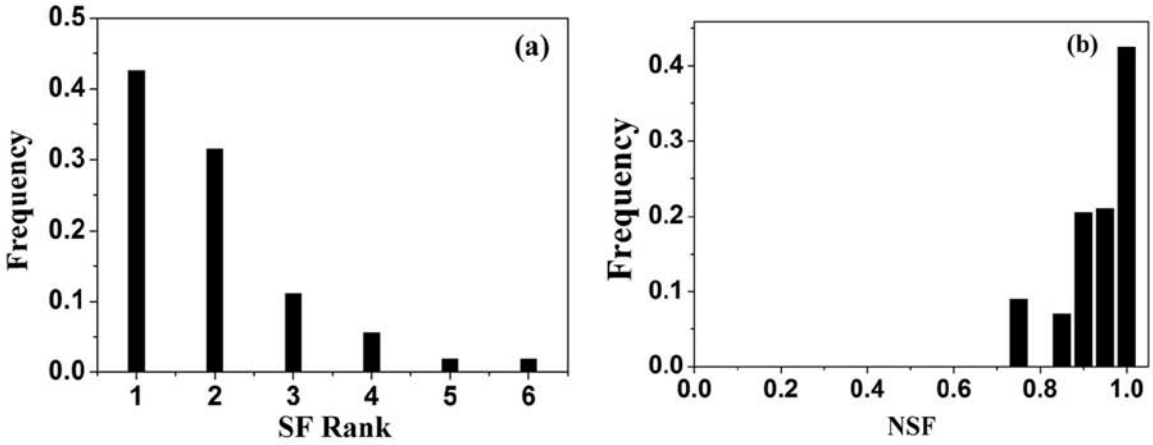

Fig. 5. (a) Frequency of SF ranks (here "1" is the highest and "6" the lowest) corresponding to the active variants of primary twin and (b Frequency of NSF associated with variants of primary twins.

Secondary twinning

The SFs of the secondary twins in the C-T1 and T1-C double twin were examined separately and plotted with different color in Fig. 6. Fig. 6 (a) exhibited the frequency of each SF rank in the form of histograms and Fig. 6 (b) showed the frequency of NSF associated with variants of secondary twins. It is seen that the accuracy of SF in predicting variants selection of the secondary twinning declines to 40%. Note that the variants having the second rank of SF in the C-T1 secondary twins still have a very high proportion (see red bar in Fig. 6 (a)).

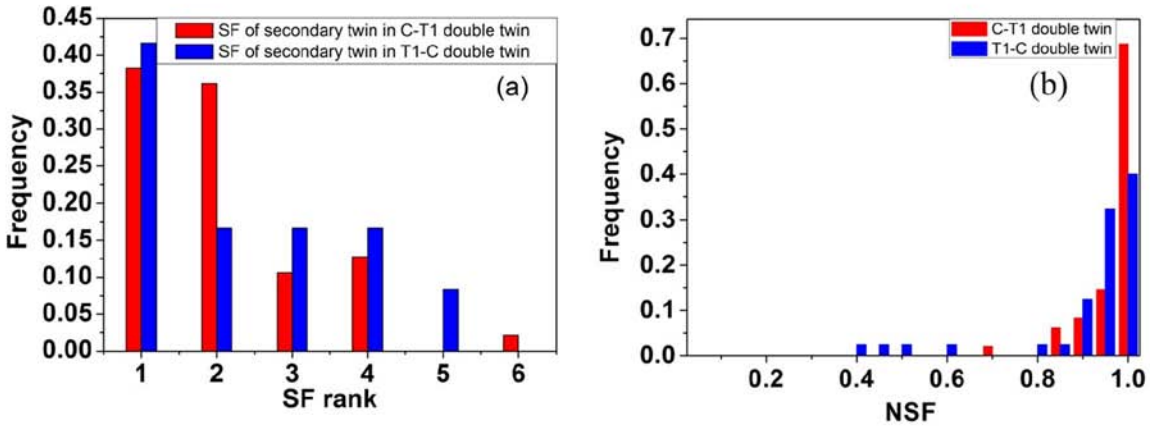

Fig. 6. (a) Frequency of SF ranks (here "1" is the highest and "6" the lowest) corresponding to the active variants of secondary twin in C-T1 (red) and T1-C (blue) double twin and (b) is the frequency of NSF associated with variants of secondary twins

3.2. Plastic energy analysis

A twin variant will be activated if the energy of deformation which is used to create the twin was sufficient and the internal energy of the material would decrease with this operation. We have considered here that the material is an ideal (i.e., no strain hardening) rigid- plastic body to calculate the energy of deformation. Because the elastic energy is restored when the twin is created, we restrict to the plastic energy of deformation which is calculated by the equation:

$$W_{Twin} = \sigma_{ij}\varepsilon_{ij} \quad (1)$$

Where σ'_{ij} is the critical resolved shear stress required (=shear stress τ expressed in the sample frame) to activate the twinning system and σ_{ij} is the corresponding twinning deformation. In the case of channel die compression, the deformation is equivalent to in-plane compression and the compressive force is applied in the sample normal direction (the third axis 33). In a grain, the stress applied to a twinning system is composed of

the macroscopic applied stress and an additional local stress resulting from the interaction of the considered grain with the neighboring grains. Since we restrict to relatively small deformation degrees, we neglect the local stress resulting from the interaction with the neighboring grains. The stress applied to a twinning system is thus restricted to the macroscopic compressive stress $\sigma_{33,}$ which corresponds to the Sachs (or static model) hypothesis. The twinning system will be active when the resolved shear stress reaches the corresponding critical value σ'_{33}. When the twinning system is active, the corresponding deformation energy expressed in the macroscopic coordinate system is given by the above Eq. (1). We introduce the grain size effect by expressing the critical resolved shear stress according to a Hall Petch (HP) type equation:

$$\sigma = \sigma_0 + \frac{k}{\sqrt{L}} \tag{2}$$

with σ_0 and k constants, σ_0 representing the stress when the length of the grain is infinite. L is the free path of the twin before encountering an obstacle (grain boundary, precipitate or other twins). Then the deformation energy can be expressed as:

$$\begin{aligned} W &= (\sigma_0 + \frac{k}{\sqrt{L}})\varepsilon_{33} \\ &= \sigma_0\varepsilon_{33} + \frac{k}{\sqrt{L}}\varepsilon_{33} \end{aligned} \tag{3}$$

In Eq. (3), σ_0 and k are unknowns. Taking into account that twinning is activated when the size of a grain exceeds a certain value below which only

crystal glide can be activated, we can deduce that the second term of the equation is dominant. Rearranging Eq. (3) we obtain:

$$\frac{W-\sigma_0\varepsilon_{33}}{k}=\frac{\varepsilon_{33}}{\sqrt{L}} \tag{4}$$

In the right hand term of Eq. (4), ε_{33} and L, are accessible to the experiment. In the following we will mainly focus on this term, $\frac{\varepsilon_{33}}{\sqrt{L}}$. Clearly, the length (L) of the free path of a twin lamella in a grain can be visualized with its boundary traces on the sample observation plane. The maximum longitudinal length of the twin lamella appearing on the sample observation plane is determined as L for each twin variant. In the present work, the $\frac{\varepsilon_{33}}{\sqrt{L}}$ term is calculated in the sample coordinate system. For simplicity, the displacement gradient tensor

$$e_{ij}=\begin{pmatrix}\frac{\partial u}{\partial x} & \frac{\partial u}{\partial y} & \frac{\partial u}{\partial z}\\ \frac{\partial v}{\partial x} & \frac{\partial v}{\partial y} & \frac{\partial v}{\partial z}\\ \frac{\partial w}{\partial x} & \frac{\partial w}{\partial y} & \frac{\partial w}{\partial z}\end{pmatrix} \tag{5}$$

where *u, v* and *w* are the displacement components and *x, y*, and *z* are the coordinates in the sample system, was first expressed in an orthonormal reference frame defined by the related twinning elements. The unit vector normal to the twinning plane, the unit vector normal to the shear plane and the unit vector in the twinning direction define this reference frame. In this frame the displacement gradient tensor has a particularly simple form:

$$e_{ij} = \begin{pmatrix} 0 & 0 & s \\ 0 & 0 & 0 \\ 0 & 0 & 0 \end{pmatrix} \tag{6}$$

With $s = \frac{|\gamma^2 - 3|}{\gamma\sqrt{3}}$ for the (10-12) twin and $s = \frac{2(\gamma^2 - 2)}{3\gamma}$ for the (11-22) twin where $\gamma = {}^{c}/_{a}$ ratio of titanium, the displacement gradient tensor for the two types of twins can be obtained as:

$$e_{ij} = \begin{pmatrix} \frac{\partial u}{\partial x} & \frac{\partial u}{\partial y} & \frac{\partial u}{\partial z} \\ \frac{\partial v}{\partial x} & \frac{\partial v}{\partial y} & \frac{\partial v}{\partial z} \\ \frac{\partial w}{\partial x} & \frac{\partial w}{\partial y} & \frac{\partial w}{\partial z} \end{pmatrix} = \begin{pmatrix} 0 & 0 & s \\ 0 & 0 & 0 \\ 0 & 0 & 0 \end{pmatrix} = \begin{cases} \begin{pmatrix} 0 & 0 & 0.218 \\ 0 & 0 & 0 \\ 0 & 0 & 0 \end{pmatrix} & for\ \{11\bar{2}2\}\ twin \\ \begin{pmatrix} 0 & 0 & 0.175 \\ 0 & 0 & 0 \\ 0 & 0 & 0 \end{pmatrix} & for\ \{10\bar{1}2\}\ twin \end{cases} \tag{7}$$

Through coordinate transformation, this displacement gradient tensor can be expressed in the crystal coordinate system (here we choose the orthonormal reference system set to the hexagonal crystal basis and the setting follows the Channel 5 convention, i.e. $e_2//a_2$ and $e_3//c$). With the Euler angles measured by SEM/EBSD that represent a set of rotations from the sample coordinate system to the orthonormal crystal basis, this tensor can be further transformed into the macroscopic sample coordinate system. If G is the coordinate transformation matrix from the macroscopic sample coordinate system to the orthonormal twin reference system, the displacement gradient tensor with respect to the sample coordinate system can be expressed as:

$$(e_{ij}^{sample\ frame}) = G(e_{ij}^{crystal\ frame})G^{-1} \tag{8}$$

Thus the deformation tensor in the macroscopic sample coordinate system can be obtained as the symmetrized displacement gradient:

$$\varepsilon_{ij} = \frac{1}{2}(e_{ij} + e_{ji}) \tag{9}$$

With Eq. (9), the energy term $\varepsilon_{33}/\sqrt{L}$ in Eq. (4) can thus be calculated.

The energy term $\varepsilon_{33}/\sqrt{L}$ in Eq. (4) has been calculated for all the examined grains. Here, the ranks referring to the decreasing order of energy term corresponding to each twin variant of primary and secondary twins were calculated separately. Further, for each energy term rank, the frequency of being selected is calculated and plotted in Fig. 7. The results indicate that in the case of primary twin, the prediction is correct in 85% of the cases using the energy term as a variant selection criterion, and in 95% of the cases of secondary twin. The variant selection strongly depends on the energy because the free path length for twin variant is included in this calculation. According to the previous study, normally the selection of twin variant is dependent on the grain shape. In the equiaxed grains, the free path for each variant is almost the same, so several variants can form together in one grain. However, in most instances of elongated grains, only one variant can be activated because of the longer free path. Also for the case of elongated grains, although the activation of the twin variant changes the dimensions of the grain, it does not change the free path length of this variant. Thus this variant can form repeatedly as long as it does not create conditions more favorable for another variant. Under such conditions, the appearing twins can continue to grow until all the parent grain is completely twinned. In most cases, primary twins that accommodate the secondary twins usually show the appearance of lamellae, i.e. secondary twins always form in parent grains of uneven shape (primary twin). The conditions of being active of secondary twin variants are thus largely dependent on the free path. This is also the reason why the energy term is

highly accurate in view of predicting the variant selection of secondary twinning.

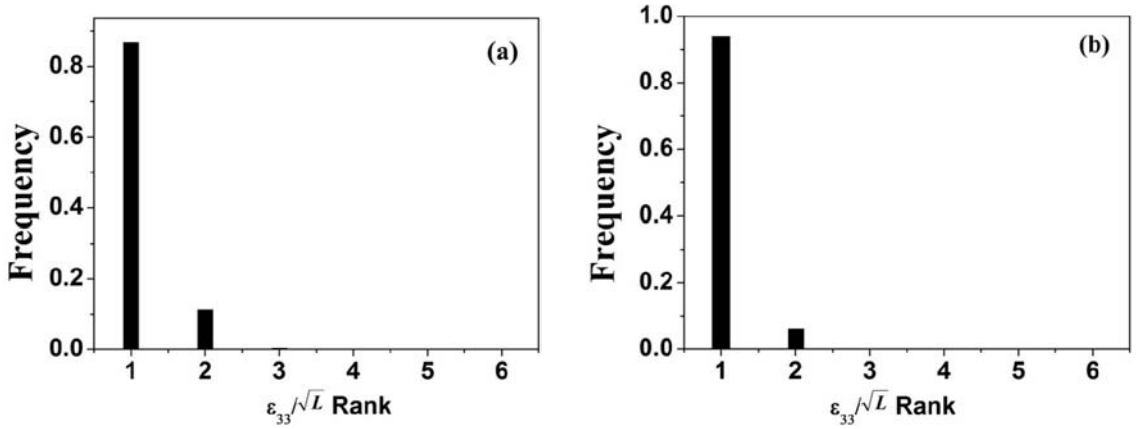

Fig. 7. Frequency of energy term ranks ("1" is the highest and "6" is the lowest) corresponding to the active variants of secondary twin.

3.3. Geometric features of double twins analysis

The geometric features of the combination of C and T1 twins were illustrated in Fig. 8, where the twin elements of primary and secondary twin, twin plane (TP), shear direction (SD) and shear plane (SP), were plotted as poles in a pole figure, in a reference frame bound to the primary twinning system, as seen in Fig. 8. The poles corresponding to the secondary twin elements were represented in stereographic projection by symbols defined in the figure caption of Fig.8 . In each variant group there are two geometrically equivalent variants, one was represented by a filled symbol and the other an open symbol. Martin et al. [Martin et al. (2010)] suggested that in the magnesium, the growth potential is strongly related to the angles of shear plane normal (SPN) and SD between primary and secondary twins because primary twins very efficiently grow along the SPN and SD and the growth of the secondary twins is primarily limited by the lengths of the

primary twin along these directions. Therefore, the variants of double twins with small angles between SPN and SD of primary and secondary twins could easily be activated from the point of view of the growth potential. In the case of titanium, the corresponding angles were summarized in table 3. The C-T1 double twin agrees well with this theory (Fig. 8 (a)). Group B has the lowest angles of TP and SD between primary and secondary twin (see Table 3), i.e. the growth of secondary twin variants belonging to group B suffer the least limitation from their primary twins. In Fig. 4, it is seen that group B was dominant and took the proportion up to 78.9%. However, this theory seems less convincing in the case of the T1-C double twin.

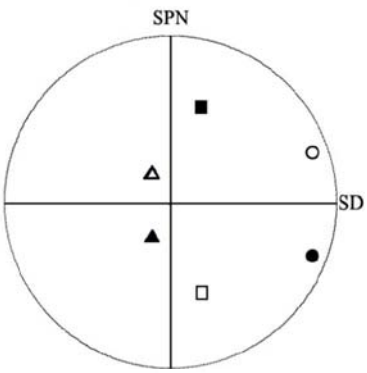

Group A in C-T1 double

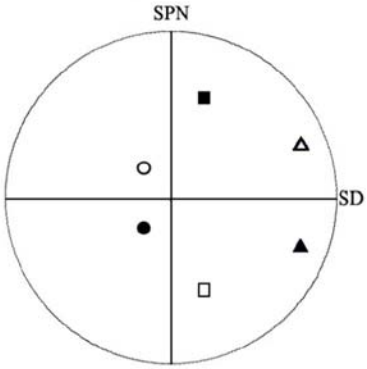

Group B in C-T1 double

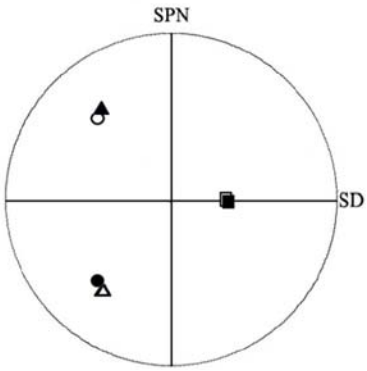

Group C in C-T1 double

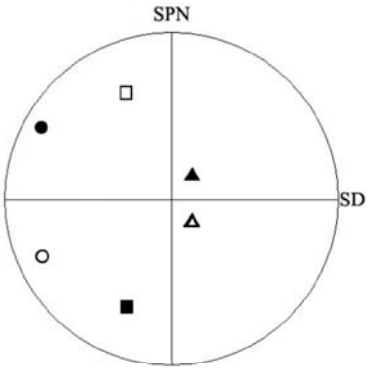

Group A in T1-C double

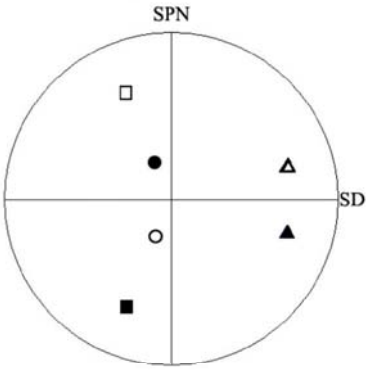

Group B in T1-C double

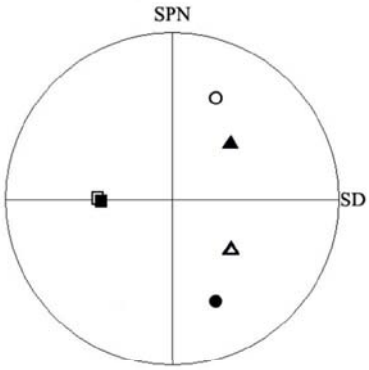

Group C in T1-C double

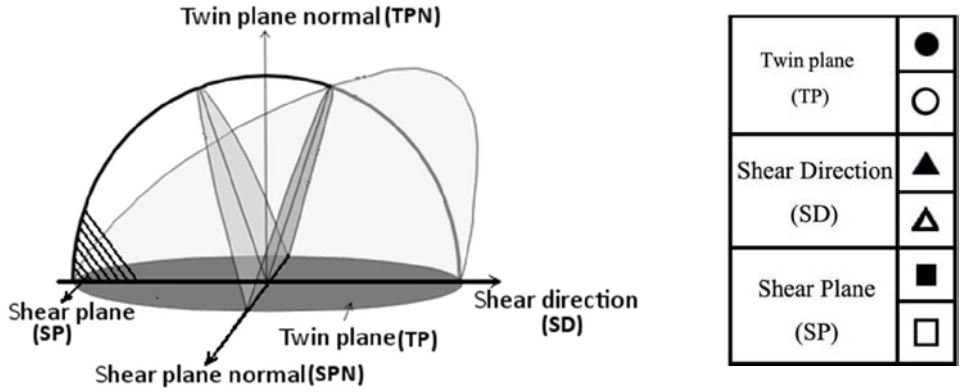

Fig. 8: Stereographic plots of the twin plane normal, shear direction and shear plane normal for group A, B and C in the C-T1 and T1-C double twins are represented with different symbols.

In Table 3 it can be deduced that group B should be predominant according to the theory. Our experiment, on the contrary, exhibited a reverse result. Also in Fig. 4, the Group C took a high proportion of 66.7% and group B was not spotted.

Table 3: Angles between twinning elements associated with variants groups of double twins

C-T1 double twins

Variant groups	Angle between primary and secondary twin's TP	Angle between primary and secondary twin's SD	Angle between primary and secondary SPN
A	84.1°	103.5°	30°
B	27.4°	23.7°	30°
C	66.9°	123.6	90°

T1-C double twins

Variant groups	Angle between primary and secondary twin's TP	Angle between primary and secondary twin's SD	Angle between primary and secondary SPN
A	84.1°	76.5°	30°
B	27.4°	23.6°	30°
C	66.9°	55.3°	90°

3.4. Effect of the twinning in the adjacent grain

As we know, twinning is a shear along the twin direction on a succession of atom layers parallel to the twin plane. When the twinning shear encounters boundaries (grain, twin or phase boundary), it leads to the accumulation of deformation energy and the formation of a local, boundary-centered high energy region which consequently, induces the activation of a new twin shear in the adjacent grain [Yoo (1969)]. On OIM micrographs, it appears that this twin shear crosses the grain boundaries and continues in the adjacent grain. In our observation, however, the most common case is that twins do not cross the boundaries. Therefore, aiming at these twins straddling boundaries, a statistical analysis of the angle between the twin planes on each side of the boundary was carried out. From the results displayed in Fig. 9, it can be deduced that for those twins whose twin planes do not deviate beyond 20°, there is a high tendency to cross the boundary. On the contrary, those twins with larger deviation, generally terminate at the boundary.

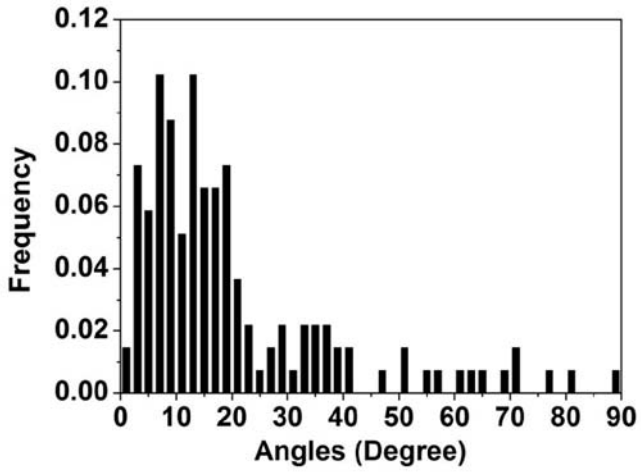

Fig. 9. Frequency of the angles between the twin planes on each side of the boundary.

4. Evolution of misorientation distribution and texture

The misorientation distribution gives the misorientation information between each pixel and its neighboring pixels in the OIM micrograph. It is quite sensitive to the twin boundaries since twin boundaries result in peaks in the misorientation distribution associated to the angles corresponding to the misorientation characteristic of the twin systems. In order to eliminate the small angle misorientations caused by dislocations, only those angles higher than 10° are included in the analysis. The misorientation distribution of initial, 16% and 35% deformation steps were shown in Fig. 10 to present the evolution as a function of the deformation degree. It is seen that at 16% deformation (Fig. 10 (b)), a 65° misorientation peak and a 85° misorientation appear, suggesting that the C twinning was dominant at this deformation stage, it occurs about twice as frequently as the T1 twinning. This result is reasonable considering that the initial texture favours the occurrence of C twin. An relatively hidden peak around 88° appearing as a shoulder on the right side of the dissymmetric T1 peak can also be guessed, which corresponds to the C group of the C-T1 double twin. When deformation continues to 35%, the frequency of the C twin was remarkably decreased and the three peaks correspond to three variant groups of the C-T1 double twin at 41°, 48° and 88° were noticeably increased. Based on the curve chart in Fig. 10 (C), variants in the group C occur about twice as frequently as the Group A or B and no evident difference in frequency is observed between Group A or B.

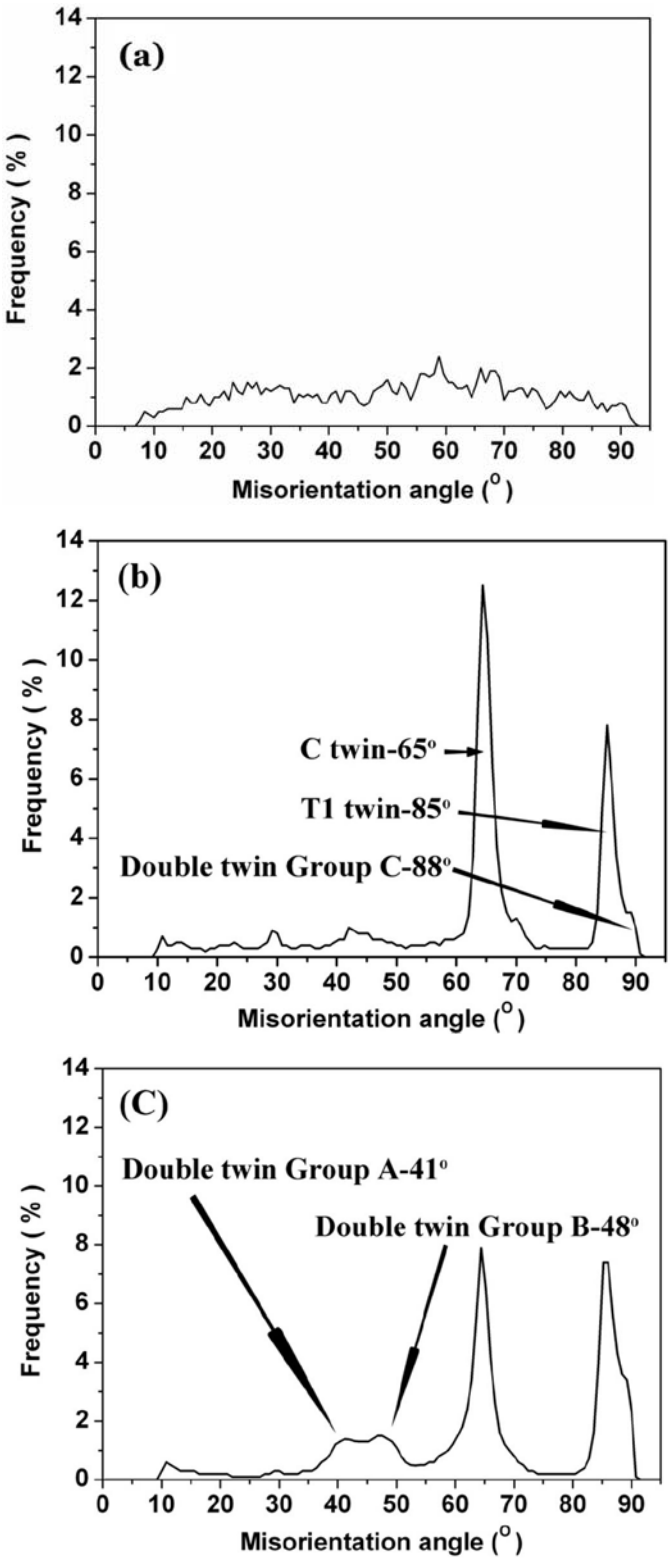

Fig. 10. The misorientation distribution at (a) initial, (b) 16% and (c) 35% deformation degree.

The texture evolution was presented in Fig. 11 by a set of {0002} and {10-10} pole figures at the deformation steps of initial, 16%, 24% and 35%. It is seen that the texture evolution was characterized by the shift of the two strong maxima from the former TD to RD in the {0002} PF. The maximum level decreased from 16 at initial (see Fig. 11 (a)) to 9 at 35% reduction stage (see Fig. 11 (e)). From the texture evolution displayed through Figures 11(a) to (e), it could be inferred that this deformation mode showed similarity to rolling. The free direction of the channel die is equivalent to the rolling direction since the elongation of the sample is allowed in both deformation modes. Similarly, almost no elongation occurs in the transverse direction of rolling whereas the transverse direction is blocked in the channel die. In our channel die compression tests, the free direction corresponded to the former TD and the blocked to the former RD. Thus the evolution of the texture was in new stable orientations with two maxima towards the former RD. This study corroborates the conclusion that twinning provides contributes significantly to the texture evolution, as also reported in the literature [Chun et al. (2005), Bao et al. (2010a)].

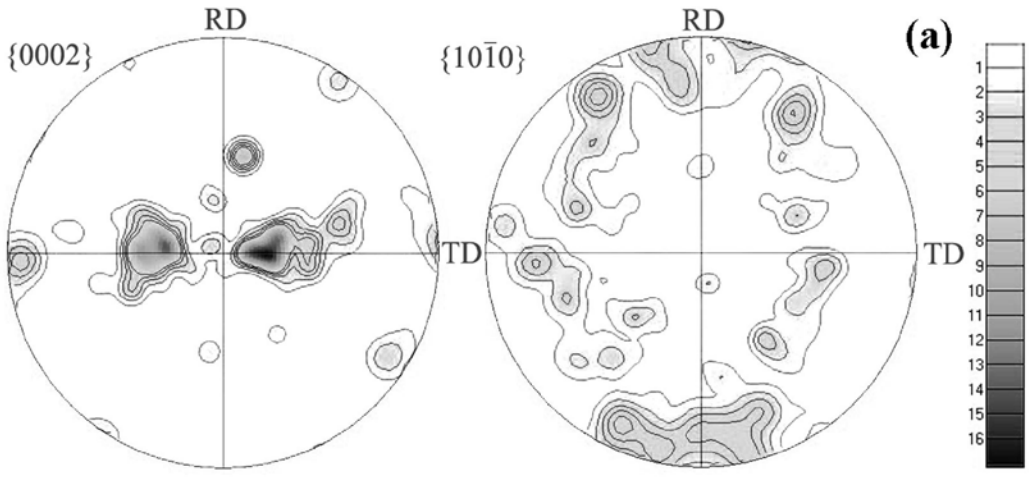

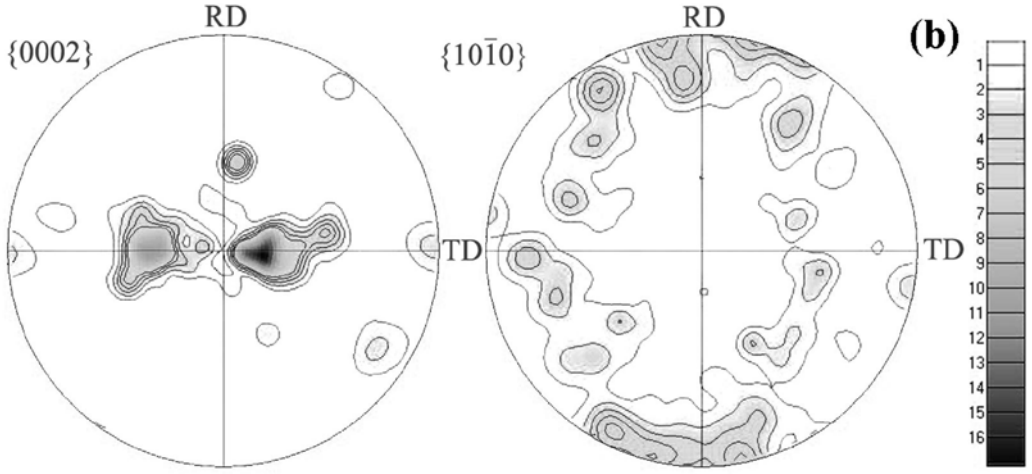
RD
{0002}
RD
{10$\bar{1}$0}
(b)
TD
TD
1
2
3
4
5
6
7
8
9
10
11
12
13
14
15
16

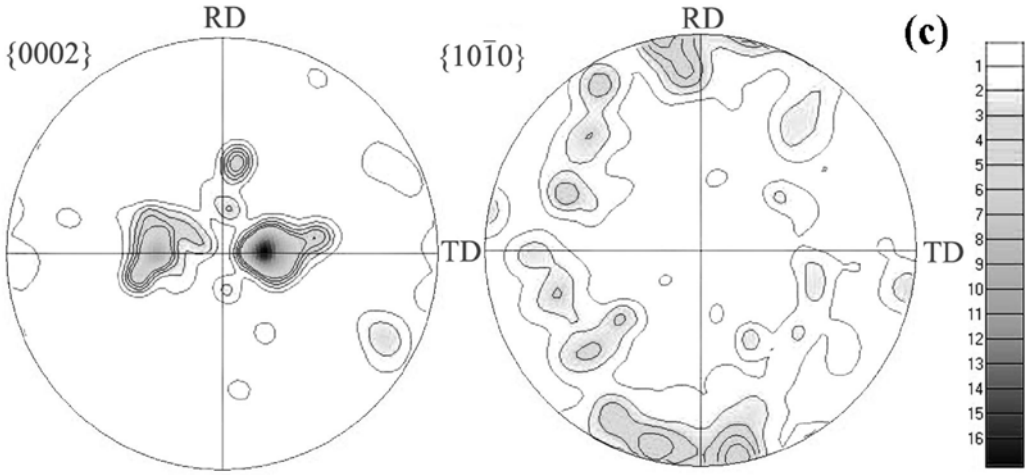
RD
{0002}
RD
{10$\bar{1}$0}
(c)
TD
TD
1
2
3
4
5
6
7
8
9
10
11
12
13
14
15
16

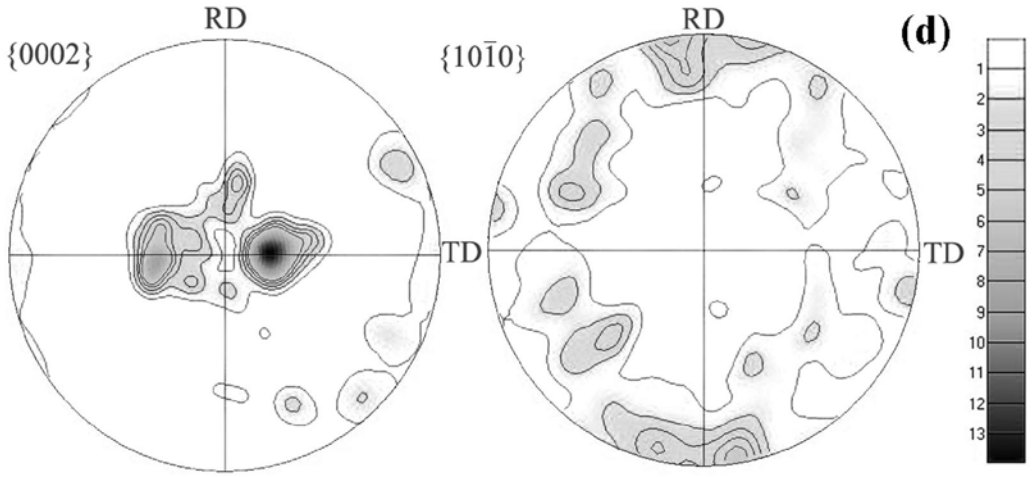
RD
{0002}
RD
{10$\bar{1}$0}
(d)
TD
TD
1
2
3
4
5
6
7
8
9
10
11
12
13

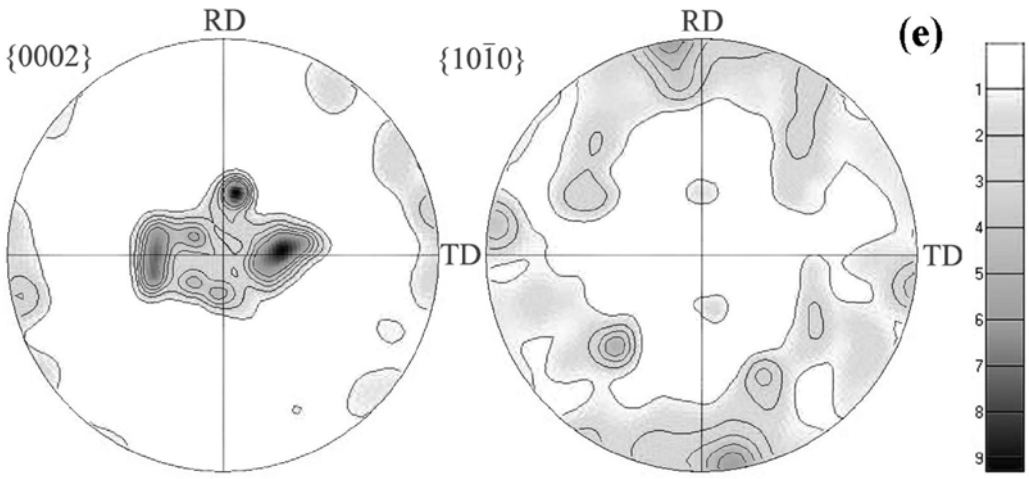

Fig. 11. The {0002} and {10-10} pole figures measured at (a) initial, (b) 8%, (c) 16%, (d) 24% and (e) 35% deformation degree.

Discussion

The occurrence of twinning is governed by various factors, such as the orientation, the size, the shape of parent grain, the boundaries, and even the slip activity [Yoo (1981)]. Due to symmetries of the crystal lattice, several potential twins are in competition, so that it is necessary to clarify the mechanisms of the variant selection process.

In this study, as verified by the experimental results, the deformation energy gave an excellent accuracy up to 85%, the Schmid Factor (SF) a still acceptable accuracy of 50%, as the variant selection criterion. The reason of high accuracy of the deformation energy criterion, as compared to the SF criterion, can be explained by the fact that the calculation not only involves the deformation energy associated with the creation of a twin variant, but also the effect of the size and shape of the parent grain. This is quite effective in the case of a non-homogeneous microstructure or non-

equiaxed parent grain. When a twin forms in a grain, it cuts the parent grain and thus changes the shape and dimensions of this grain, generally subdividing the initial parent grain into three domains. The twin can be considered as a new grain with its own dimensions and crystallographic orientation. When a twin forms, the size of the parent grain is modified and thus the critical stress on each possible twin variant will change according to the HP law. As a result, variants which did not have a sufficient level of stress through the SF can nevertheless be activated in a newly created domain, despite the orientation of the initial parent grain not having changed. This explains why in equiaxed grains, several variants can appear. However, in the elongated grains, although the activation of the twin variant changes the dimension of the grain, it does not change the length of the free path of this variant. Thus this variant can form repeatedly, at least as long as it does not create conditions more favorable for another variant. In such conditions, the twins activated can continue to grow until the whole grain is twinned. A twin can thus be regarded as a new grain, which is a slightly different point of view when considering secondary twinning. Generally, this new grain (i.e. the primary twin) presents an elongated shape (at least at the early stage of its formation). Thus there will generally be only one activated variant in this existing primary twin. In fact, this concept strongly depends on the size of the twin, since, as previously discussed, when a grain is fully twinned, there can be several secondary twin variants thereafter.

With respect to a homogeneous microstructure, the geometric SF that is the factor transforming the applied stress into the resolved shear stress on

the twin plane and along the twin direction, should in principle be conclusive in the variant selection. But the local stress tensor effectively applied to the grain does not coincide with that derived from the macroscopic applied stress tensor. Thus, the geometric SF thus may be not pertinent in some cases, notably when in one parent grain, the first and second highest SFs of variants are very close (NSF very close to 1). As seen in Fig. 5 and Fig. 6, the high frequency of the rank 2 SF probably results from this deviation between the local stress tensor and macroscopic applied stress tensor. Moreover, the high proportion of NSF range from 0.8 to 1.0 (not including 1.0) in Fig. 5 (b) and Fig. 6 (b) also supports this interpretation. It could be inferred that the true frequency of rank 2 SF should be about 15 to 20% lower than the calculated value in Fig. 5 and Fig. 6. If it was possible to calculate the true local stress state, the accuracy using SF in variant selection could increase dramatically.

It can therefore be concluded that the deformation energy can be adopted as an effective criterion in variant selection, and SF should not be completely abandoned but used as a complementary criterion in the case of homogeneous microstructure.

Conclusion

In this study, an investigation of the effect of various factors on twin variant selection in double twins was performed. All possible misorientations corresponding to double twin combinations of {10-12}, {11-21} and {11-22} were calculated with respect to the sample coordinate frame. This leads to

the crystallographic characterization of each double twin variant. The main conclusion can be summarized as follows:

1. The twinning order does affect the resulting misorientation induced by double twinning, even though they are identical in misorientation angle and have symmetrically equivalent axes. All the double twin variants are classified into 15 orientation variant groups rather than 10 geometric variants groups.
2. Strong variant selection takes place in the C-T1 and the T1-C double twinning. The Group B is predominant with respect to the two others in the C-T1 double twin (78.9%). In the case of the T1-C double twin, the predominant variant group is the Group C (66.7%).
3. Schmid factor analysis was performed on the primary twin and secondary twin respectively. SF gave an accuracy of about 50% for predicting the primary twin variant selection and about 40% for the secondary twin variant selection. The relative inaccuracy is probably due to the deviation between the local stress tensor and macroscopic applied stress tensor.
4. A new calculation associated with deformation energy was described to assess the influence of deformation energy on the variant selection. It gave an excellent accuracy up to 85% for predicting the primary twin variant selection and about 95% for the secondary twin variant selection.
5. The twins formed will induce in the adjacent grains variants to be activated across the boundary as long as the angles between the twin

planes are not beyond 20°. No influence of geometric features was found on the variant selection in the double twinning.

6. It is suggested that deformation energy rank of each variant should be adopted as a main criterion in predicting variant selection, and the Schmid factor used as an additional second criterion.
7. Twinning affects the texture evolution by the reorientation of the crystallographic lattice from the former stable orientation of the parent grain into the new stable orientation of the twin. The stable orientations depend on the deformation mode, like rolling or channel die compression for example.

Acknowledgement

This study was supported by the Federation of Research for Aeronautic and Space (Fédération de Recherche pour l'Aéronautique et l'Espace Thème Matériaux pour l'Aéronautique et l'Espace : project OPTIMIST (optimisation de la mise en forme d'alliage de titane).

References

Akhtar A. Basal slip and twinning in α-titanium single crystals *Metallurgical and Materials Transactions A*. 1975, vol. 6 pp. 1105-1113.

Bao L. Lecomte J. S. Schuman C. Philippe M. J. Zhao X. Esling C. Study of plastic deformation in hexagonal metals by interrupted in-situ EBSD measurement. Advanced Engineering Materials. 2010a. Vol. 12, pp. 1053-1059.

Bao L. Schuman C. Lecomte J.S. Philippe M.J. Zhao X. Zuo L. Esling C. Study of Deformation Mechanisms in Titanium by Interrupted Rolling and Channel Die Compression Tests. *Computers, Materials & Continua*. 2010b, Vol.394, pp. 1-15.

Barnett M. Keshavarz Z. Beer A. Ma X. *Non-Schmid behaviour during secondary twinning in a polycrystalline magnesium alloy.* Acta Materialia, 2008, Vol. 56. Pp. 5-15.

Capolungo L. Marshall P. E. McCabe R. J. Beyerlein I. J. Tomé C. N., Nucleation and

growth of twins in Zr: A statistical study. *Acta Materialia,* 2009, Vol. 57 pp. 6047-6056.

Chun Y.B.Yu S.H. Semiatin S.L. Hwang S.K. Effect of deformation twinning on microstructure and texture evolution during cold rolling of CP-titanium Materials Science and Engineering A 2005, Vol. 398, pp. 209-219.

Fundenberger J.J. Philippe M.J. Wagner F. Esling C. Modelling and prediction of mechanical properties for materials with hexagonal symmetry (zinc, titanium and zirconium alloys). *Acta Materialia*. 1997, Vol. 45, pp. 4041-4155.

Kocks U. F. Westlake D. G. The importance of twinning for the ductility of HCP polycrystals, *AIME MET SOC TRANS.* 1967, Vol. 239, pp. 1107-1109.

Lebensohn R. A. Tome C. N. A study of the stress state associated with twin nucleation and propagation in anisotropic materials. Philosophical Magazine A. 1993, Vol. 67, pp. 187-206.

Mahajan S. Williams D.F. Deformation twinning in metals and alloys. *International Materials Reviews.* 1973, Vol. 18, pp. 43-61.

Martin E. Capolungo L. Jiang L. Jonas J.J. Variant selection during secondary twinning in Mg-3%Al. *Acta Materialia*. 2010, Vol. 58, pp. 3970-3983.

Partridge P.G. The crystallography and deformation modes of hexagonal close-packed metals*. International Materials Reviews*. 1967, Vol. 12, pp. 169-194.

Philippe M.J. Esling C. Hocheid B. Role of twinning in texture development and in plastic deformation of hexagonal materials. *Textures and Microstructures*. 1988, Vol. 7 pp. 265-301.

Philippe M.J. Serghat M. Van Houtte P. Esling C. Modelling of texture evolution for materials of hexagonal symmetry-II. Application to zirconium and titanium α or near α alloys. *Acta Metallurgica et Materialia*. 1995, Vol. 43 pp. 1619-1630.

Rosi F. D. Perkins F. C. Seigle S. S., Mechnism of plastic flow in titanium at low and high temperatures. *Trans. Met. Soc. AIME,* 1956, pp. 115-122.

Vedoya P. Pochettino A. Penelle R. Plastic Anisotropy of Titanium, Zirconium and Zircaloy 4 Thin Sheets. *Textures and Microstructures.* 1988, Vol. 8 pp. 601-610.

Yoo M.H. Interaction of slip dislocations with twins in HCP metals. *Trans. Met. Soc. AIME*. 1969, Vol. 245, pp. 2051-2060.

Yoo M.H. Slip, twinning, and fracture in hexagonal close-packed metals. *Metallurgical and Materials Transactions A*. 1981, Vol. 12 pp. 409-418.

Zaefferer S. A study of active deformation systems in titanium alloys: dependence on alloy composition and correlation with deformation texture. *Materials Science and Engineering A*. 2003, Vol. 344, pp. 20-30.

Chapter 5: Conclusions and prospects

This chapter lists the main conclusions obtained in the present work and some suggestions for future work based on the findings, conclusions and problems identified in the course of the present work.

5.1 Conclusions

The present work attempts to improve the understanding of the contribution of deformation twinning to the plastic deformation of hexagonal T40 titanium alloy, as well as establishing a criterion for the twin variants selection. From the experimental data and theoretical investigations, the following important conclusions can be drawn:

Twinning occurs in grains having specific orientations. Generally, in rolling and compression, compression twinning occurs in the grains with their c axis close to the compressive force; tension twinning occurs in the grains with their c axis perpendicular to the compressive force.

The twinned part of a grain can be considered as a new grain. When twins grow within the grain, they can consume almost the whole matrix. In this case the primary twinned area is much larger than the remaining matrix and thus represents the “new grain” for possible subsequent secondary twinning. Special attention should be paid when determining the twinned volume fraction. With the EBSD technique, a large twinned volume fraction could be demonstrated. This contradicts the conventional judgement that the twinned part is always smaller in a twinned grain than the remaining part of the parent grain, as was generally concluded from optical microscopy. Only step by step EBSD orientation mapping allows an unambiguous determination of the twinned volume fraction.

In rolling and compression, it appears that the growth of {10-12} tension twin variants and {11-22} compression twin variants exhibit different characteristics. {10-12} tension twins usually exhibit only one variant per

grain. Even if another variant was activated, it would be rapidly absorbed by the first variant. This predominant twin variant grows very fast until almost no original parent is left, showing predominant variant system (PVS). This is because the {10-12} tension twins form under the resolved compressive force that is almost perpendicular to the c axis of the parent grain. In this situation, only two variants have a high Schmid factor and the misorientation between the two variants is only 9.98°. Hence, in a given grain, {10-12} twin lamellae of these two variants can easily merge into one another. In contrast, it is easy for the {11-22} compression twin to activate more than one variant, and they collide with each other and block growing, showing multiply variants system (MVS). This is because that as a compression twin, {11-22} twin forms under the resolved compressive force that is parallel to the c axis of the matrix. Since all the six {11-22} twin variants have symmetrical orientation relations by a 60° rotation around the c axis, the six variants should have the same Schmid factor under a compressive force parallel to the c axis. In our experimental observations, for the grains with {11-22} compression twins, the applied compressive force always deviates to some extent from the c axes, therefore usually three or four variants have a relatively high Schmid factors and these variants are activated simultaneously. PVS is inclined to occur in elongated grains and MVS is inclined to occur in equiaxed grains.

The order of the twinning does affect the resulting misorientation induced by double twinning, even though they are identical in misorientation angle and have symmetrically equivalent axes. The set of all the double twin

variants are classified into 15 orientation variant groups rather than 10 geometric variants groups.

In this study, two sets of double twins were observed, C-T1 double twins and T1-C double twins respectively. All the variants of these two sets of double twins are classified into 3 groups by symmetrically equivalent rotation with respect to the parent crystal, namely Group A (41.3° about <1-543>), Group B (48.4° about <5-503>) and Group C (87.9° about <4-730>). Strong variant selection takes place in these two double twinning systems. The Group B is predominant with respect to the two others in the C-T1 double twin (78.9%). In the case of the T1-C double twin, the predominant variant group is the Group C (66.7%).

Schmid Factor (SF) analysis was performed on the primary twin and secondary twin respectively. SF gave an accuracy of about 50% for predicting the primary twin variant selection and about 40% for the secondary twin variant selection. The relative inaccuracy is probably due to the deviation between the local stress tensor and the macroscopic applied stress tensor. A new calculation associated with deformation energy was described to assess the influence of the deformation energy on the variant selection. It gave an improved accuracy up to 85% for predicting the primary twin variant selection and about 95% for the secondary twin variant selection.

The twins formed will induce in the adjacent grains variants to be activated across the boundary as long as the angles between the twin planes are not beyond 20°. No influence of geometric features was found on the variant

selection in the double twinning. It is suggested that deformation energy rank of each variant should be adopted as a main criterion in predicting variant selection, and the Schmid factor used as an additional second criterion.

Twinning affects the texture evolution by the reorientation of the crystallographic lattice from the former stable orientation of the parent grain into the new stable orientation of the twin. The stable orientations depend on the deformation mode, like rolling or channel die compression for example.

5.2 Prospects

The following are some suggestions for future work based on the findings, conclusions and problems identified in the course of the present work.

In order to study the deformation mechanisms in titanium, many efforts are required on twinning, gliding and the interaction between them. In the present study, we focused on the twinning and extended the discussion a little to the gliding. Therefore, some prospects could be suggested as follows:

1. The interrupted “in situ” EBSD method is an effective way to study the deformation twinning in detail. With this approach, various deformation modes could be studied, such as shear, tensile test and ECAP… So far, the deformation in this approach is limited within 35% due to the poor EBSD index ratio after larger plastic deformation. A

solution for this problem would be quite useful in the view of future work.

2. The in situ deformation (tensile and shear tests) experiments in the chamber of SEM/EBSD with microgrids deposited on the sample surface would be another interesting approach to study the local strain (thus stress) distribution in polycrystalline titanium during deformation.

3. Further studies could be concentrated on dislocations and slips, with TEM technique. Additional detailed investigation on deformation mechanisms could be performed using Burger vector identification methods in the TEM.

THESE

Présentée *à*

UNIVERSITÉ PAUL VERLAINE-METZ

Par

BAO Lei

Pour l'obtention du grade de:

Docteur de l'Université Paul Verlaine-Metz

Spécialité: Mécanique des matériaux

Option: Sciences des Matériaux

Contribution to the Study of Deformation Twinning in Titanium

Soutenue le 21Juin 2011 à Pékin devant le jury composé de:

Claude ESLING	Professeur à l'Université Paul Verlaine de Metz, France	Directeur de thèse
Xiang ZHAO	Professeur à Northeastern University, Chine	Directeur de thèse
Christophe SCHUMAN	Maître de conférences à l'Université Paul Verlaine de Metz, France	Co-directeur de thèse
Yandong WANG	Professeur à Beijing Institute of Technology, Chine	Rapporteur
Alain VASSEL	Docteur à Association TITANE, France	Rapporteur
Lei WANG	Professeur à Northeastern University, Chine	Rapporteur
Elisabeth GAUTIER	Directeur de recherche CNRS, France	Examinateur
Liang ZUO	Professeur à Northeastern University, Chine	Examinateur
Yongqing ZHAO	Professeur à Northwest Institute for Nonferrous Metal Research, Chine	Membre du Jury
Yafeng LU	Professeur à Northwest Institute for Nonferrous Metal Research, Chine	Membre du Jury
Isabelle MORELON	Docteur, International Program Manager ANR, Non-thematic Department, France	Invité
Jean-Sébastien LECOMTE	Ingénieur de recherches CNRS, Arts Metiers Paris-TECH, France	Invité
Philippe MARTINEAU	Conseiller adjoint, Service pour la Science et la Technologie, Ambassade de France en Chine, France	Invité

LEM3 - UMR CNRS 7239 Université Paul Verlaine-Metz - Île du Saulcy - 57045 METZ Cedex 1

Contents

Résumé

Le titane et ses alliages sont largement utilisés dans les domaines aéronautique, spatial, de l'armement, du génie civil, dans des applications commerciales et biomédicales en raison de sa résistance à la rupture élevée, d'une bonne ductilité et d'une grande biocompatibilité. Les mécanismes de la déformation plastique du titane ont été étudiés en détail par le passé, particulièrement sur l'étude de la déformation par maclage car il a une grande influence sur les propriétés mécaniques.

Une méthode d'essais "in situ" en EBSD basée sur des tôles polies et colées ensemble a été développée dans cette étude et utilisée en laminage et en compression plane. Avec cette méthode, des mesures EBSD sont effectuées à chaque étape de la déformation dans la même zone comprenant un grand nombre de grains. Par conséquent, l'information sur l'orientation de ces grains à chaque l'étape de la déformation est mesurées.

Le maclage apparait dans les grains qui ont des orientations particulières. En règle générale, la réorientation induite par le maclage aligne l'axe c de la partie maclées vers les orientations stables de la texture de laminage, de sorte qu'aucun autre maclage secondaire peut être induit. Le maclage secondaire se produit uniquement lorsque le macle primaire envoie l'axe c loin des orientations stables. Pour les grains maclés, la rotation du réseau de la matrice est semblable à celle des grains ayant une orientation cristallographique identique mais sans macles.

Deux types de systèmes de macles ont été activés au cours de la déformation à la température ambiante: des macles de tension (10-12) et des macles de compression (11-22). Dan le maclage primaire, les résultats montrent que les variantes de macle ayant des facteurs Schmid supérieurs à 0.4 ont une bonne chance d'être actifs. Les comportements des deux types de maclage sont complètement différents. Dans la déformation en compression, les macles (11-22) montrent le comportement de type multiplication des variants (Multiply Variants System: MVS) alors que les macles (10-12) montrent le type de maclage prédominant (Predominant Twin System: PTS). Cette étude présente deux types de macles doubles dénommées C-T1 (= macle primaire de Compression et macle secondaire de Tension) et T1-C (= macle primaire de Tension et macle secondaire de Compression). Tous les variants sont classés seulement en trois groupes: A, B et C par symétrie cristallographique. Les désorientations de ces 3 groupes par rapport à l'orientation de la matrice sont respectivement de 41.34°, 48.44° et 87.85°.Une forte de sélection de variant se déroule dans le maclage double. Pour les macles doubles CT, 78.9% des variantes appartiennent à la B et pour T1-C, 66.7% des variantes appartiennent à C. Le facteur de Schmid joue un rôle prépondérant dans la sélection des variants des macles doubles. Les caractéristiques géométriques, associant " volumes communs " et l'accommodation de la déformation ne contribuent pas de manière significative à la sélection des variants.

Summary

Titanium and its alloys are widely used in aviation, space, military, construction and biomedical industry because of the high fracture strength, high ductility and good biocompatibility. The mechanisms of plastic deformation in titanium have been studied in detail, especially deformation twinning since it has a great influence on the ductility and fracture strength.

In this study, an interrupted "in situ" SEM/EBSD investigation based on a split sample of commercial titanium T40 was proposed and performed in rolling and channel die compression. This approach allows to obtain the time resolved information of the appearance of the twin variants, their growth, the interaction between them and the interaction with the grain boundaries or twin boundaries. With the orientation data acquired by the EBSD technique, we calculated the Schmid factor, crystallographic geometry, and plastic energy associated with each variant of primary twins, secondary twins and double twins to investigate the lattice rotation, the activation of twins, the growth of twins, and the variant selection criterion.

In this observation, two types of twin systems were activated: {10-12} tension and {11-22} compression twins. Secondary twins were also activated, especially the twin variants with the highest Schmid factors (e.g. higher than 0.4). The growth of the two

types of twin is quite different. The {11-22} twin shows Multiple Variants System (MVS) whereas the {10-12} twin shows Predominant Variant System (PVS).

The twinning occurs in grains that have particular orientations. Generally, the reorientation induced by the twinning aligns the c-axis of the twinned part to the stable rolling texture orientations, so that no further secondary twinning can be induced. The secondary twinning occurs only when the primary twinning orientates the c-axis of the primary twins far away from the stable orientations. For twinned grains, the lattice rotation of the matrix is similar to that of the grains having a similar crystallographic orientation but without any twin.

Two sets of double twins were observed in this study, classified as C-T1 and T1-C double twins respectively. All the variants of C-T1 and T1-C double twins were classified into three groups: A, B and C according to the crystallographic symmetry. The misorientations of theses three groups with respect to the matrix are 41.34°, 48.44° and 87.85°. Strong variant selection took place in double twinning. In C-T1 double twins, 78.9% variants belong to group B whereas in T1-C double twins, 66.7% variants belong to group C. The plastic energy and Schmid factor both play important roles in the variant selection of double twinning. Geometrical characteristics, like the common volume or strain accommodation do not contribute significantly to the variant selection.

Introduction générale

Plusieurs classes de matériaux à structure cristalline hexagonale présentent actuellement un intérêt pour des applications techniques ainsi que pour la recherche fondamentale. Les exemples sont: les alliages de titane, de magnésium, le béryllium ou encore le zirconium. Dépendant de leurs propriétés, ils sont utilisés dans beaucoup d'applications différentes (aéronautique, transport, nucléaire, biomédical...). Leurs propriétés mécaniques sont intensivement étudiées afin de connaître les possibilités et les limites de leur mise en forme. Plus particulièrement nous nous intéressons ici au cas du titane, l'intérêt de ce matériau réside principalement dans sa légèreté, tenue à la corrosion. Le titane est le plus souvent allié avec l'aluminium, le fer, le chrome, le vanadium, le molybdène, le tantale, le niobium et le manganèse. Mais aussi avec des éléments légers comme l'oxygène, le carbone et l'azote (éléments alphagènes par opposition aux éléments précédent qui étaient bétagènes). On le trouve la plupart du temps sous la forme de minerai.

Néanmoins, l'utilisation de ce matériau passe par sa mise en forme et l'application de différents procédés. Lors de sa mise en forme, de grandes

déformations plastiques sont appliquées au matériau, il est donc primordial de connaître son comportement aux grandes déformations. L'état actuel de la recherche dans ce domaine nous renseigne principalement sur des déformations relativement faibles et pour des tests simples. De grandes déformations plastiques, cependant, impliquent le développement d'une anisotropie plastique qui est particulièrement forte dans les polycristaux hexagonaux déjà marquée aux faibles déformations.

1. Bases de compréhension

Nous nous intéressons ici aux mécanismes de déformation microscopiques pouvant opérer dans les métaux à structures hexagonales. Une déformation permanente peut être engendrée par diffusion des défauts ponctuels, glissement de défauts linéaires (dislocations) également appelés glissement cristallographique, glissement aux joints de grains, maclage ou transformation martensitique. Cependant les trois principaux mécanismes observés dans les structures hexagonales lors de déformations plastiques sont le maclage, le glissement aux joints de grains et bien sur le glissement cristallographique.

1.1. Maclage

Le maclage joue un rôle important dans la déformation plastique. On observe surtout le maclage dans les matériaux dont le nombre de symétries est réduit comme les matériaux à structures hexagonales. Une partie du cristal est cisaillée entre deux plans qui vont former les interfaces avec la partie non déformée. Le réseau maclé prend une orientation symétrique par rapport au réseau non maclé (voir figure 1). Le plan de symétrie sera le plan de maclage.

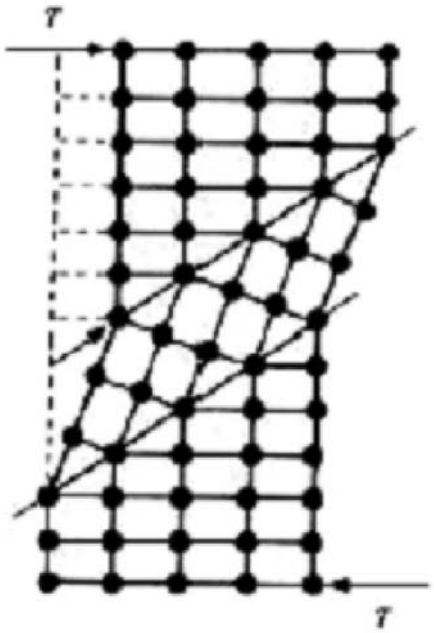

Figure 1 Illustration du maclage

Le taux de cisaillement induit est donné par la géométrie du système de maclage (plan et direction cristallographique de maclage) dans la maille cristalline.

Le maclage provoque une réorientation du réseau cristallin, ce qui peut alors faciliter le glissement cristallographique. Le maclage pourra orienter les systèmes de glissement de façon à rendre le glissement cristallographique plus propice. Cependant, en subdivisant les grains, le maclage augmente la densité d'obstacles s'opposant au passage des dislocations. Il entraîne ainsi un durcissement par écrouissage.

La contrainte critique de maclage semble être indépendante de la température mais il existe une température de transition entre maclage et glissement qui dépend de la vitesse de déformation, de la taille de grain et de l'énergie de faute d'empilement. La taille des grains joue un rôle non négligeable sur la contrainte de maclage σ_T , dans la loi de Hall et Petch la constante k_T est distincte de la constante k_S utilisée pour le glissement:

$$\sigma_T = \sigma_{T0} + k_T d^{-1/2}$$

Quant à l'effet des textures sur le maclage, Gray et al. (Gray, Kaschner et al. 1999) ont montré qu'elle avait un important effet dans les métaux à faible symétrie. Ils l'ont démontré pour le magnesium et le zirconium. Ils ont

montré notamment que les contraintes de maclage étaient différentes en traction et en compression dès lors de la présence de texture.

Cependant, en cisaillement simple et à une température relativement élevée (au delà de 200°C), le maclage ne semble pas opérer de façon significative dans les métaux hexagonaux.

1.2. Glissement cristallographique

Passons maintenant à la description du mécanisme de déformation par glissement cristallographique. Le glissement cristallographique est un mécanisme qui opère dans tous les matériaux cristallisés : métaux et alliages métalliques, roches (calcites) ou encore polymères cristallisés. Ce mécanisme a déjà été observé avant le XX^{ème} siècle. Des métallurgistes ont observé au microscope optique, sur des polycristaux déformés, des lignes ou stries régulières qu'ils ont appelées « lignes de glissement ». En réalité, par la suite, au Microscope Electronique à Balayage, ces lignes de glissement étaient en réalité des marches. La formation de ces marches résulte directement du mécanisme de déformation : des parties du cristal (ou polycristal) glissent les unes sur les autres sur des plans cristallographiques bien définis (les systèmes de glissement). Ce mécanisme est dû au mouvement des dislocations dans ces plans de glissement. Une

dislocation peut être activée par une contrainte appliquée au cristal. Sous une contrainte suffisante, la dislocation glisse à travers le cristal. Elle produit un petit déplacement (de vecteur de Burgers b) de la surface parcourue par rapport aux autres parties du cristal. Lors du glissement d'une dislocation, le volume reste inchangé, car le glissement se produit par cisaillement entre des plans parallèles du cristal. Dans le réseau cubique face centré, ce sont les vecteurs de Burgers du type <110> , dans le cubique centré : <111> . Dans les matériaux à structures hexagonales, il existe plusieurs familles de systèmes de glissement, avec des vecteurs de Burgers de type <a> et <c+a>. Un système de glissement est défini par un plan de glissement (repéré par sa normale unitaire) et par une direction de glissement contenue dans ce plan. Le tableau 1, présente les différentes familles de système de glissement opérant dans les structures hexagonales.

On notera ici que pour les matériaux hexagonaux la notation de Miller-Bravais {*hkil*} est adoptée. Les indices *h, k* et *i* ne sont toutefois pas indépendants; la relation suivante existe entre eux : $h+k+i=0$. Ci-dessous la représentation des différentes familles de système de glissement dans la maille élémentaire hexagonale.

Tableau 1 Familles de systèmes de glissement dans les cristaux h.c.p

Familles	Nombre de système de	Systèmes
Basales {0001}<11-20>	3	2
Prismatiques {10-10}<-11-20>	3	2
Pyr. <a> {10-11}<-12-10>	6	4
Pyr. <c+a>/A {01-11}<2-1-1-3>	12	?
Pyr. <c+a>/B {11-22}<-2113>	6	5

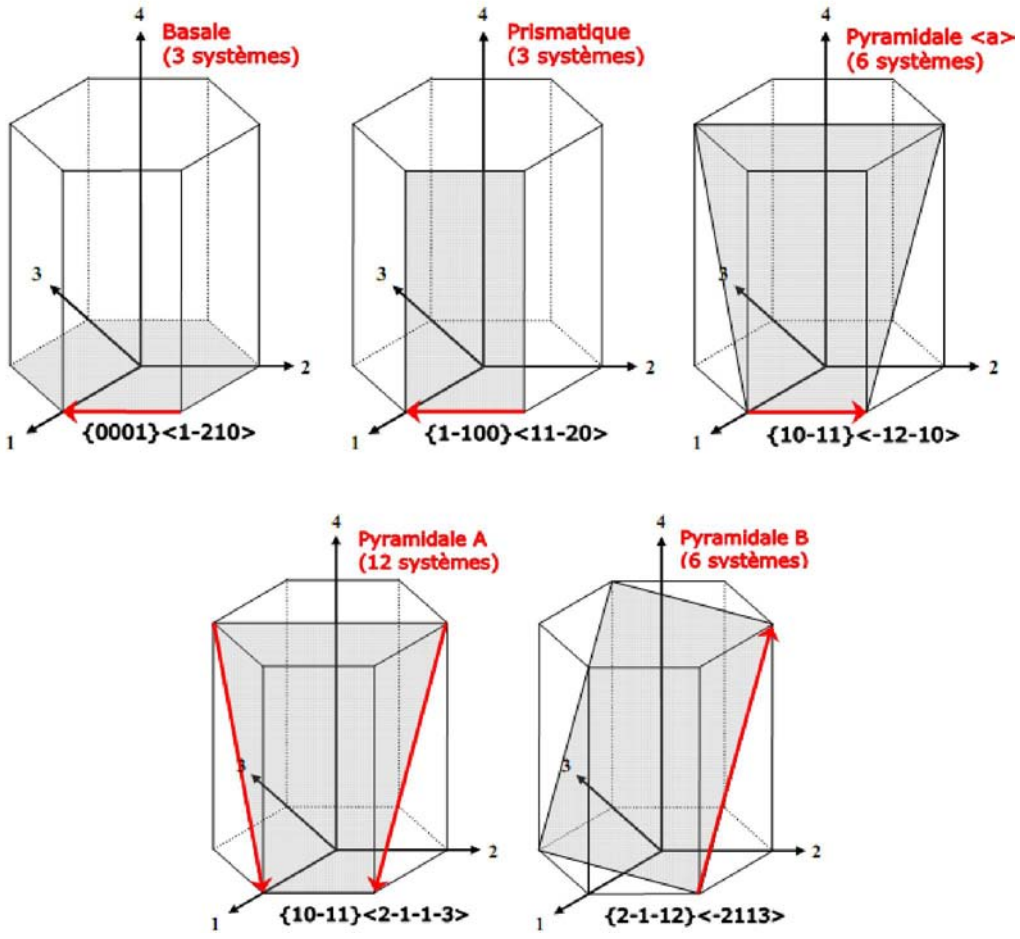

Figure 2 Position des systèmes de glissement dans la maille hexagonale

2. Plasticité cristalline des titan dans la littérature

Les matériaux à structure hexagonale tels que le béryllium ou le magnésium sont particulièrement intéressants du fait de leur légèreté, le magnésium notamment pour l'industrie automobile, des ordinateurs ou encore des matériels sportifs. Les propriétés du titane sont particulièrement appréciées par l'industrie aérospatiale, aéronautique ou encore biomédicale. Le zirconium est quand à lui essentiellement étudié pour son utilisation dans les réacteurs nucléaires. Cependant, ils ne présentent pas autant de « facilités » de mise en forme que les matériaux cubiques par exemple, ses systèmes de glissement sont la plupart du temps plus difficiles à activer, le maclage devient alors plus fréquent dans ces matériaux. Il devient alors important de connaître leurs caractéristiques de déformations, notamment les contraintes de cisaillement critiques résolues de leurs différentes familles de systèmes de glissement, l'activité de maclage, de recristallisation dynamique… Ces questions ont fait l'objet de beaucoup de travaux ces dernières années et restent d'actualité. Les matériaux hexagonaux peuvent être également très fragiles par rapport à certains autres matériaux. Diverses techniques d'amélioration de ces

propriétés mécaniques, comme l'application d'une hyper déformation, ont alors été développées et sont actuellement le sujet de beaucoup d'études.

Nous proposons au travers de cette section une présentation des principaux travaux ayant trait à la plasticité cristalline, à l'évolution de texture et aux différents mécanismes de déformation prenant place des les matériaux hexagonaux lors d(Koike 1987)e leur déformation. Il est question du titane sur lequel ce travail est appliqué.

Les textures dans le titane ont fait l'objet de beaucoup d'études et notamment durant un laminage (à chaud ou à froid). Nous pouvons citer entre autres les travaux de Koike(Koike 1987) en 1987 pour le laminage à froid, de Lee et al. (Lee, Esling et al. 1988) et Nourbakhsh et al. (Nourbakhsh and O'Brien 1988) en 1988 pour un laminage à froid. En 1994, Kailas et al. (Prasad, Biswas et al. 1994) étudient l'influence de la texture initiale sur les instabilités de la microstructure du titane durant une compression pour des températures comprises entre 25 et 400°C. Par la suite, en 1997, Lebensohn et Canova (Lebensohn and Canova 1997) proposent une modélisation auto-cohérente pour simuler l'évolution de texture dans le titane, ils l'appliquent à du laminage et montrent notamment que le modèle mène à de meilleurs prédictions de texture quand les deux phases

(alpha et beta) présentent dans l'alliage de titane sont considérées. En 1999, Singh et al. (Singh, Bhattacharjee et al. 1999) décrivent l'évolution de texture dans un alliage de titane Ti-10V-4.5Fe-1.5Al durant un laminage et un recuit, ils comparent les textures obtenues avec celles obtenues pour d'autres alliages de titane mais aussi avec celles d'alliages de métaux cubiques (tantale et acier). Plus récemment nous pouvons citer Chun et al. 2005 (Chun, Yu et al. 2005), qui étudient l'effet de la déformation par maclage sur la microstructure et l'évolution de texture durant un laminage à froid. Ils montrent notamment que l'activité de glissement et de maclage dépend de la réduction imposée par le laminage. En 2005, Bozzolo et al. (Bozzolo, Dewobroto et al. 2005) examinent la microstructure et la texture dans des tôles de titane faiblement allié laminées à 80% dans le but d'étudier le grossissement de grain et les effets de la recristallisation dynamique.

De façon plus générale Bache et Evans, proposent en 2001 (Bache and Evans 2001) une étude sur l'impact de la texture sur les propriétés mécanique d'un alliage de titane. En 2003, Zaefferer (Zaefferer 2003) étudie l'activité des mécanismes de déformations dans différents alliages de titane et sa dépendance au regard de leurs compositions. En 2007, Wu

et al. (Wu, Kalidindi et al. 2007) simulent l'évolution de la texture ainsi que le comportement en contrainte-déformation du titane durant de grandes déformations plastiques. Ils prennent en considérations le glissement et le maclage et obtiennent de bonnes prédictions.

3. Méthodes Expérimentales

3.1. Matériels et Préparation des échantillons

Le matériau utilisé est une tôle de titane T40 (titane commercialement pur) d'épaisseur 1,5mm dont la composition chimique est donnée dans le tableau 2. Avant déformation, la tôle a été recuite à 750°C pendant 2 heures pour obtenir une microstructure complètement recristallisée et obtenir une taille de grain moyenne de 200µm.

Tableau 2 : composition chimique du T40

Élements	H	C	N	O	Fe	Ti
Composition ppm (wt.)	3	52	41	1062	237	Balance

Les échantillons de T40 recristallisés ont été dabord polis mécaniquement avec du papier abrasif (600#, 1200#, 2400# jusqu'au papier 4000# (Struers standard)) puis polis électrolytiquement dans une solution de 200 ml

d’acide perchlorique et 800 ml de méthanol sous 17V (30 secondes) à la température de 20°C.

3.2. Essais MEB/EBSD interrompus

Les échantillons ont été laminé a froid ou déformé en compression plane en plusieurs passes, premièrement pour obtenir un certain taux de déformation et ensuite pour un taux de déformation donné accroître ce taux.

Pour réaliser cet essai interrompu ‘’in situ’’ une surface de 500×300 μm^2 a été polie soigneusement et repérée par quatre micro indentations. Les orientations de tous les grains présents dans la surface ont été mesurées par MEB/EBSD avant et après chaque incrément de déformation.

Le mode opératoire pour le laminage et pour la compression plane est illustré par la figure 3.

Les 2 tôles de l’assemblage sont collées pour éviter d’avoir un glissement relatif des 2 parties durant la déformation et ainsi maintenir une bonne qualité de surface pour les mesures MEB/EBSD.

L’évolution de l’orientation des grains ainsi obtenu durant la déformation sera donnée sous forme de figures de pôles et par les champs de rotation des orientations.

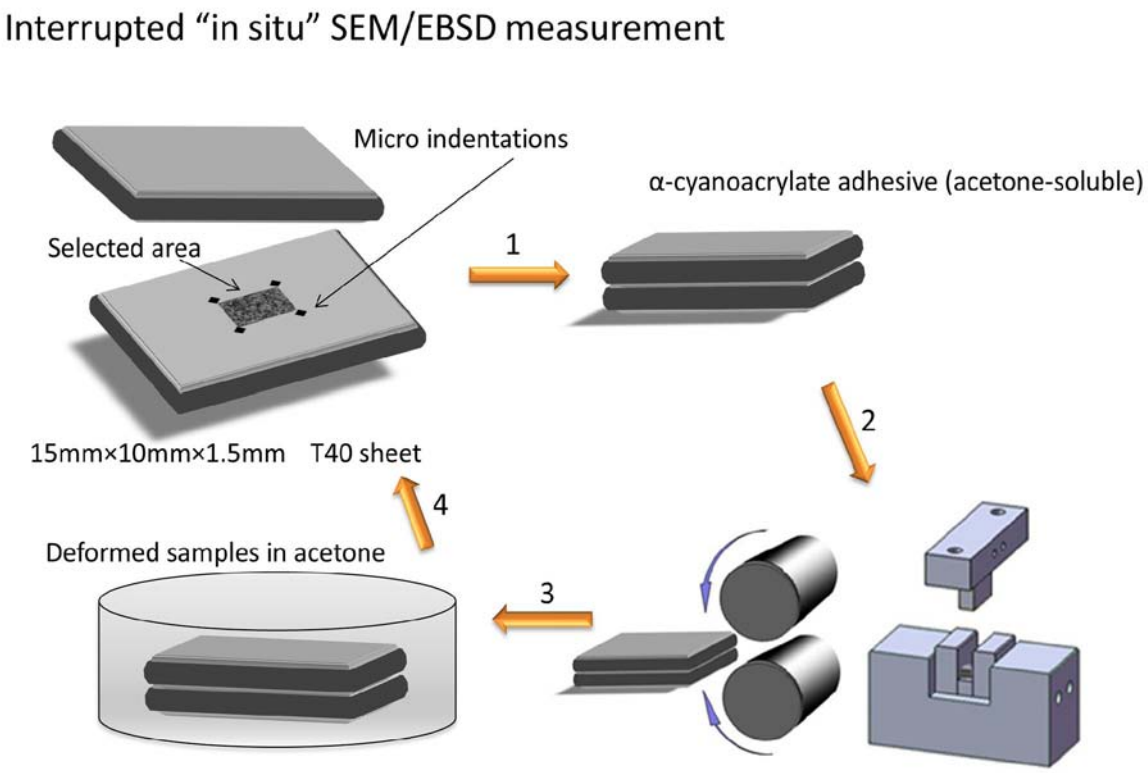

Figure 3: Synoptique d’un essai interrompu : Étape 0 après polissage, on effectue un marquage de la zone puis on fait un EBSD. Étape 1 : on colle les 2 échantillons. Etape 3 on déforme soit en laminage soit en compression. Étape 4 : on place l’assemblage dans de l’acétone pour dissoudre la colle. On revient à l’étape 0 où l’on fait un EBSD. Et le cycle peut recommencer.

4. Conclusion Générale

Le présent travail vise à améliorer la compréhension de la contribution des macles de déformation lors de la déformation plastique d'un alliage de titane T40, ainsi que de l'établissement d'un critère de sélection de variant de macles. À partir des données expérimentales et des études théoriques, les conclusions importantes suivantes peuvent être tirées:

Le maclage se produit dans les grains ayant des orientations spécifiques. Généralement, lors du laminage et de la compression plane, le maclage de compression se produit dans les grains qui ont leur axe c parallèle à la force de compression (ou légèrement incliné); le maclage de tension se produit dans les grains avec leur axe c perpendiculaire la force de compression.

La partie maclée d'un grain peut être considérée comme un nouveau grain. Lorsque les macles grandissent dans le grain, elles peuvent consommer pratiquement toute la matrice. Dans ce cas, la zone principale maclées est beaucoup plus grande que la matrice restante et représente donc le ''nouveau grain'' pour d'éventuels maclages secondaires ultérieurs. Une attention particulière doit être accordée lors de la détermination de la fraction volumique maclée. Avec la technique EBSD, une fraction volumique maclée plus grande peut être trouvée. Ceci contredit l'opinion selon

laquelle la partie maclée est toujours plus petite dans un grain maclé que dans la partie restante du grain parent, comme cela a été généralement conclu par microscopie optique. Seule la technique EBSD en suivant étape par étape l'évolution de la cartographie d'orientation permet une détermination sans équivoque de la fraction volumique maclée.

Lors du laminage et de la compression plane, il apparaît que la croissance des variants de macles de tension {10-12} (notées T1) et des variants de macles de compression {11-22} (notées C) présentent des caractéristiques différentes. Les macles de tension {10-12} présentent généralement un seul variant par grain. Même si un autre variant a été activé, il sera rapidement absorbé par le premier variant. Ce variant de macle prédominant croit très vite jusqu'à ce qu'il ne reste plus de matrice ; ceci montre le système de variant prédominant (PVS). C'est parce que les macles de tensions {10-12} se sont formées avec une force de compression parallèle à DN alors que les axes c du grain parent sont dans DT (perpendiculaire à DN). Dans cette situation, seuls deux variants ont un haut facteur de Schmid et la désorientation entre les deux variants n'est que de 9,98 °. Ainsi, dans un grain donné, ces deux variants de macles {10-12} peuvent facilement se fondre l'un avec l'autre. En revanche, il est facile pour les macles de

compression {11-22} d’activer plus d'un variant. Ceux-ci entrent en contact les uns avec les autres et se bloquent. C’est le système de variants multiples (MVS). C'est parce que les macles de compression {11-22} sont formées avec une force de compression parallèle à DN qui est parallèle à l'axe c de la matrice. Comme tous les six variants de macle {11-22} ont des relations d’orientation symétrique par une rotation de 60 ° autour de l'axe c. Les six variants devraient avoir le même facteur Schmid sous une force de compression parallèle à l'axe c. Dans nos observations expérimentales, pour les grains ayant des macles de compression {11-22}, la force de compression appliquée dévie toujours dans une certaine mesure des axes c des grains, donc seulement trois ou quatre variants auront des facteurs Schmid relativement élevés. Ces variants seront activés simultanément. PVS est enclin à se produire dans les grains allongés et MVS est enclin à se produire dans les grains équiaxes.

L'ordre d’apparition du maclage affecte la désorientation résultante induite par le maclage double (maclage secondaire), même si elles sont identiques en angle de désorientation et ont des axes symétriquement équivalents. L'ensemble de tous les variants de macles secondaires sont classés en 15 groupes de variant d'orientation plutôt qu’en 10 groupes de variants

géométriques.

Dans cette étude, deux paires de maclage double ont été observées, C-T1 et T1-C respectivement. Tous les variants de ces deux paires de macles doubles sont classés en 3 groupes par rotation symétriquement équivalente par rapport au cristal parent, à savoir le groupe A (41,3 ° autour de <1-543>), le groupe B (48,4 ° autour de <5-503>) et le groupe C (87,9 ° autour de <4-730>). Une forte Sélection de variant a lieu dans ces deux systèmes de maclage double. Le groupe B est prédominant par rapport aux deux autres dans les deux C-T1 (78,9%). Dans le cas de T1-C, le groupe de variants qui prédomine est le groupe C (66,7%).

L'analyse du facteur de Schmid (SF) a été réalisée sur les macles primaires et secondaires respectivement. SF a permis, avec une précision d'environ 50% de prédire la sélection de variant de macle primaire et avec une précision d'environ 40% pour la sélection du variant de macle secondaire. L'imprécision relative est probablement due à l'écart entre le tenseur des contraintes locales au niveau du grain et le tenseur des contraintes macroscopiques appliqué. Un nouveau calcul associé à l'énergie de déformation a été proposé pour évaluer l'influence de l'énergie de déformation sur la sélection de variant. Ce modèle a donné une précision

de 85% pour prédire la sélection de variant de macle primaire et 95% environ pour la sélection du variant de macle secondaire.

Les variants de macle formées dans un grain pourront induire dans les grains adjacents des variants qui vont être activés à travers le joint de grain tant que les angles entre les plans de macle ne sont pas au-delà de 20 °. Il n'a pas été trouvé d'influence des caractéristiques géométriques sur la sélection de variant dans le maclage double. Il est suggéré de prévoir que le calcul de l'énergie de déformation de chaque variant doit être adopté comme principal critère de sélection de variant, et que le facteur de Schmid soit utilisé comme un critère supplémentaire secondaire.

Le maclage affecte l'évolution de la texture par la réorientation de la maille cristallographique de l'ancienne orientation stable du parent vers la nouvelle orientation stable de la macle. Les orientations stables dépendent du mode de déformation, comme le laminage ou la compression plane par exemple.

Références

Bache, M. and W. Evans (2001). "Impact of texture on mechanical properties in an advanced titanium alloy." Materials Science and Engineering A **319**: 409-414.

Bozzolo, N., N. Dewobroto, et al. (2005). "Texture evolution during grain growth in recrystallized commercially pure titanium." Materials Science and Engineering A **397**(1-2): 346-355.

Chun, Y. B., S. H. Yu, et al. (2005). "Effect of deformation twinning on microstructure and texture evolution during cold rolling of CP-titanium." Materials Science and Engineering A **398**(1-2): 209-219.

Gray, G. I., G. Kaschner, et al. (1999). Advances in Twinning. proceedings of an international symposium, San Diego, Warrendale, Pa: Minerals, Metals & Materials Society.

Koike, M. (1987). "Hot-rolling texture in titanium sheet." Tetsu to Hagane-Journal of the Iron and Steel Institue of Japan **73**.

Lebensohn, R. A. and G. R. Canova (1997). "A self-consistent approach for modelling texture development of two-phase polycrystals application to titanium alloys." Journal Name: Acta Materialia; Journal Volume: 45; Journal Issue: 9; Other Information: PBD: Sep 1997: 3687-3694.

Lee, H., C. Esling, et al. (1988). "Development of rolling texture in titanium." Textures and Microstructures **7**: 317-337.

Nourbakhsh, S. and T. D. O'Brien (1988). "Texture formation and transition in Cold-rolled titanium." Materials Science and Engineering **100**: 109-114.

Prasad, Y., S. Biswas, et al. (1994). Influence of Initial Texture on the Microstructural Instabilities During Compression of Commercial Alpha-Titanium at 25 Degrees to 400 Degrees INDIAN INST OF SCIENCE BANGALORE.

Singh, A., A. Bhattacharjee, et al. (1999). "Microstructure and texture of rolled and annealed [beta] titanium alloy Ti-10V-4.5 Fe-1.5 Al." Materials Science and Engineering A **270**(2): 225-230.

Wu, X., S. R. Kalidindi, et al. (2007). "Prediction of crystallographic texture evolution and anisotropic stress-strain curves during large plastic strains in high purity [alpha]-titanium using a Taylor-type crystal plasticity model." Acta Materialia **55**(2): 423-432.

Zaefferer, S. (2003). "A study of active deformation systems in titanium alloys: dependence on alloy composition and correlation with deformation texture." Materials Science and Engineering A **344**(1-2): 20-30.